THE FACTORS AFFECTING THE OPTIMAL PERFORMANCE OF EDDY-CURRENT MACHINES.

A Thesis submitted for the Degree of Master of Philosophy

by

Henry Donald Luddington Clark

at

The University of Aston in Birmingham

during

September, 1977.

THE FACTORS AFFECTING THE OPTIMAL PERFORMANCE OF EDDY-CURRENT MACHINES

HENRY DONALD LUDDINGTON CLARK

SUMMARY

This thesis presents an examination of the factors which influence the performance of eddy-current machines and the way in which they affect the optimality of those machines.

After a brief introduction to the types of eddy-current machine considered, the applications to which these machines are put are examined. A list of parameters by which to assess their performance is obtained by considering the machine as part of a system. In this way an idea of what constitutes an optimal machine is obtained.

The third chapter then identifies the factors which affect the performance and makes a quantitative evaluation of that effect. Here the various alternative configurations and components are compared with regard to their influence on the mechanical, electromagnetic, and thermal performance criteria of the machine.

Chapter four contains a brief review of the methods of controlling eddy-current machines by electronic methods using thyristors or transistors as the final control element.

Where necessary, the results of previous workers in the field of electrical machines have been extended or adapted to increase the usefulness of this thesis.

Key Words

Machines, Eddy-current, Design.

ACKNOWLEDGEMENTS

The author would like to acknowledge the valuable guidance given by his supervisor, Professor E.J. Davies, during the course of his research, and the constructive criticism of this work offered by Dr. M.T. Wright.

The joint financial assistance given by Heenan Drives Limited, Worcester, and the Science Research Council is also gratefully acknowledged.

Finally, the author acknowledges the diligent efforts of Miss N.P. Freeman who typed the manuscript of this thesis.

CONTENTS

LIST OF SYMBOLS

a	cross sectional area of conductor, m^2
A	cross sectional area of coil space, m^2
b	temperature coefficient of resistivity 1/K
B	magnetic flux density, T
b	strip thickness, m
c	eccentricity, m
d	depth of plating, m
D	diameter, m
e	eccentricity coefficient
E	electromotive force, V
f	factor
F_x	magnetomotive force, A
F	force, N
g	airgap length, m
i	current, A
I	current, A
J	moment of inertia, kg m^2
J_x	current density, A/m^2
k_n	arbitrary constant
L	active length, m
m	saturation index
m	mass, kg
MLT	mean length of turn, m
n	rotational speed, rev/sec
N	number of turns

N_s	number of slots
p	pole pairs
P	Power, W
q	degree of interdigitation
r	radius, m
R	resistance, Ω
s	fractional slip
S	reluctance, H^{-1}
t	time, s
T	torque, Nm
ΔT	temperature rise, K
v	velocity, m/s
V	voltage, V
α	slot depth/airgap length ratio
β	slot width/airgap length ratio
γ	mass density kg/m
δ	Carter's coefficient
ε	flux utilisation coefficient
η	efficiency
θ	angle, radians
κ	pole arc-pole pitch ratio
κ'	tooth width-tooth pitch ratio
λ	pole wavelength, m
Λ	permeance, H
μ	permeability, H/m
ρ	resistivity, Ω m

ϕ magnetic flux, Wb

ψ pole face taper factor

ω angular velocity, rad/s

Suffices

a active

ac fundamental component

c coil

eff effective, overall

g airgap

i input

l lost

m maximum

net net, resultant

o output, reference quantity

r reaction

t related to time or temperature

ϕ flux producing

Variations on these symbols may occur in the text; where this is the case the new symbol or meaning has been stated.

1. INTRODUCTION

1.1 Eddy Currents

When a homogeneous, electrically conducting material is subjected to a time varying magnetic field, electrical currents are found to be induced in it. This phenomenon was first demonstrated by Francois Arago in 1824. Arago found that by rotating a copper disc near a permanent magnet it would also rotate in the same direction as the disc. He was unable to explain the reason for this occurrence, and it was not until 1831 that Michael Faraday discovered the principle of electromagnetic induction, the key to Arago's problem.

Faraday found that an electric current could be made to flow in a conductor by moving it through a magnetic field. He formulated the notion that an electric force was produced which was proportional to the rate at which lines of magnetic flux were cut.

Lenz, in 1834, postulated that any current that flowed under such circumstances would be in such a direction as to oppose the change producing it. In 1845 Neumann formulated Faraday's and Lenz' rules into the law

$$E = - \frac{d\phi}{dt} \qquad (1.1)$$

which is now known as Faraday's Flux Cutting Rule.

When an induced electromotive force causes currents to flow in a bulk conductor they are known as Eddy or

Foucault Currents. The first term refers to the analogy between electrical and hydraulic eddies, whilst the second comes from the name of the French physicist Léon Foucault, who is credited with postulating the existence of such currents in Arago's disc experiment.

1.2 Eddy-current Machines

If the eddy currents are generated by the motion of an electromagnet system relative to a conductor, a force will be produced by the interaction of the applied field and the reaction field of the eddy currents. This force will be in such a direction as to attempt to reduce the relative motion.

In an eddy-current machine of the type depicted in Fig. 1.1 this force manifests itself as a torque tending to rotate the driven member in the same direction as the driving member. This simple machine consists of two parts separated by a short radial airgap. One is an electrical conductor in which the eddy currents flow. This is known as the loss member and may be in the form of a drum or a disc, Fig. 1.2, in a rotating machine. The other component is an electromagnet system which produces a space varying flux density around the airgap. It is usually referred to as the rotor or field member.

If one of the members is held stationary a retarding torque will be applied to the other, driven, member when excitation is supplied to the field member. This arrange-

ment finds applications as a brake, a retarder and a dynamometer. In the first case the machine is used to absorb excess energy from a system. When used as a supplementary brake for road vehicles it is known as a retarder. The dynamometer absorbs the mechanical power generated by prime movers whilst at the same time allowing torque and speed to be measured, and hence the power output.

The energy absorbed by an eddy-current machine appears in the form of heat. The eddy-currents flowing in the loss member produce heat by the Joule effect. The basic relationship obtaining here is a power balance.

Under steady-state conditions:

The thermal power dissipated = Mechanical power absorbed

or

$$P_D = T\omega \qquad (1.2)$$

where P_D = thermal power, W

T = braking torque, Nm

ω = angular velocity, rad/s.

The eddy-current machine is also capable of operating as a torque transmitter. If both members are free to rotate independently, then a torque on one shaft will be balanced by an equal torque on the other. As the torque is transmitted from one shaft to the other this machine is termed a coupling. Relative motion or slip, must exist between the two members for a torque to be produced.

Considering the power balance again, under steady conditions:

$$T\omega_i = T\omega_o + \text{losses} \qquad (1.3)$$

where T is the torque transmitted, Nm

ω_i is the angular velocity of the input or driving member, rad/s.

ω_o is the angular velocity of the output or driven member, rad/s.

or $\text{losses} = T\omega_i - T\omega_o$

$= T(\omega_i - \omega_o)$

$= T\omega_s$ where $\omega_s = \omega_i - \omega_o$

the efficiency, $\eta = \dfrac{\text{Power in - losses}}{\text{Power in}}$

$$= \frac{T\omega_i - T\omega_s}{T\omega_i} \qquad (1.4)$$

defining fractional slip, $s = \dfrac{\omega_s}{\omega_i}$

then $$\eta_{p.u} = 1 - s \qquad (1.5)$$

i.e. the efficiency of an eddy-current coupling varies directly as the ratio of output to input speeds. This is consistent with equation (1.2) as in a brake the fractional slip, s, is always unity.

The eddy-current coupling has been found to make an excellent variable-speed drive. By means of an electronic control system furnishing a small excitation power, the coupling can be made to yield a continuously variable

output from a constant speed drive motor. In its most common form, the coupling is driven by a three phase induction motor.

1.3 THE OPTIMISATION PROBLEM

The various machines illustrated in Plates 1, 2, 3 and 4, show the development of eddy-current machines over the past 32 years. In common with many other engineering products the form of the machine has changed little throughout its history.

Despite many years of development no clear consensus has emerged as to what constitutes the ideal or optimal machine. Of the alternatives available for the loss member and rotor, and various constructional arrangements, no systematic study has been made. The reasons for this surprising omission are twofold. First, no adequate theory was available for many years which accurately described the electromagnetic phenomena occurring in the machine. Second, no rational criteria exist by which to judge the performance of the machine on its own. The former problem is now gradually being resolved by a series of progressively more elaborate studies (see Section 1.4). The latter, however, is insoluble. It is only in the context of the whole system that the performance of eddy-current machines can be evaluated.

This thesis sets out to review progress in the study of eddy-current machines, and having done that

to use the best available theories to evaluate the manifold alternatives available to the designer of these machines.

1.4 RELEVANT LITERATURE

Although the historical development of the theory of eddy-current machines is interesting it is not strictly relevant to a study such as is contained in this thesis. For the interested reader a good review of the works of Rudenberg et al is contained in the thesis of Wright[9].

It was not until 1946, and the publications of papers by Gibbs[1], that any kind of comparative discussion of the options available to the machine designer was offered. Gibbs discussed the various types of rotor available and then proceeded to offer his theory of the operation of eddy-current couplings. Although he demonstrated its accuracy by means of worked examples it is not given in an immediately useful form. The third part of the paper contains methods of tailoring the performance of the machine by changing the number of poles or altering the loss member resistivity. Methods of cooling were also covered. Whilst Gibbs made a valuable contribution to the understanding of the eddy-current coupling, the effect of machine parameters was still obscure.

A great deal of light has been shed upon this aspect by the work of Davies[2]. He extended the work of Gibbs to

obtain equations for the peak torque, $\hat{T}_m$, and the slip speed for peak torque, $\hat{n}_m$, in terms of machine parameters. Accompanied by a generalised equation applying to any machine with a solid iron loss member, Davies offered a tested method[4] of predicting the performance of eddy-current machines. In his second paper Davies[3] refined his theory to take into account the possibility of using materials other than pure iron for the loss member. Having already shown that the theory applied to hetero-polar rotors, he used a homopolar rotor in the second paper and showed that the theory was equally applicable. The appendix to this paper is the first attempt at the optimisation of rotors. Considering a machine of a certain diameter, pole number and the same loss member, Davies demonstrated the effects of utilising different rotors.

Further, to test Davies' theory, James[6] carried out an extensive experimental investigation using both solid iron and end-ring loss members. He showed that a machine employing a drum with copper rings, attached at the ends of the active region, obeyed Davies' theory over the range $0.2 < n/n_m < 4$. In doing so, James raised the problem of how to account for end effects. The simple loss-member resistivity multipliers advocated by Gibbs and James can give useful results in certain circumstances. The assumption, however, that the end region currents are governed by Laplace's Equation

does not allow for the frequency dependence which exists in practice.

Two papers from outside the domain of eddy-current machines that give alternative approaches to end-effects, are those by Russell and Norsworthy[7], and Woolley and Chalmers[8]. The former considers the losses in a screened rotor induction motor, whilst the latter concerns end effects in a solid rotor induction motor. Although neither of these papers is directly concerned with eddy-current machines, relevant results are given which are discussed further in Section 3.5.2.

Wright[9] successfully tackled both the effects of copper plating a ferromagnetic loss member and the prediction of transient torque response at constant slip speed[5]. In the course of his experiments he made use of salient pole and partially interdigitated rotors, providing useful information about their relative merits[10]. This work on copper-faced couplings neatly bridges the gap between Davies' work on solid iron couplings and that of Bahler and Van der Hoek[11] on non-magnetic loss member machines.

Jackson[12] is one of the most recent authors to work on eddy-current machines. His work shows that the absolute speed of machines does not have a direct bearing on their performance, but that the relationship of that speed to the speed for peak torque does. This experimental machine,

which operated up to 14000 rev/min, still obeyed Davies' theory. Jackson is the first author to give more than a passing mention of temperature effects. He draws attention to the marked effect of temperature upon peak torque, T_m, and slip speed at peak torque, n_m. Extensive consideration is given to the heat transfer mechanisms in the machine.

Where useful, proven relationships have been employed from the above papers to derive tables or graphs. The design methods enumerated later in the thesis thus extend the usefulness of these papers. Prior to this work it was necessary to decide upon what constituted optimal performance. To do this, several papers concerning eddy-current machines and their applications were useful.

A review of variable speed drives and their applications by Laithwaite[13] gave both some factors to be considered when choosing a drive and a comparison of various types of drive.

Bloxham and Wright[14] show the usefulness of the eddy-current coupling as a variable speed drive. They explain the essentials of coupling construction and operation and give examples of industrial applications. Another paper[15] by the same two authors consider the economic aspects of the eddy-current coupling variable speed drive. They make the point that there are three elements to the overall cost of a coupling, capital,

operating and maintenance costs. When all these are considered the eddy-current coupling becomes an attractive proposition as a variable speed drive.

Under the auspices of another manufacturer Flack, Grant and Parker[16] also discuss applications of eddy-current couplings and brakes.

Wright[17] presents a general theory of losses in eddy-current couplings. With particular reference to pump drives he discusses the economics of using an eddy-current coupling compared with an a.c. commutator motor. Since cost is an important element in the optimality of a machine, this paper gives a useful insight into the competitiveness of an eddy-current coupling for this type of application.

Another application for the eddy-current machine is as a supplementary vehicle brake or retarder. The requirements for this application are discussed by Reed[18]. In a mainly descriptive paper he considers the different available types and the conditions under which they operate.

In a similar manner Scharff[19], Reverdin and Borione[20], and Breton[21], describe the evolution and application of the double disc machine as a retarder.

Despite the established use of eddy-current machines as brakes and dynamometers, no recent works of any relevance appear to have been published.

2. OPTIMISATION AND OPTIMAL PERFORMANCE

2.1 INTRODUCTION

In this chapter the philosophy of optimisation and the methods of achieving optimality are considered. With regard to eddy-current machines various applications are considered in detail to obtain a definition of what is required of an optimal machine.

2.2 OPTIMISATION

2.2.1 The Meaning of Optimisation

Optimisation is taken to mean the process of designing something so that if fulfils as closely as possible the required conditions.

In its simplest form, the optimisation problem consists of two conflicting parameters whose values must be determined so that a third parameter achieves a 'best' value. In graphical form this problem is represented by a three-dimensional surface. The highest peak or the deepest trough represents the optimum conditions, depending upon whether the definining parameter was to be maximised or minimised.

2.2.2 Analytical Optimisation

This method of optimisation entails selecting an 'objective function' which represents the 'goodness' of the machine. The objective function is an analytical relationship in terms of all the design variables. An attempt is then made to minimise the objective function, which may, for instance, be the cost of the machine. A variety of methods

is available for minimisation,[22] which in theory should enable a minimum to be obtained. The multi-dimensional expression required for the objective function will have many minima and uncertainty will exist as to whether the lowest or global minimum has been found. There are, however, sophisticated, if complicated Gradient Divergence techniques which largely overcome this problem.

For electromagnetic machine optimisation, the lack of suitable analytic relationships between design parameters makes this approach difficult. The eddy-current machine with a multiplicity of alternative forms is even less suitable for this type of optimisation.

2.2.3 The Pragmatic Approach

The pragmatic approach relies to a greater extent on the use of engineering judgement. Approximate relationships are used for each aspect of the design which is optimised successively. This procedure will work well when the variables are substantially independent; human judgement is unreliable when three or more interdependent variables are involved. Essentially this approach involves splitting the design into manageable sections and identifying optimal conditions.

With a device like the eddy-current machine,where there are few exact analytic relations yet many variables, this second approach seems more appropriate. It is this piecewise approach that has been adopted in the subsequent sections.

2.3 OPTIMAL PERFORMANCE

2.3.1 Introduction

In Chapter 1 it was explained that eddy-current machines act as controllable transmitters and absorbers of mechanical power. Consequently, they are always adjuncts to a system containing a load and/or a drive motor, the performance of the machine being assessed in terms of the overall system performance. The suitability of the machine for its allotted purpose largely determines its degree of optimality.

2.3.2 Factors Affecting the Choice of Machine

In order to determine what parameters measure the optimality of a machine it is instructive to consider the factors which influence the choice of machine initially. The machine which best satisfies these requirements must be closest to optimum.

These factors may be classified under the following headings:

(i) Performance

(ii) Reliability

(iii) Maintainability

(iv) Overall cost

(v) Noise level

(vi) Weight/Power ratio

(vii) Size/Power ratio

(viii) Simplicity of operation

(ix) Simplicity of Installation

(x) Safety

(xi) Resistance to Hostile Environment

The above list shows the most common factors to be considered when selecting a machine for a given application. The first four are probably the most important in the majority of instances. These, however, are not independent of the other factors. Indeed this is a recurrent problem in optimisation studies. No one aspect can be considered in isolation.

2.3.3 Performance

2.3.3.1 The Factors Comprising Performance

The performance required of an eddy-current machine depends greatly upon the nature of the load. This topic is discussed at length in Section 2.4.

Meanwhile, the performance characteristics of eddy-current machines will be considered. These characteristics may be expressed by the following:

(a) The steady-state Torque-slip curve

(b) The power dissipation capacity

(c) The transfer function.

2.3.3.2 The Steady-state Torque-Slip Curve

Fig. 2.1 shows a typical family of torque-slip curves for a small commercial eddy-current coupling. Each curve represents a different value of excitation current. The

dashed curve A shows the torque-slip characteristic of the coupling when cold. The continuous lines show the torque after thermal equilibrium has been established. The effects of temperature are more marked in some machines than others (see Section 3.4.4). The two main temperature sensitive variables are the loss member resistivity and the length of the active airgap. Whilst little can be done to mitigate the former effect, an axial airgap arrangement greatly reduces the latter.

The dot-dash line, B, shows the heat dissipation limit of the machine. Torque and slip combinations beyond this limit are not permitted for continuous operation.

The straight line, C, gives the maximum torque of the drive motor, here a small three phase induction motor running substantially at constant speed and driving the loss member.

Other important performance characteristics given in Fig. 2.1 are, the initial slip for rated torque, which should be small for high efficiency, and the torque at maximum slip, which is the torque available to accelerate the load from rest.

Conventionally, the performance parameters are specified under certain conditions of temperature and altitude for an air cooled machine. Should these conditions be deviated from derating may be necessary. Typically, the maximum slip loss should be reduced by 1.8% per degree C for air inlet temperatures above 20° C, and by 1.5% for every 100m in excess of

1000m altitude above sea level.

2.3.3.3 The Power Dissipation Capacity

The slip loss in an eddy-current coupling appears as heat in the loss member. It must be removed under continuous running conditions, otherwise overheating and consequent failure will occur. The power dissipation capacity will often restrict the performance in the high torque and slip regime. This restriction is confined to air cooled machines. In common with many electrical machines cooling becomes progressively more difficult as the diameter increases (see Section 3.4.1). Whilst the losses increase as D^{2+} L the cooling area only increases as DL. Practically, this means that forced air cooling and eventually liquid cooling must be employed to removed the slip losses as the size increases.

Fig. 2.2 shows the heat dissipation capacity of an air cooled machine where the loss member and integral cooling fan are driven by the drive motor. The curve has two distinct portions, the second is as a result of the maximum loss member temperature being reached, and the first is due to the excitation coil temperature limit. These limits on cooling capacity are represented on the torque-slip graph by a family of constant-power hyperbolae for various input speeds (curve B on Fig. 2.1).

2.3.3.4 The Transfer Function

There are two elements which determine the transient response of an eddy-current machine, the time constants of

the machine and those of the controller.

The torque response at constant slip speed depends to a large extent on the type of machine. Wright et al[5,9] have carried out extensive investigations in this area (see Section 4.2).

Speed changes at constant torque are predominantly governed by the combined inertia of the machine and the rest of the system.

It should be noted that a coupling is only capable of accelerating a load or maintaining constant speed. In the absence of sufficient friction, a retarding torque must be provided for deceleration. This is normally furnished by an eddy-current or friction brake.

The controllability, for want of a better term, relates to the ease and accuracy of control. The control system for the eddy-current machine is intended to make the machine perform in a predetermined manner. Control is effected by means of a variable direct current supply connected to the excitation windings. Open-loop control constrains the machine to operate on the torque-slip curve for that particular current. Closed-loop control, however, is more versatile in that speed, torque, or some other parameter can be made to alter according to the desired conditions. Most often speed or torque are controlled, although any other variable can be controlled if a suitable transducer is available.

Accuracy of control depends upon the quality and complexity of the controller and transducers, and the transient response of the machine. It is possible to improve upon the natural response of the machine by forcing, momentarily exceeding the rated coil current, and inversion, causing the field current to decay rapidly by reversing the supply. In this way effective response times can be reduced by a factor of two or three.

The most significant feature of eddy-current machine control equipment is its low power rating. As the machine itself acts as the power control element it is only necessary to supply the I^2R losses of the excitation coil. Typically these are only 1 to 2% of the power rating of the machine.

2.3.4 Reliability and Maintenance

These two topics have been combined, as for most purposes they are inextricably linked.

The eddy-current machine should be inherently reliable. The small number of parts that wear, the bearings, and brushes and sliprings, if correctly selected, should have a long and predictable life. Correct design of the other components should ensure that other failure modes do not occur, providing that the machine is operated within its ratings.

The level of reliability required of a coupling is comparable with that of the squirrel cage induction motor

which usually drives it.

Inevitably some components become consumed as the machine operates. It is the purpose of preventive maintenance to replace these before failure occurs. Preventive maintenance is usually restricted to lubrication of the bearings and replacement of the brushes, if fitted. Modern machines have endeavoured to eliminate the maintenance requirement entirely by adoption of 'sealed for life' bearings and brushless construction. It is shown in Section 3.3.13 that this elimination of maintenance, by the adoption of brushless construction, is achieved at the expense of performance and greater complexity. Whether this is justifiable or not depends upon the application to which the machine is put.

2.3.5 Overall Cost

The overall cost of a machine is a quantity expressing the sum of initial, running, and maintenance costs over the life of the machine in terms of present value. It is an important factor in selecting a machine. The running costs of eddy-current couplings are often assumed to be inherently high. This assumption is often erroneous as the efficiency of an eddy-current drive system depends largely upon the nature of the load (Section 2.4). There is, however, another factor to be considered, the relationship between machine performance and efficiency.

2.3.6 The Effect of Drive Performance on Running Costs

2.3.6.1 Losses

A typical drive system employing an eddy-current

coupling consists of, an induction motor, a coupling and a load. (Fig. 2.3).

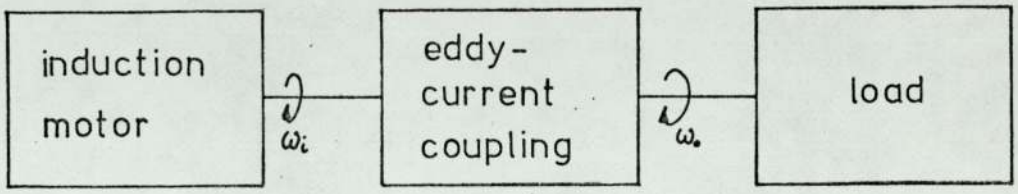

Fig. 2.3 Typical Eddy-current Drive System

The running costs clearly depend upon the efficiency with which the motor and coupling deliver power to the load. The principal losses in the system are:

(a) The slip loss of the induction motor, which typically is about 5% of the input power under full load conditions.

(b) The slip loss of the coupling, which varies according to the design of the coupling. It is about 10% of the input power under full torque and maximum output speed conditions.

(c) The excitation loss, being the power supplied to the field windings to control the coupling. Typically it is around 2% of the transmitted power.

and

(d) The friction and windage losses in the coupling which are typically 2% of full power and sensibly constant.

Of these the slip and excitation losses are largely determined by the design of the coupling. Two different types of coupling will be considered to evaluate the effect of their performance on the running costs.

2.3.6.2 The Drives Used for Comparison

Coupling A is chosen to be representative of the average currently available machine.

Coupling B is a predicted next generation machine. By using the design techniques covered in this thesis, it is believed that significant improvements can be achieved over present day designs.

The properties of these two machines are summarised below:

	Coupling A	Coupling B
Max. Power, (kW)	10	10
Initial Slip, (pu)	0.1	0.05
Extn. loss, (W)	200	100
Cost, (£)	400	440

Fig. 2.4 Summary of the Properties of Couplings A and B

Fig. 2.4 shows that both initial slip at rated torque and excitation power have been halved in the improved coupling B. This is assumed to have been achieved at a 10% increase in cost. Whilst these figures are necessarily speculative, they will serve to show that in view of the rapid increase of energy costs in recent years, such perform- improvements are worth striving for.

2.3.6.3 The Present Value Criterion

The circumstances under which savings will be made, may be calculated using discounted cash flow methods[23] to determine the present value of the running costs. The annual running costs can be estimated for a variety of loads and discounted using the well known formula:

$$(PV) = R\{\frac{1-(1+r)^{-n}}{r}\} \qquad (2.1)$$

where (PV) = the present value, £ $\frac{(PV)}{R}$ = Discount factor

R = the annual cost, £

r = the discount rate, p.u.

n = the length of the period, years.

2.3.6.4 Choice of Discount Rate

The choice of discount rate is important to the realism of the calculations. The rate is determined principally by the cost of capital and is therefore of similar magnitude to the minimum lending rate. At the time of writing (Spring 1977), interest rates in the U.K. vary monthly. Until some stabilisation of the economy is attained, the use of discounted

cash flow methods must rely on past experience and reasonable assumptions. In the short term interest rates of 10% seem realistic.

2.3.6.5 The Effect of Inflation

Inflation, the term used to describe the rise of wages and prices simultaneously, further complicates the cost calculations. In this context it means that the annual cost of energy to the drive system will increase. Equation 2.1 can be easily modified to take this into account. As it stands Equation 2.1 is the sum of a geometric progression. Thus:

$$(PV) = R(1+r)^{-1} + R(1+r)^{-2} \text{ --------- } R(1+r)^{-n} \qquad (2.2)$$

Inflation, however, causes the annual cost R, to increase, thus:

$$R_n = R(1+i)^n \qquad (2.3)$$

where R_n is the annual cost in the year n

i is the per unit inflation rate

and so the present value progression becomes

$$(PV) = R\frac{(1+i)}{(1+r)} + R\frac{(1+i)^2}{(1+r)^2} \text{ --------- } +R\frac{(1+i)^n}{(1+r)^n} \qquad (2.4)$$

The term $(\frac{1+i}{1+r})$ occurs throughout and thus enables an 'effective' discount rate, r', to be employed, where:

$$r' = 1-(\frac{1+i}{1+r}) \qquad (2.5)$$

Currently the rate of inflation is greater than the discount rate, which implies a negative effective discount rate. Using a negative rate in the Present Value equation means that the (P V) exceeds the sum of annual costs. Clearly the technique cannot realistically be employed.

Unlike electromagnetic theory, which is governed by a set of immutable laws and relationships, economics does not have such time-independent laws. Under the present circumstances the best which can be done is to make the optimistic assumption that the average trends of the past will apply to the future. Accordingly, an effective discount rate of 5% ($r' = 0.05$) has been selected for the subsequent calculations.

The importance of selecting an accurate value for the discount rate can be seen by plotting discount factors against time for various rates, Fig. 2.5. Alternatively, discount factors can be plotted against discount rate for various periods, Fig. 2.6. These show that the longer the period or the higher the discount rate, the less is the importance of money paid in the latter years of the period.

2.3.6.6 Application of the Discount Factors

In the following examples a discount rate of 5% has been used. The effect of other rates can be seen by using Figs. 2.5 and 2.6. Knowing the difference in running costs, the difference in present value can be found and either,

the suitability of the two machines, or the amount available for improving the existing machine estimated.

2.3.6.7 Estimation of Running Costs

For simplicity, the following assumptions have been made:

(a) The excitation power is constant

(b) Each drive delivers the same power to the load,

(c) The drive motor in each case has the same efficiency and cost.

The input power to the motor is

$$P_{in} = \frac{P_{LOAD}}{\eta_m \eta_c}$$

where P_{LOAD} - load power, Kw

η_m - motor efficiency

η_c - coupling efficiency

The energy consumption of the motor is obtained from the product of input power and running time. To this must be added the excitation energy.

2.3.6.8 Constant Speed Load at Maximum Drive Power

Here the drive is operating under constant load conditions at full speed.

Assuming:

(i) The system operates for 2000 hrs. per annum

(ii) Energy costs are 2p/kW hr

(iii) $r' = 0.05$

then the annual running cost for A and B are £448 and £424 respectively. After only two years B has used £44 less energy, thereby more than offsetting the assumed £40 difference in initial cost. The table, 2.1, illustrates this point.

	Drive A	Drive B	A - B
Initial Cost, £	400	440	-40
Total Cost, £; year 1	826	844	-18
" " " " 2	1233	1229	4
" " " " 3	1619	1593	26
" " " " 4	1990	1945	45

Table 2·1

The break-even period may be calculated by setting the present value of the difference in running costs equal to the initial cost difference.

i.e.

$$C_{iB} - C_{iA} = (R_A - R_B)\{\frac{1-(1+r)^{-n}}{r}\} \qquad (2.6)$$

where C_{iA} - initial cost of coupling A

C_{iB} - initial cost of coupling B

R_A - annual running cost of coupling A

R_B - annual running cost of coupling B

which gives

$$n_b = \frac{\log\left| 1 - \frac{C_{iB} - C_{iA}}{R_A - R_B}.r \right|}{\log\frac{1}{1+r}} \qquad (2.7)$$

where n_b is the break even period.

2.3.6.9 Constant Power Load-Variable Speed

The example given in the previous section represented a drive operating at high efficiency. An application where the overall efficiency is lower is that of a winder drive. The nature of this type of load is discussed later in Section 2.4.3.4, where it is shown that the overall energy efficiency depends upon the range over which the drive must operate.

e.g. If the speed range is 8:1 then the overall efficiency is 0.18 times the maximum speed efficiency.

	Drive A	Drive B
Max. Efficiency, %	90	95
Overall ,, ,%	16·3	17·1
Mean Input Power, kW	6·3	5·9
Annual Running Cost, £	252	236

Breakeven Period = 2·7 yrs

Table 2·2

The lower power demand of this application results in a longer break-even period. Nevertheless, the improvements to the drive efficiency are probably still worth achieving.

It should be noted that the drive is rated at 10 kW yet is only capable of driving a 1 kW load. This is necessary owing to the requirement for the drive to operate at low speed and hence low efficiency. It is conceivable that the use of a gearbox or multi-speed motor to vary the coupling input speed might result in a cheaper system overall. This type of evaluation can also be easily carried out using the foregoing techniques.

2.4 APPLICATIONS FOR EDDY-CURRENT MACHINES

2.4.1 Dynamometers

The eddy-current machine has been successfully employed as a dynamometer for measuring the power output of prime movers and other machines which generate mechanical power. By attaching one member of the dynamometer to a torque arm, and the other to the output shaft of the machine to be tested, an adjustable retarding torque may be applied by varying the excitation current.

The steady-state performance of a dynamometer is usually given in the form of a power absorption envelope. The line AB in Fig. 2.7 (p 29) shows the low speed performance of the dynamometer[12]. When testing motors which produce large torques near stall, it is desirable that the gradient of AB should be as large as possible.

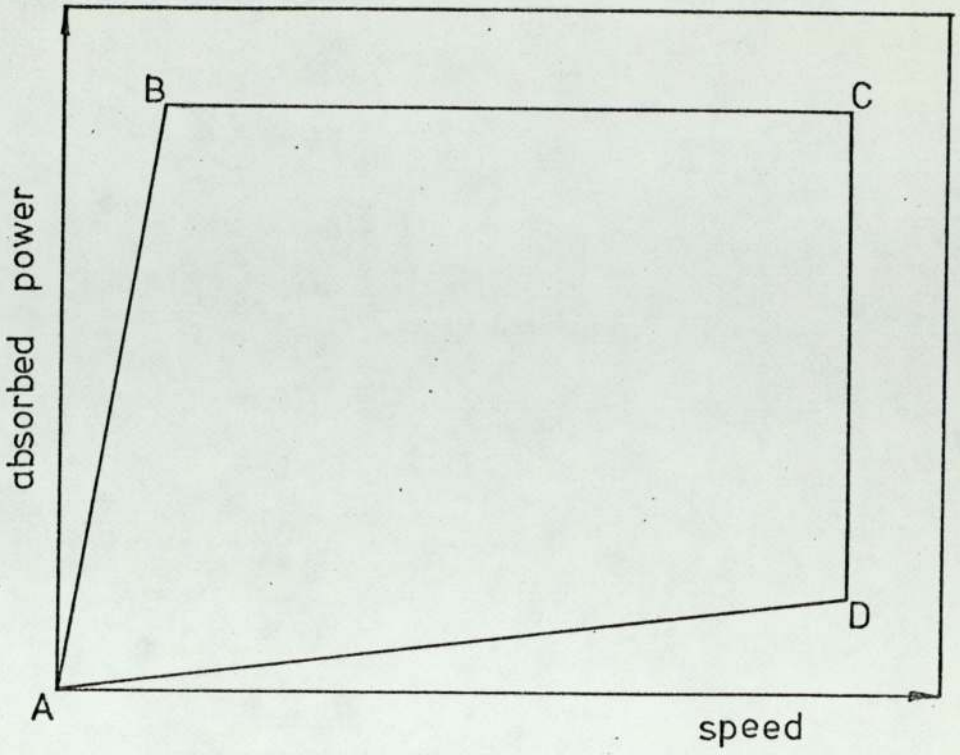

Fig. 2.7 Typical Dynamometer Power Envelope

The maximum power which can be absorbed by the dynamometer is shown by BC. Eddy-current dynamometers absorb mechanical energy by converting it into heat. The maximum power is determined by the rate at which the cooling system can remove the heat.

The line CD indicates the maximum speed at which the dynamometer may operate. Ideally this should be in excess of the speed of the machine being tested. Gas turbines, for instance, operate at speeds up to 15,000 rev/min. The use of speed reducing devices such as gears or belts is undesirable on account of their indeterminate losses. It

is preferable that the dynamometer should be connected directly to a turbine. The maximum speed of the dynamometer is usually set by the ability of the rotor to withstand the centrifugal forces at elevated temperature.

The last side of the power absorption envelope, AD, represents the power absorbed when no excitation is being applied. It is the minimum load that the dynamometer will apply. This unavoidable drag force is caused by the existence of friction and viscosity inside the dynamometer. Clearly, the closer AD is to the speed axis, the better, as the range of the dynamometer is maximised.

Transient performance is also an important consideration in assessing a dynamometer. The ability of the dynamometer rapidly to load and unload the prime mover is sometimes required for the simulation of shock loads. The simulation of real situations is another use for eddy-current dynamometers. Here the dynamometer is controlled by a computer program to simulate, say, town driving conditions for emission tests on a petrol engine.

2.4.2 Brakes

2.4.2.1 Introduction

A brake is used to apply a mechanical retarding force to a system, as a means of controlling the magnitude and rate of change of speed. Two types of eddy-current brake are in common use, the industrial brake and the vehicle brake.

2.4.2.2 The Industrial Brake

For as long as the eddy-current coupling has been employed as a variable speed drive, the eddy-current brake has been used to complement it. Owing to the inability of the eddy-current coupling to decelerate the load, it is necessary to provide the retardation by means of a brake. Frequently, the brake is incorporated into the casing of the coupling (Plate 3). Driving and braking torques are then available and by means of two excitation units accurate control of small or metastable loads can be effected. The performance characteristics desired of the brake are determined by the nature of the load and the type of control stratagem adopted.

2.4.2.3 The Vehicle Brake or Retarder

The eddy-current brake also finds application as a supplementary brake for heavy road vehicles, (Fig. 2.8). In this context it is known as an eddy-current retarder.

Conventional friction brakes give good performance when applied for short periods. Sustained or repeated braking, however, renders them liable to fade. Fade is the term used to describe the loss of braking force caused by overheating of the friction surfaces. Accordingly, it is becoming increasingly common to fit supplementary braking systems to vehicles susceptible to brake fade. The eddy-current retarder is ideally suited for this application.

The main requirement of a retarder is that it should

be capable of relieving the friction brakes of the need to operate under conditions likely to produce overheating and fade. The descent of long hills is a typical instance, when gentle braking must be made continuously to maintain a safe road speed. In practice this means that the retarder must be capable of absorbing a power similar to that produced by the vehicle engine for periods of up to 15 mins., without exhibiting the catastrophic fade of friction brakes.

It is desirable that the retarder is light and compact as it is often fitted after manufacture. At present retarders have a mass of about 2% of the gross vehicle mass[18]. As a result of friction and windage a small retarding torque will always be present even when unexcited. This loss of useful engine power is undesirable and in a good retarder must be minimised. The additional weight and slight loss of power are usually offset by the monetary savings made by the extended friction brake life.

2.4.3 Couplings

2.4.3.1 Variable Speed Drives

In the power transmission mode the eddy-current machine is known as a coupling. It is used to control the power transmitted from a drive motor to a load. The efficiency with which it does so is largely determined by the nature of the load. The following sections show how the load affects the efficiency of the system and the design of the coupling.

2.4.3.2 Generalised Coupling Loads

According to Wright[17] the torque speed characteristic of many loads can be expressed as a polynomial,

$$T = \sum_{n=o}^{\infty} A_n \omega^n \qquad (2.7)$$

where T - torque, Nm

A_n - load coefficient

ω - load angular velocity rad/s

n - index

It can be simply shown that the slip loss at fractional slip s is

$$P = \sum_{n=o}^{\infty} A_n \omega_o^{n+1} \, s(1-s)^n \qquad (2.8)$$

where ω_o - input speed of the coupling

and the conditions under which this is a maximum are given by

$$\frac{\partial P}{\partial s} = 0$$

Many loads only require a single term in the polynomial to be represented adequately.

e.g. n = -1, a constant power winder

n = 0, a constant torque

n = 1, torque proportional to speed

n = 2, a pump or fan load.

So for a single term load

$$P = A\omega_o^{n+1}\, s(1-S)^n \qquad (2.9)$$

The slip at maximum loss, s_{max} is given by

$$s_{max} = \frac{1}{n+1}$$

and the maximum loss is then

$$P_{max} = A\omega_o^{n+1}\, \frac{n^n}{(n+1)^{n+1}} \qquad (2.10)$$

Comparing this loss with the rated power of the drive yields a per unit loss

$$\frac{P_{max}}{P_{rated}} = \frac{n^n}{(n+1)^{n+1}} \qquad (2.11)$$

This shows (Fig. 2.9) that the greater is n the smaller is the loss. The overall energy efficiency of the drive system depends upon the torque - Speed-time relationship and the nature of any associated losses. Examples of a pump drive (n=2) and a winder drive (n=1) follow.

2.4.3.3 Pump Drive

The characteristic of a pump load is that the torque is roughly proportional to the square of the speed.

Substituting n=2 into equation 2.11 yields,

$$\frac{P_{max}}{P_{rated}} = \frac{4}{27}$$

i.e. the maximum loss in the coupling is about 15% of the

full load power. It has been shown[17] that an eddy-current pump drive can have a comparable efficiency with an a.c. commutator motor in such circumstances.

The power-speed requirement of the pump is shown in Fig. 2.10 along with the loss in the coupling. In terms of the coupling torque-slip curve, for steady-state operation, a drooping characteristic of the type in Fig. 2.11 is suitable. A low initial slip is also desirable to give high efficiency. The relatively small slip loss means that adequate cooling is quite easily achieved even with large machines (500 kW). The only time when excessive heat may be produced is during acceleration from rest.

2.4.3.4 The Winder Drive

2.4.3.4.1 Description

In contrast to Section 2.4.3.3, a load which is very demanding of an eddy-current coupling is the centre driven winder.

Fig. 2.12 shows the situation obtaining in a partially wound coil. The eddy-current coupling drives the coil spindle so that the line speed and tension remain substantially constant.

The velocities are related thus,

$$v = \omega r$$

and the forces,

$T = Fr$ (assuming, for the moment, that the material is massless)

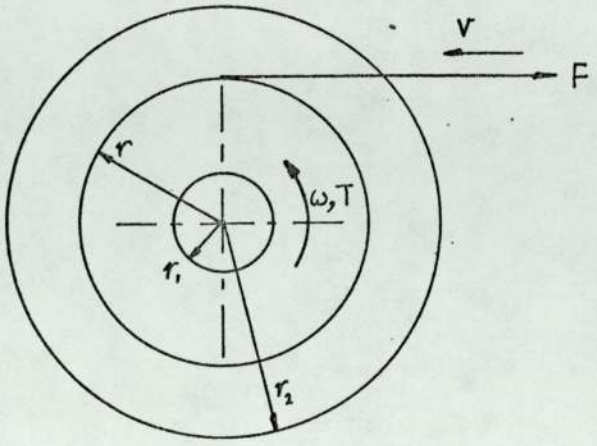

Fig. 2.12 Centre Driven Winder

The power required is,

$$Fv = T\omega = \text{constant}$$

whence

$$T\alpha \frac{1}{\omega}$$

i.e. the coupling must transmit maximum torque at minimum output speed (maximum slip).

If that material thickness is b then,

$$\delta r = \frac{bv\delta t}{2\pi r} \qquad (2.12)$$

as $\delta t \to 0$ $\quad \int r dr = \frac{1}{2\pi} \int bv\, dt$

and

$$\frac{r^2}{2} = \frac{bvt}{2\pi} + \text{constant} \qquad (2.13)$$

at $t = 0$ $\quad r = r_1$

$$\therefore \quad r = \sqrt{r_1^2 + \frac{bvt}{\pi}} \tag{2.14}$$

The instantaneous efficiency,

$$\eta = \frac{\omega}{\omega_{in}} = \frac{V}{r\omega_{in}} \propto \frac{1}{r} \tag{2.15}$$

Fig. 2.13 shows how r and $\frac{1}{r}$ vary with time. The radius, torque and power input all vary as the square root of time, and the instantaneous efficiency as the inverse of the square root. It can be seen that the efficiency falls rapidly to a low value.

2.4.3.4.2 Overall Efficiency

The overall efficiency is dependent upon the build up ratio, B, where $B = r_2/r_1$.

The overall efficiency, $\eta_o = \frac{\text{energy output}}{\text{energy input}}$

$$\eta_o = \frac{\int_o^t Fv\,dt}{\omega_{in} \int_o^t Fr\,dt}$$

$$= \frac{\frac{Fv\pi}{bv} \cdot (r_2^2 - r_1^2)}{\frac{\omega_{in} F 2\pi}{bv} \left(\frac{r_2^3}{3} - \frac{r_1^3}{3} \right)}$$

$$= \frac{3}{2} \cdot \frac{V}{\omega_{in}} \cdot \left(\frac{r_2^2 - r_1^2}{r_2^3 - r_1^3} \right)$$

$$= \frac{3}{2} \frac{V_{in}}{\omega_{in} r_1} \cdot \left(\frac{B^2-1}{B^3-1}\right)$$

i.e. $\eta_o = 3/2$. Maximum Efficiency. $\left(\frac{B^2-1}{B^3-1}\right)$ (2.16)

The relationship between overall efficiency and build up ratio is shown in Fig. 2.14. It can be seen that for B=10, which is not uncommon, the overall efficiency will be as low as 15% of the maximum drive efficiency.

2.4.3.4.3 Inertia Effects

The foregoing analysis did not take the mass of the coil into account. This manifests itself as the angular momentum of the coil.

$$\text{Moment of Inertia, } J = \int_o^r 2\pi r \gamma r^2 dr$$

where γ is the density of the material being coiled. For simplicity the spindle is assumed to have the same mass density.

$$\therefore \quad J = 2\pi\gamma\frac{r^4}{4} \text{ per unit width of coil} \qquad (2.17)$$

now Torque = rate of change of angular momentum

$$T = \frac{d}{dt} J\omega$$

$$= \frac{d}{dt} 2\pi\gamma\frac{r^4}{4} \cdot \omega$$

$$= \frac{3}{4} \gamma \, bv^2 r \text{ per unit width} \qquad (2.18)$$

This torque is additional to that required to maintain the tension in the web. As this torque is proportional to the radius of the coil the overall efficiency remains the same.

2.4.3.4.4 Drive Requirements

Compared with the pump drive, the winder is a very severe application for an eddy-current coupling. The low efficiency of the coupling at high slip, is combined with the need to run for the major part of each wind at high torque, to give a low overall efficiency. The coupling must therefore be designed to operate at high dissipation for long periods.

The torque-slip curve of the coupling should be of the rising type where the torque increases in proportion to slip speed, Fig. 2.15. In order to accommodate different film thicknesses a tension range of four to one may be required. This implies that with a ten to one build up ratio, a forty to one torque range will be needed. If control is to be maintained at the low torques, the no-load drag torque of the coupling must be kept small. For instance, a water cooled coupling with a wet airgap might well not be suitable.

2.4.3.4.5 Control Requirement

The control system for a winder drive must endeavour to keep both tension and line speed constant. Various control schemes have been devised to achieve this constant power criterion. In general, the more delicate is the

material being handled, the more complex is the control system.

The constant tension requirement is sometimes modified so that tension is gradually reduced as the coil diameter increases. This is necessary to prevent damage being done to the inner layers of the coil.

3. FACTORS AFFECTING OPTIMAL PERFORMANCE

3.1 CATEGORISATION OF FACTORS

Having decided in the preceding chapter the parameters which comprise the performance of a machine, it is now necessary to identify the factors which affect them. When these factors are known and quantified their importance in the optimality of a machine can be found.

For convenience, these factors are divided into three areas,

(i) Mechanical Factors

(ii) Electromagnetic Factors

(iii) Thermal Factors

3.2 MECHANICAL FACTORS

3.2.1 Arrangements

The mechanical design of eddy-current machines is concerned with the strength and arrangement of the component parts. The coupling has two independent rotating members to be accommodated, whereas the dynamometer and brake have only one. By considering coupling construction, that of the other machines is implicitly covered, so it is only necessary to investigate couplings.

The eddy-current coupling, in its simplest form, consists of two members separated by a short airgap. This airgap, which may be radial (drum machines) or axial (disc machines) permits relative motion between field and loss members.

3.2.2 Axial Airgap

The primitive disc machine, Fig. 3.1, consists of a rotor and loss member affixed to separate collinear shafts, each supported by two widely spaced bearings. One of the bearings may be placed between the two members, Fig. 3.2, enabling a shorter machine to be constructed.

3.2.3 Radial Airgap

Rather more possibilities exist for the construction of the drum coupling. The simplest machine, Fig. 3.3, has one member mounted inside the other, both rotating on separate shafts. Again one of the bearings can be placed between the shafts to shorten the overall length, Fig. 3.4.

Another approach is to use a shaft running the entire length of the machine. One of the members is mounted directly onto this shaft, whilst the other is on a quill shaft, Fig. 3.5. In all these forms the outer member is cantilevered from one end. This construction becomes unsatisfactory at large diameters (>0.5m) and so a doubly supported form is used, Fig. 3.6.

3.2.4 Choice of Driving and Driven Member

Thus far, it has not been said which members is input or output, nor which is the rotor or loss member. For the disc machine only, two choices exist; rotor input and disc loss member output, and vice versa. The drum machine, however, has a further option, which member should be inside

which. Again two possibilities exist, rotor mounted inside drum and vice versa.

The choice of a particular arrangement influences the performance in several respects. The principal effects lie in the areas of

Magnetic Pull Forces	(Section 3.3.12)
Temperature Effects	(Section 3.4)
End Effects	(Section 3.5.2)

Where necessary specific mention will be made of any differences due to type of construction.

3.3 ELECTROMAGNETIC FACTORS

3.3.1 Components

The active or torque transmitting components are the rotor and its excitation coil, and the loss member. Several alternative types of each are available, the choice depending upon the desired performance.

3.3.2 Rotors

Although both members rotate in an eddy-current coupling, it is conventional to apply the term rotor to the one which produces a varying flux density pattern around the airgap. Two classes of rotor exist; the homopolar type, where the polarity remains the same, and the flux density varies, and the heteropolar type where the polarity alternates around the rotor. The homopolar type is commonly referred to as the 'inductor' type, Fig. 3.7.

3.3.3 The Inductor Rotor

3.3.3.1 Description

It can be seen (Fig. 3.7) that the inductor rotor has a series of slots cut into the active face. These slots modulate the performance of the airgap to produce a varying flux density wave from a steady applied magneto-motive force (m.m.f.). The flux density wave in the airgap of an eddy-current machine can be represented by a rectangular wave under standstill conditions. Fourier analysis of this wave resolves it into a steady component and a series of harmonics. It is these harmonics, particularly the fundamental, which generate eddy currents in theloss member, and hence provide torque transmission. The steady component of flux density serves no useful purpose, it merely reduces the flux carrying capacity of the magnetic circuit.

3.3.3.2 Fourier Series with Infinitely Deep Slots

If it is assumed that:

(a) there are infinitely deep slots

(b) the iron is uniformly permeable

(c) there is no flux fringing, and

(d) cartesian co-ordinates may be employed for the airgap region,

then the flux density wave appears thus, Fig.3.8 (p45).

The Fourier series for this wave is

$$B(\theta) = B_o \left| \kappa' + \frac{2}{\pi} \sum_{n=1}^{\infty} \frac{1}{n} \sin n\pi\kappa' \cos n\theta \right| \qquad (3.1)$$

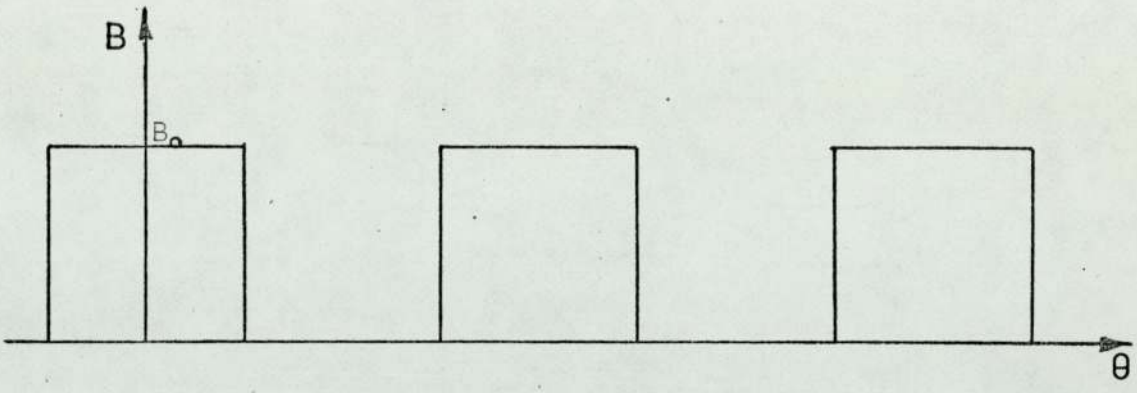

Fig. 3.8

where κ' is the tooth width/tooth pitch ratio.

Integrating the fundamental component over one half tooth pitch gives the fundamental flux per pole,

$$\phi_{ac} = B_o \int_{-\pi/2}^{\pi/2} \frac{2}{\pi} \sin\kappa'\pi \cos\theta \, d\theta$$

$$= \frac{4B_o}{\pi} \sin\kappa'\pi \quad \text{per unit area} \qquad (3.2)$$

and the total flux per pole pair is,

$$\phi_t = 2B_o\kappa'\pi \quad \text{per unit area} \qquad (3.3)$$

ϕ_{ac} and ϕ_t have been evaluated with respect to κ' and plotted in Fig. 3.9(a).

At this point is is useful to introduce a flux utilisation coefficient, ε, which is a measure of the effectiveness of the rotor in producing useful flux,

$$\varepsilon = \frac{\phi_{ac}}{\phi_t} \quad , \text{ (Fig 3.9(b))} \qquad (3.4)$$

3.3.3.3 Finite Depth Slots

Real rotors, however, do not have infinitely deep slots and so some account must be taken of the slot flux, see Fig. 3.10.

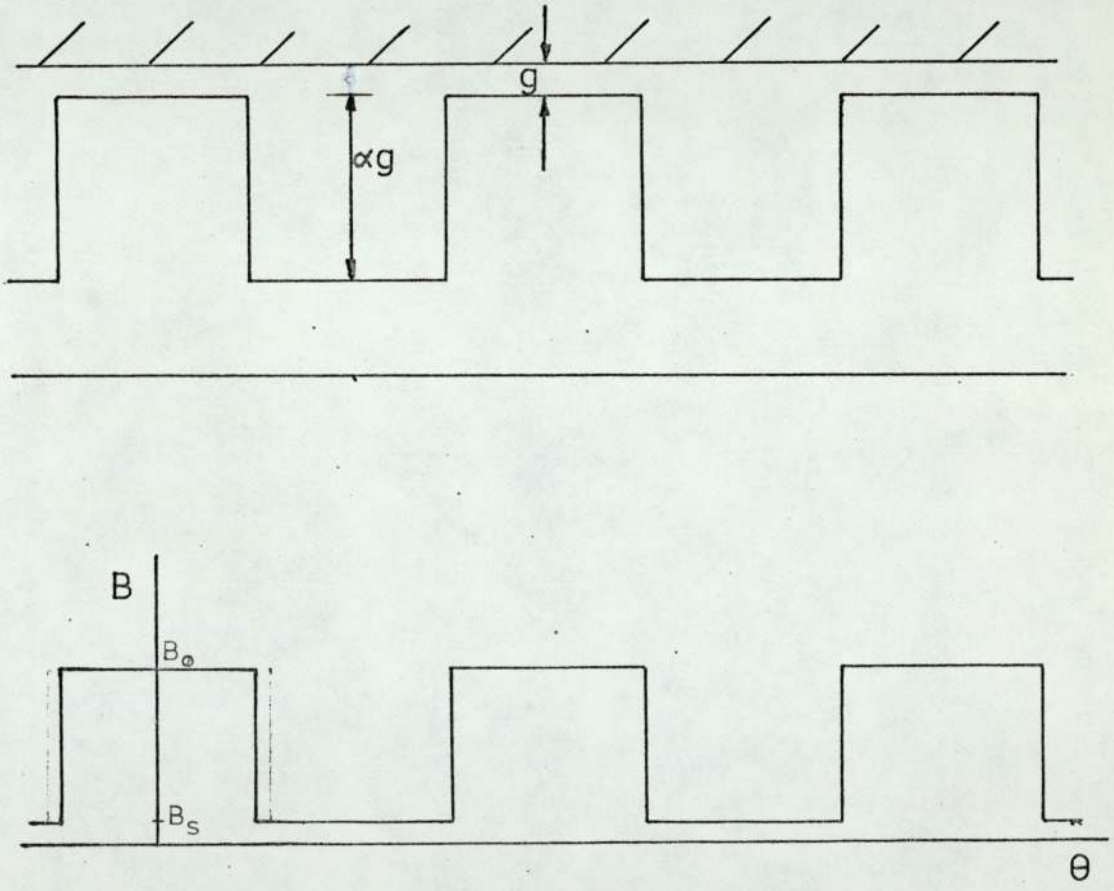

Fig. 3.10 Finite Slots

Here the airgap permeance, and hence the flux density, is taken to vary as the inverse of the airgap length.

$$\text{i.e.} \quad B_o = \mu_o \frac{F}{g} \quad \text{over a tooth}$$

$$B_s = \mu_o \frac{F}{\alpha g} \quad \text{over a slot}$$

where F is the airgap m.m.f., A

g is the airgap length, m

and α is the ratio of slot depth to airgap length.

The Fourier series then becomes

$$B(\theta) = (B_o - B_s) \left| \kappa' + \frac{2}{\pi} \sum_{n=1}^{\infty} \frac{1}{n} \sin n\pi\kappa' \cos n\theta \right| + B_s$$

$$= B_o \left(\frac{\alpha-1}{\alpha}\right) \cdot \left| \kappa' + \frac{2}{\pi} \sum_{n=1}^{\infty} \frac{1}{n} \sin n\pi\kappa' \cos n\theta \right| + B_o/\alpha \qquad (3.5)$$

Integrating the fundamental flux as before,

$$\phi_{ac} = B_o \left(\frac{\alpha-1}{\alpha}\right) \frac{4}{\pi} \sin\kappa'\pi \qquad (3.6)$$

and the total flux,

$$\phi_{t} = 2B_o \left(\frac{\alpha-1}{\alpha}\right) \kappa'\pi + \frac{4B_o\pi}{\alpha} \qquad (3.7)$$

3.3.3.4 Fringing Flux

As a further refinement the effect of fringing can be taken into account. Here the magnetic width of the slot will

appear less than the actual width.

Effective slot width = real slot width $(1-\delta)$

where δ is Carters coefficient.

This means that κ' is increased,

$$\kappa'' = \kappa' + (1-\kappa')\delta \qquad (3.8)$$

A useful approximation due to Baillie[32] is,

$$\delta \simeq \frac{5}{5+w_s/g} = \frac{5}{5+\beta}$$

where $\beta = \frac{\text{slot width}}{\text{airgap}}$

For most machines $\beta > 50$ and the effect upon ε is slight

viz: $\varepsilon \propto \beta^{1/5}$ (3.9)

3.3.3.5 Alternative Flux Utilisation Coefficient

It is interesting to note that ε is similar to that given by Gibbs.

He defines

$$\varepsilon_g = \frac{\phi_t - \phi_s}{\phi_t + \phi_s} \qquad (3.10)$$

where ϕ_t = tooth flux, i.e. the flux emanating from $\pm \lambda/4$ of the tooth centre line and

ϕ_s = slot flux

This expression implies that the useful flux is given by

$$\phi_{ac} = \phi_t - \phi_s \qquad (3.11)$$

This is indeed correct for a fundamental flux density wave

superimposed on a steady flux density. It is not however true if applied to the rectangular flux density wave of Fig. 3.10. Both flux utilisation coefficients have been evaluated using the rectangular wave assumption, and plotted in Fig. 3.11. It can be seen that whilst the two give broadly similar results, discrepancies exist near the maximum value of ε, i.e. $0.4 < \kappa' < 0.6$, when $\alpha = 15$.

3.3.3.6 Optimum κ'

It is important to draw a distinction between the best utilisation of the total magnetic flux and the maximum nett useful flux. Under ideal circumstances the latter criterion is better for judging rotor performance. Real machines, however, suffer from saturation of the magnetic circuit and so it is better to maximise ε.

In practice, since the maximum fundamental flux occurs at $\kappa' = 0.5$, and the maximum ε at $\kappa' < 0.5$, the tooth width-tooth pitch ratio is usually chosen to be about 0.45.

3.3.4 Heteropolar Rotors

The characteristic of a heteropolar rotor is that the direction of the m.m.f. is reversed between adjacent poles. This means that there is no steady flux component, and consequently much better use is made of the available flux.

3.3.5 The Distributed Winding Rotor

The distributed winding rotor[27] is similar to a d.c. machine armature. The conductors are embedded in slots in

the rotor surface, and current is passed through them via sliding contacts. By suitable connection of the windings, a series of alternating poles can be produced around the airgap. The triangular m.m.f. wave, Fig. 3.12, produced by this rotor contains a large fundamental component.

If the conductors are approximated to a uniform current sheet on the surface of the rotor and saturation effects are ignored then the flux density becomes

$$B(\theta) = B_o \frac{8}{\pi^2} \sum_{n=1}^{\infty} (-1)^{n+1} \frac{\sin(2n-1)\theta}{(2n-1)^2} \qquad (3.12)$$

where B_o = peak flux density

and as before

$$\phi_{ac} = B_o \int_o^{\pi} \frac{8}{\pi^2} \sin\theta d\theta = \frac{16}{\pi^2} B_o \text{ per pole} \qquad (3.13)$$

$$\phi_t = B_o \pi \text{ per pole pair.} \qquad (3.14)$$

and therefore

$$\varepsilon = 1.03$$

The large amount of useful flux combined with the lack of saliency, which means that armature reaction m.m.f. is more effective, make this rotor likely to be highly effective. Nevertheless, the high cost of manufacture and impossibility of brushless operation preclude its adoption in commercial machines.

3.3.6 The Salient Pole Rotor

3.3.6.1 Flux Density Wave Analysis

With a salient pole rotor, Fig. 3.13, the excitation

windings are concentrated in single slots between the poles. Large diameter rotors tend to employ individual bobbin coils, whereas small rotors may use a serpentine coil.

The flux density wave produced by these rotors may be approximated by a chorded square wave, Fig. 3.14.

Using the same idealising assumptions as for the inductor rotor the Fourier series is,

$$B(\theta) = \frac{4B_o}{n\pi} \sum_{n=1,3}^{\infty} \sin n\kappa\frac{\pi}{2} \cdot \sin n\theta \qquad (3.15)$$

where $$\kappa = \frac{\text{pole arc}}{\text{pole pitch}}$$

and so,

$$\phi_{ac} = \frac{8B_o}{\pi} \sin \frac{\kappa\pi}{2} \quad \text{per pole} \qquad (3.16)$$

$$\phi_t = 2B_o\kappa\pi \quad \text{per pole pair} \qquad (3.17)$$

$$\therefore \quad \varepsilon = \frac{4}{\pi^2} \frac{\sin\kappa\pi/2}{\kappa} \qquad (3.18)$$

These quantities are shown graphically in Fig. 3.15 where it can be seen that under ideal conditions ε is maximised as κ tends to zero. In a conflicting manner ϕ_{ac} increases with increasing κ.

3.3.6.2 Optimum κ

Like the inductor rotor, a balance must be obtained between maximum useful flux and maximum flux utilisation. There are, however, two additional factors to be taken into

account. These are the pole to pole leakage flux and the apportionment of copper and iron space.

It is shown in Section 3.3.11.2 that leakage flux begins to increase rapidly at values of κ in excess of 0.7. Whilst leakage flux does not diminish the airgap flux directly, its presence does serve to reduce the available m.m.f. at the airgap if the iron is saturated. According to Section 3.3.11.2, the proportion of leakage to active flux is substantially constant from $\kappa = 0.2$ to 0.8.

The other additional factor, the need to provide space for the excitation windings, also points to a value of $\kappa = 0.7$ as being optimum. The extra m.m.f. obtainable by increasing the coil size is lost in the increased reluctance of the poles.

As a result of all these considerations a value of $\kappa = 0.7$ is usually chosen for salient pole rotors.

3.3.7 The Lundell Rotor

3.3.7.1 Introduction

The Lundell rotor, also known as the interdigitated or imbricated type, is shown in Fig. 3.16. It can be seen that it consists of two sets of claws of opposite polarity which are meshed together to provide a heteropolar m.m.f. wave. Excitation is furnished by an annular coil which may be mounted between the two end plates, or remotely, in which case the flux is directed to the rotor through

extra airgaps, Fig. 3.39. The constructional simplicity and cheapness of this rotor make it a popular choice despite its performance being limited by long and tortuous flux paths.

3.3.7.2 Tapered Poles

The Lundell rotor gives rise to a similar airgap flux density wave to that from a salient pole rotor. The main deficiency of the Lundell rotor is the difficulty of obtaining a uniform flux density along the pole face. It is inevitable in the construction of the rotor that the pole face area will be greater than the cross-sectional area of the pole neck. One expedient commonly adopted to ameliorate this deficiency is to taper the pole faces such that they have a trapezoidal shape. If it is assumed that this does indeed achieve a uniform flux density it also causes unbalanced m.m.f. waves at each end. This unbalanced wave, Fig. 3.17, gives a reduced fundamental flux component. The Fourier fundamental for a waveform of this nature is,

$$B_1(\theta) = \frac{2B}{\pi} \left| \sin\psi\frac{\pi}{2} + \sin(2\kappa-\psi)\frac{\pi}{2} \right| \sin\theta, \qquad (3.19)$$

and

$$\phi_{ac} = \frac{8B}{\pi} \sin\kappa\frac{\pi}{2} \cos(\kappa-\psi)\frac{\pi}{2} \qquad (3.20)$$

The situation exists at the ends of the active region of the rotor. It is not unreasonable to assume that the average fundamental flux can be represented by the mean of three regions, the two ends and the middle where the usual

symmetrical chorded rectangular wave applies.

$$\text{i.e} \quad \phi_{ac} = \frac{8B}{\pi} \sin \frac{\kappa\pi}{2} \left(\frac{1+2\cos(\kappa-\psi)\frac{\pi}{2}}{3} \right) \qquad (3.21)$$

where ψ is the taper factor (see Fig. 3.18)

This function is evaluated and tabulated for $\kappa=0.7$ in Fig. 3.19. It can be seen that the torque ($\alpha\phi_{ac}^{3}$) will be reduced by 10% when $\psi = 0.9$. In most machines this signifies a taper angle of around 10^{o}. Tapers greater than this would be unacceptable. A balance must be obtained between the enhancement of the axial flux density distribution and the reduction of fundamental flux.

3.3.7.3 Pole Shape

Another way in which the pole shape is varied results from the attempt to make most use of rotor length. Some common pole shapes are depicted in Fig.3.20. The first, Fig.3.20a gives a uniform flux density at the expense of active length. Extending the length of the pole, Figs. 3.20b and (c), creates problems with achieving uniform flux density distribution and gives rise to saturation in the neck of the pole. Section 3.3.9 deals with a method of estimating the effectiveness of elongating the pole face.

3.3.8 The Partially Interdigitated Rotor

3.3.8.1 Description

As implied by the name, this type of rotor comprises similar claws to the Lundell type, but only partly enmeshed.

This gives rise to the type illustrated in Fig. 3.2.1. Here the end regions give a homopolar flux density pattern, whilst the central region has a heteropolar nature.

A machine employing this type of rotor will have a performance intermediate between an inductor and a Lundell machine.

3.3.8.2 Degree of Interdigitation

A new quantity is needed in order to define a partially interdigitated rotor. This is the degree of interdigitation, q,

where $q = \frac{\text{length of heteropolar zone}}{\text{active length of rotor}}$

This quantity varies from 100% which is a Lundell rotor, to 0% which is an inductor rotor.

The analysis of the m.m.f. pattern with different q is given in the next section on the Evaluation of Different Rotors.

3.3.9 The Evaluation of Different Rotors

3.3.9.1 Method

For a rotor of a given diameter, overall length, pole number etc., it is well known[3] that,

$$Tm \alpha L F_g^2 \qquad (3.22)$$

where T_m is the maximum torque

L is the active length

F_g is the fundamental airgap m.m.f.

for an effectively two-dimensional machine.

If then, F_g varies along the z-axis of the airgap it should be possible to obtain a measure of the various pole shapes by evaluating this function. Suppose that Fg varies thus, Fig. 3.22

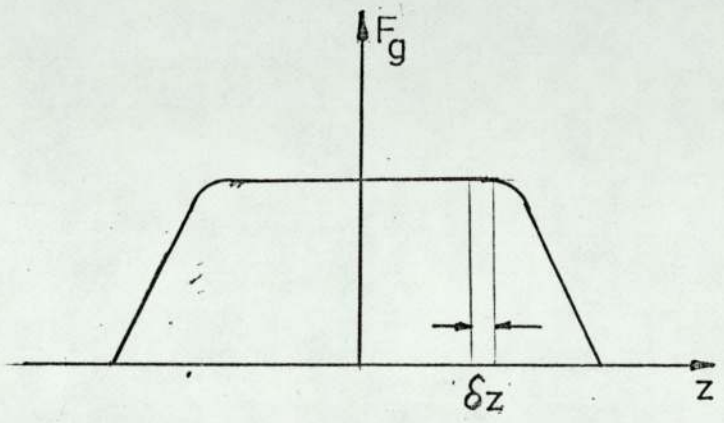

Fig. 3.22 Axial Fundamental m.m.f. Distribution

then the element of torque δT produced by the element of length δz will be

$$\delta T = \kappa |F_g(z)|^2 \delta z \qquad (3.23)$$

if the variation in Fg is not so large as to cause a large difference in n_m, the slip speed at peak torque, then it is not unreasonable to integrate Equation 3.23 to obtain the total peak torque.

$$T = \kappa \int_0^L |F_g(z)|^2 dz$$

$$= k \overline{F_g^2} L \qquad (3.24)$$

where k is a constant

and $\overline{F_g^2}$ is the mean square value of $F_g(z)$.

The magnitude of the fundamental m.m.f. wave at any z is obtained from the peripheral airgap m.m.f. wave in the manner of Section 3.3.3. Since this magnitude depends solely on the change in amplitude of the airgap wave, it is only necessary to know the way in which the wave varies from pole to pole.

In order to determine the relative torque producing ability of different pole shapes, and the effect of partial interdigitation, an assumed m.m.f. distribution must be used. These are depicted in Figs. 3.23 and 3.24. They are derived on the basis of constant m.m.f. over the third of the pole nearest to the neck, dropping linearly to zero at the pole ends. This is a compromise between a constant flux criterion from, say, saturation in the pole neck, and a uniform axial m.m.f. distribution, which would result from the assumption of infinite permeability.

3.3.9.2 Salient Pole Rotor

The active length of this rotor is taken to be two thirds of the overall length to allow for the end turns of the coil. With a peak airgap m.m.f. of F Amperes, the amplitude change is 2F.

$\therefore$ $F_g \propto 2F$

$F_g^2 \propto 4F^2$ over the active length.

$$\therefore \quad Tm = k.\ \frac{2}{3}L.4F^2$$

$$= \frac{8}{3}kLF^2 \qquad (3.25)$$

3.3.9.3 Inductor Rotor

Here the active length is also two thirds of the total. The amplitude change of m.m.f. is only F.

$$F_g \alpha F$$

$$F_g^2 \alpha F^2$$

$$Tm = \frac{2}{3}kLF^2 \qquad (3.26)$$

i.e. one quarter of that given by the salient pole rotor.

3.3.9.4 Lundell and Partially Interdigitated Rotors

With this type of rotor a value for the mean of the square of the fundamental m.m.f. is obtained in a piecewise manner from Figs. 3.23 and 3.24. This is then multiplied by the active length of the rotor, which is the same for all, to obtain the relative peak torques.

The relative slip speeds for peak torque may be obtained from the inverse of the mean fundamental m.m.f. Although these values will be approximate, they do indicate the general trend.

Table 3.1 summarises the most important results which are also plotted in Fig. 3.25.

TABLE 3.1

	Torque p.u.	$\frac{n_m}{n_{m\,(lundell\ b)}}$
Salient Pole	1.33	0.75
Lundell a	0.67	0.75
Lundell b	1.0	1.0
Lundell c	0.92	1.13
P.I. 66%	0.69	1.3
P.I. 33%	0.50	1.5
P.I. 0%	0.39	1.8
Inductor[1]	0.33	2.25

[1]Note that this rotor is not optimal as $\kappa' \simeq 0.35$

3.3.9.5 Discussion

Table 3.1 shows that under the assumptions made, the salient pole rotor gives most torque at smallest slip, and the inductor least torque at highest slip. This accords well with results obtained in practice. It also shows that the peak torque of a partially interdigitated rotor drops as the degree of interdigitation is reduced, which is as expected.

The most interesting result is that for the Lundell rotor, which means that the elongated pole of Fig. 3.20(b) is best.

A more realistic assessment of rotor performance

could be made, along with an investigation of the effects of varying radial pole depth, by the use of conducting paper analogues.

3.3.10 Excitation Power

3.3.10.1 Introduction

Power is dissipated in the excitation windings when current flows to produce the airgap m.m.f. Although this power is small it is not insignificant as it determines the size of the control equipment and the temperature rise of the coil.

3.3.10.2 The Excitation Coil

Consider a coil of wire wound in the form of an annulus. It may be specified by the following:

MLT - mean length of turn, m

N - number of turns,

A - overall cross-sectional area, m^2

a - cross-sectional area of a conductor, m^2

ρ - resistivity of the conductors, Ωm

F - m.m.f. produced, A

J - current density A/m^2

The resistance, R, of such a coil is,

$$R = \frac{N \times MLT \times \rho}{a}$$

To produce a given m.m.f., the current flowing must be

$$I = \frac{F}{N}$$

and so the power loss must be,

$$P_c = I^2R = \frac{F^2}{N^2} \cdot \frac{N \times MLT \times \rho}{a}$$

$$= \frac{F^2 \times MLT \times \rho}{Na} \qquad (3.27)$$

Na, the actual cross sectional area of all the conductors, is substantially constant for a given type of conductor. The power loss is then also constant for a coil producing a constant m.m.f.

The area occupied by a coil is given by,

$$\text{Area} = \frac{F}{J \times \text{packing factor}} \qquad (3.28)$$

The necessity for introducing a packing factor arises because the interturn insulation and the interstices between conductors reduce the area available for conduction. Typically, round section wires have a packing factor of about 0.6 and strip conductors about 0.9.

3.3.10.3 Salient Pole Windings

The windings of a salient pole rotor run in slots between the poles, each pole has the area of one adjacent slot for the winding associated with it.

$$\text{Slot Area} = \frac{\pi D^2}{4} \cdot \frac{1}{2p} \cdot (1-\kappa) \times \text{a constant} \qquad (3.29)$$

The constant in this expression depends upon the amount by which the pole shoes are undercut and the core diameter of the rotor. A value of around 0.5 is common for rotors

where $D \simeq 0.2m$.

If the airgap, g, is 0.3 mm

the diameter, D is 200 mm

the number of pole pairs, p, is 6

then the coil area will be

$$A_c \simeq 2.6 \times 10^{-3}(1-\kappa) \times 0.5 \quad m^2$$

The m.m.f. required to produce a flux density of 1.2T (the maximum normally achieved in eddy-current machines) is

$$F = \frac{1.2}{\mu_o} \times 0.3 \times 10^{-3} = 286A$$

If the current density in the conductors is restricted to no more than $4.65A/mm^2$ then the total conductor area must be

$$A_{cn} = \frac{286}{4.65} \simeq 61.5 \text{ mm}^2$$

allowing for imperfect filling of the slot means that for round wires an area of at least $\frac{61.5}{0.6} = 103 \text{ mm}^2$ is required. This would be sufficient if the iron were infinitely permeable and no m.m.f. were required to force the flux through the magnetic circuit. Practically, this is not so, about three times the m.m.f. being needed to overcome the iron reluctance. Usually this is so when $\kappa = 0.7$, being the accepted optimum for a salient pole rotor.

As machines become larger, cooling problems predominate and so fewer poles may be employed. This results in lower torques and hence lower heat losses, and also relieves the pressure on coil space.

3.3.10.4 Excitation Power

If the rotor is taken to be 65 mm long the mean length of turn will be about 230 mm, and hence the power dissipated will be

P_c = 9.7 watts per pole

∴ Total power for the whole rotor = 9.7 x 12 = 116 W.

3.3.10.5 Lundell and PI Rotors

The marked difference in this class of rotors is that the coil space is unaffected by the number of poles or the pole arc-pole pitch ratio.

A rotor of similar overall dimensions to that of Section 3.3.10.3 having a coil generating the same m.m.f. consumes only 19 watts, regardless of pole number. This is a great advantage over the salient pole rotor, the ability to have a large number of poles at low excitation power.

3.3.11 Magnetic Leakage

3.3.11.1 Introduction

As a result of the proximity of the poles to one another in an eddy-current machine, substantial leakage of magnetic flux can occur. Whilst this does not directly affect performance, it does impose an extra burden upon the magnetic circuit. Increased m.m.f. losses owing to saturation will occur if leakage fluxes reach an appreciable proportion of the total flux.

A useful method for estimating the magnitude of the leakage flux is that due to Pohl[33]. He originally applied this procedure to salient pole rotors but it can be readily applied to Lundell rotors.

3.3.11.2 Pohl's Method for Salient Poles

Referring to Fig. 3.26, there are four leakage paths to be considered,

(1) Pole shoe side leakage

(2) pole side leakage

(3) pole shoe flank leakage

(4) pole flank leakage

and the main flux path 5.

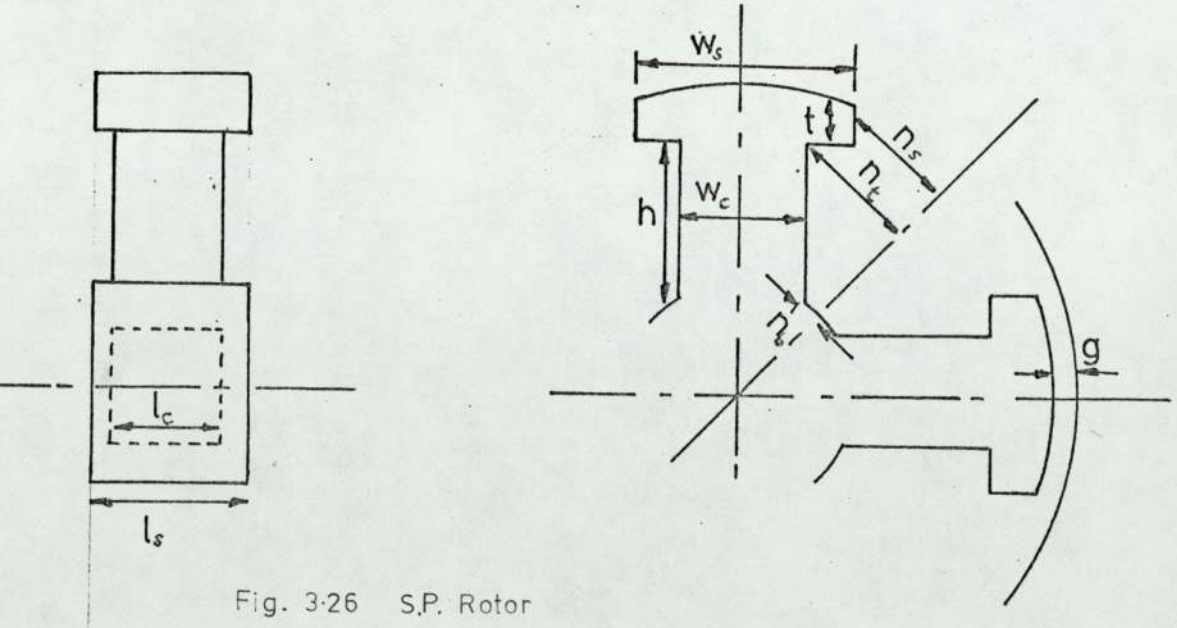

Fig. 3.26 S.P. Rotor

Pohl obtained expressions for the leakage permeance of each of these paths. When re-arranged into the symbols used in this thesis they are:

(i) Pole shoe side leakage permeance,

$$\Lambda_1 = 4\frac{\mu_o \cdot \ell_s (t+g)}{(1-\kappa)\lambda} \qquad (3.30)$$

(ii) Pole shoe flank leakage permeance,

$$\Lambda_2 = \frac{8}{\pi}\,\mu_o (t+g)\left|\log_e\left(1+\frac{\pi}{2}\,\frac{\kappa}{(1-\kappa)}\right)\right| \qquad (3.31)$$

(iii) Pole side leakage permeance

$$\Lambda_3 = \mu_o h\,\frac{\ell_c}{n_c}\left|\frac{\delta+1}{\delta-1}\left(1-\frac{\log_e \delta}{\delta-1}\right)\right| \qquad (3.32)$$

where $\delta = \dfrac{n_t}{n_b}$

(iv) Pole flank leakage permeance

$$\Lambda_4 = \mu_o\,\frac{4}{\pi}\,h\,A\log_e\left(1+\frac{\pi}{4}\,\frac{w_c}{n_c}\right) \qquad (3.33)$$

where $A = \dfrac{\delta+1}{\delta-1}\left(1-\dfrac{\log_e \delta}{\delta-1}\right)$

Using these equations to calculate the leakage fluxes, a set of results was obtained for a 150 mm diameter, six pole pair rotor. These are plotted in Fig. 3.27, along with the ratio of leakage flux to leakage flux plus airgap

flux. The leakage flux itself increases steadily as κ increases. The proportion of leakage flux, however, reaches a minimum around $\kappa = 0.5$ and is substantially constant for $0.2 < \kappa < 0.8$.

Recalling what was said in Section 3.3.6.2 about the apportionment of copper and iron space, it is clear that best use of the rotor is made when κ is around 0.7. Here the proportion of useful flux to total flux is approaching a maximum.

3.3.11.3 Lundell Poles

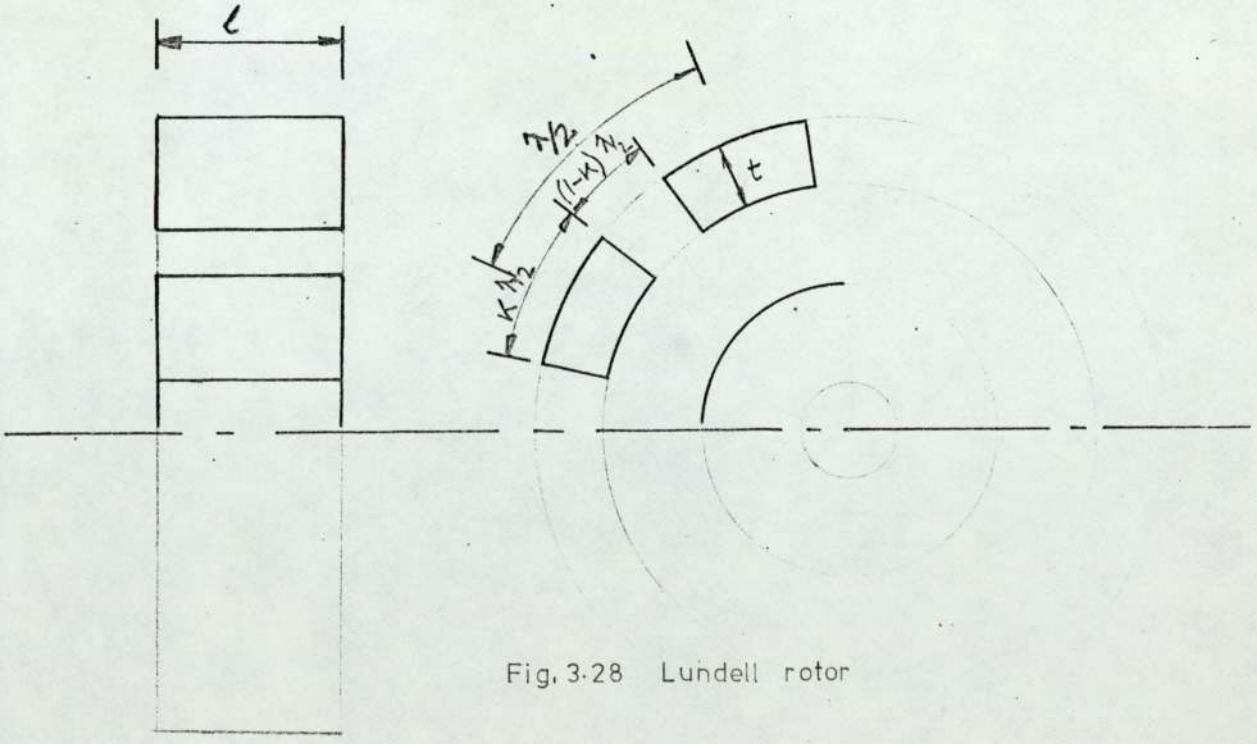

Fig. 3.28 Lundell rotor

The pole side leakage permeance is given by

$$\Lambda_1 = \frac{2\mu_o t \ell}{(1-\kappa)\frac{\lambda}{4}} \quad \text{per pole} \tag{3.34}$$

The pole back leakage is obtained by considering an assumed flux path thus, Fig. 3·29 ,

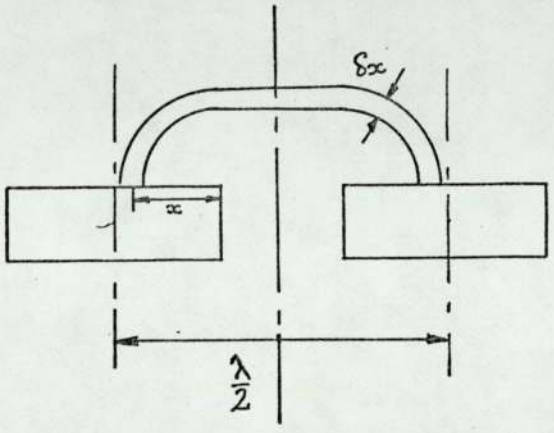

Fig. 3·29

The permeance of the path at x is

$$\Delta\Lambda = \frac{\mu_o \ell \, dx}{\frac{\pi x}{2} + (1-\kappa)\frac{\lambda}{4}}$$

which upon integration gives

$$\Lambda_2 = \frac{4}{\pi}\mu_o \ell \, \log_e\left(1 + \frac{\pi\kappa}{2(1-\kappa)}\right) \tag{3.35}$$

If desired, the permeances of other paths may be obtained in a similar fashion to improve the accuracy of the estimate.

The airgap permeance is approximately given by,

$$\Lambda g = \mu_o \frac{\kappa}{g} \frac{\lambda}{2} \ell \text{ per pole} \qquad (3.36)$$

By calculating the magnetic flux traversing the airgap, and the leakage flux for varying κ, the curve, Fig. 3.30, was obtained. A very similar shape to that for salient poles indicates that $\kappa = 0.7$ is optimum for this type of rotor also. Under these conditions, for similar rotors, the leakage flux is twice as large for the Lundell rotor as it is for the salient pole type.

3.3.11.4 The Effects of Magnetic Saturation on Leakage Flux

The results obtained in the foregoing section were derived on the basis of infinite permeability of the iron. Under conditions of low flux density this is reasonable. When, however, the material of the magnetic circuit is required to sustain high flux densities, the relative permeability drops to a low value. Further magnetisation, caused by increasing the excitation coil m.m.f., will thus take place as if the whole rotor were made of air. The proportion of leakage to useful flux then increases as the rotor iron becomes more saturated.

3.3.11.5 The Variation of Leakage Flux with Size

Consider the two leakage permeances obtained for the Lundell rotor, equations 3.34 and 3.35. The first is a function of the pole wavelength whereas the second is not.

This may be at first surprising. When, however, it is realised that the area and length of the pole back leakage both increase with wavelength, the constancy of Λ_{L2} can be appreciated.

For constant κ,

$$\Lambda_{L1} \alpha t\ell$$

$$\Lambda_{L2} \alpha \ell$$

In section 3.5 it is shown that t and l are likely to be proportional to diameter and that λ will be approximately constant in a range of similar machines.

$$\Lambda_{L1} \alpha D^2$$

$$\Lambda_{L2} \alpha D$$

Under these conditions the airgap permeance of a pole will remain nearly constant. Therefore, as the size of the rotor is increased the leakage flux will increase faster than the airgap flux.

3.3.12 Magnetic Forces

3.3.12.1 Unbalanced Magnetic Pull

This force arises from a difference in flux density within the machine. In a disc machine the force will occur as an axial thrust tending to shorten the airgap, or as a radial force in drum machines. Their effect is to increase the load on the bearings and so they must be allowed for at the design stage.

In the drum machine the radial force tends to cancel out owing to an equal force diametrically opposed. Anisotropy of the material in the magnetic circuit or eccentricity of the airgap gives rise to an unbalanced force. Since both of these effects will exist to some extent in a real machine the stiffness of the shafts, etc., must be increased.

An axial thrust is inherent in a single disc machine as depicted in Fig. 3.1. The force can be largely cancelled by arranging either for a purely axial flux through the disc or for the use of another disc to provide an equal and opposite thrust.

3.3.12.2 Unbalanced Magnetic Force Caused by Eccentricity of the Airgap

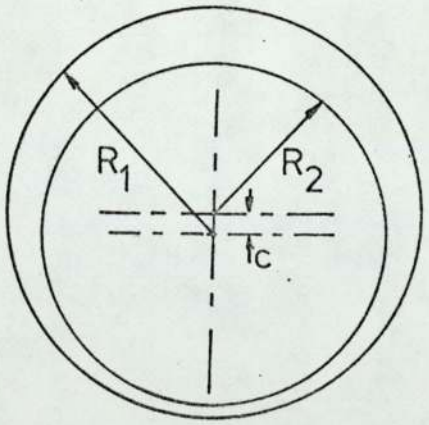

Fig. 3.31 Eccentric Radial Airgap

If the distance between the centres is c

the drum radius is R_1

the rotor radius is R_2

the nominal airgap is $g_o = R_1 - R_2$

it can be shown[24] that the airgap length at angle θ is

$$g \simeq g_o + c \cos\theta \tag{3.36}$$

when $R_1 \simeq R_2 >> g_o$

Assuming a constant m.m.f. across the airgap the radial force per unit area at angle θ can be shown to be

$$\frac{P_r}{A} = \frac{1}{2} \mu_o \frac{F^2}{g^2} \tag{3.37}$$

The radial force acting on an element $d\theta$ at radius r is

$$P_r(\theta) = \frac{1}{2} \mu_o \frac{F^2 L_a r}{(g_o + c \cos\theta)^2} d\theta \tag{3.38}$$

by integrating the vertical component of this force around the airgap, the net force acting on rotor and drum can be obtained,

$$P_{net} = \int_o^{2\pi} \frac{1}{2} \mu_o \frac{F^2 L_a r \cos\theta}{(g_o + c \cos\theta)^2} d\theta$$

The CRC Handbook of Tables for Mathematics[25] gives the following for the result of such an integration

$$\int \frac{\cos\theta}{(g_o + c\cos\theta)^2} d\theta = \frac{\sin\theta}{(g_o^2 - c^2)(g_o + c \cos\theta)} +$$

$$- \frac{c}{(g_o^2 - c^2)} \int \frac{d\theta}{g_o + c\cos\theta} \qquad (3.39)$$

+ constant

Using equation 3.39 the final result for the force is

$$P_{net} = \frac{\mu_o L_a r F^2 c\pi}{(g_o^2 - c^2)^{3/2}} \qquad (3.40)$$

Owing to symmetry the horizontal components cancel.

This result applies to a smooth airgap, the effects of saliency may be accounted for by multiplying equation 3.40 by κ, the pole arc-pole pitch ratio.

It is interesting to compare this result with that given by Miles Walker[26]. He obtains an expression for the force along a diameter, makes an approximation valid at small eccentricities and integrates around the airgap. The result given by him, converted into SI units is,

$$\text{Force per unit area} = \frac{\mu_o F^2 c}{2 g_o^3} \qquad (3.41)$$

which is the same as equation 3.40 if $c^2 << g_o^2$.

This force will be stationary in space if the eccentricity results from misalignment of the shafts carrying the drum and rotor. These components will be subject to a force rotating at their speed of rotation. If, however, the force arises from poor machining of one of the components relative to its centre, the unbalanced force will rotate in space at the speed of the defective member. The other member

will thus experience a force rotating at slip speed.

If an eccentricity, e, is defined where,

$$e = \frac{c}{g_o} \tag{3.42}$$

it will vary between zero and unity.

From equation 3.40 all other factors being constant

$$F_{net} \alpha \frac{c}{(g_o^2 - c^2)^{3/2}}$$

$$\alpha \frac{e}{(1-e^2)^{3/2}} \tag{3.43}$$

The variation of this force with eccentricity is plotted in Fig. 3.32. Since the restoring force applied by the bending of the shaft is likely to vary directly as the deflection, c, it can be seen that this is a metastable condition. If the eccentricity exceeds a certain value it will continue to increase until rotor and drum touch. This cannot be permitted to happen in an eddy current machine, so eccentricities in excess of about 0.3 must be prevented from occurring.

3.3.12.3 Saturation Effects

This is one instance when the existence of magnetic saturation has a favourable influence. The onset of magnetic saturation will tend to limit the magnetic force, as the flux density in the airgap will not normally rise above 1.5T.

3.3.13 Brushless Machines

3.3.13.1 Parasitic Airgaps

The simple machine Figs 3.33 and 3.34, utilises sliding electrical contacts in the form of sliprings and brushes to conduct the excitation current to the rotating field coil. If it is desired to eliminate the possible unreliability and the need to maintain these components, they can be replaced by sliding magnetic contacts. This is achieved by inserting two parasitic airgaps in the magnetic circuit between a stationary field coil and the pole structure of the rotor. In this way rotation of the poles is allowed whilst excitation is furnished from a stationary coil.

Parasitic airgaps may be created in several ways, Figs. 3.37 to 3.41 . Although these methods all remove the need for brushes and sliprings, certain penalties are incurred owing to the presence of the parasitic gaps, and the attendant modifications to the structure of the machine necessitated by their presence.

The first and most obvious drawback of this form of construction is the additional reluctance in the magnetic circuit caused by the presence of extra airgaps. It is for this reason that they are frequently termed 'parasitic' in that they detract from the performance of the machine. An appreciable m.m.f. similar to that across the active airgap, has to be generated to drive the magnetic flux across the parasitic gaps. If the excitation coil is not enlarged it

is clear that the total flux in the circuit will be substantially reduced. The amount of the reduction will depend upon the degree of saturation in the magnetic circuit (Section 3.3.13.2).

In order to estimate the effect of the parasitic airgaps it is useful to resort to an electrical analogue of the magnetic circuit. By dividing the machine into discrete elements, mesh or nodal analysis may be carried out. A complete analytical solution is impossible owing to the non-linear nature of the B-H curve of iron. For the purpose of this general investigation, certain assumptions about the state of the iron enables analysis to be accomplished easily.

3.3.13.2 The Effect of Parasitic Airgaps

3.3.13.2.1 Magnetic Circuit Analogue

Considering the basic machine, Fig. 3.33, it is simplest to investigate the effect of separating the pole structure from the coil and core by means of short airgaps, Fig. 3.38. For the moment, the feasibility of this operation is not considered. If this machine is regarded as the simplest form of brushless design, it can be used as the basis from which to evaluate more practical designs.

Ignoring leakage paths, the magnetic circuits of the two types of machine can be represented as shown by Figs. 3.35 and 3.36.

Whilst using this simple analogue it is necessary to

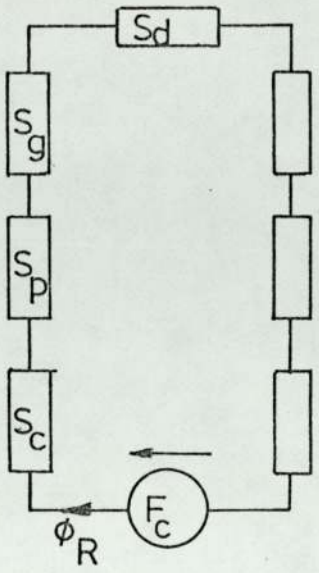

Where S_d - drum reluctance, H^{-1}

S_g - airgap " , H^{-1}

S_p - pole " , H^{-1}

S_c - core " , H^{-1}

F_c - coil m.m.f. " , A

ϕ_R - magnetic flux, Wb

Fig. 3.35 Electrical Analogue of Simple Rotating Coil m/c

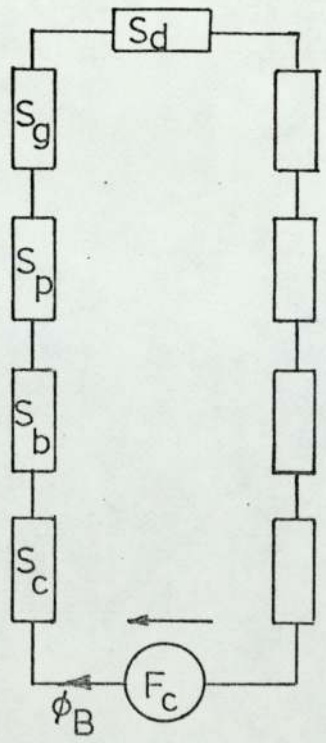

Where S_b - parasitic airgap reluctance, H^{-1}

ϕ_B - magnetic flux, Wb

Fig. 3.36 Electrical Analogue of Simple Brushless Machine

assume that the iron has constant permeability. Then the equation

$$F = S\phi$$

is linear.

It can be seen that for a rotating coil machine, Fig. 3.35,

$$\phi_R = \frac{F}{S_d+2(S_g+S_p+S_c)} \qquad (3.44)$$

and for the brushless machine, Fig. 3.36,

$$\phi_B = \frac{F}{S_d+2(S_g+S_p+S_c+S_b)} \qquad (3.45)$$

If all other parameters of the machine remain constant then a measure of the change in performance is given by the ratio ϕ_B/ϕ_R. This ratio evidently depends upon the relative total circuit reluctances and the degree of saturation of the iron. The two extreme cases are, when,

(a) the iron has infinite permeability

(b) the iron is heavily saturated.

3.3.13.2.2 Infinite Permeability

In this instance,

$$S_d = S_p = S_c = 0$$

and so

$$\frac{B}{R} = \frac{S_g}{S_g+S_b} \qquad (3.46)$$

For manufacturing reasons the airgap length is usually dependent upon its mean diameter. In this example it is assumed that the lengths of active and parasitic gaps are the same. This does not, however, mean that their reluctances are equal, as the parasitic gap is smooth and the active gap is slotted. Assuming that their diameters and active lengths are similar, the flux ratio may be conveniently expressed in terms of Carter's coefficient. This quantity expresses the ratio of the reluctances of smooth and slotted airgap. For two otherwise identical airgaps,

$$K_g' = \frac{S_{slotted}}{S_{smooth}}$$

where K_g' is Carter's coefficient.

For the brushless machine,

$$K_g' = \frac{S_g}{S_b}$$

therefore the flux ratio from equation 3.46

$$\frac{\phi_B}{\phi_R} = \frac{S_g}{S_g+S_g/K_g'} = \frac{1}{1+1/K_g'}$$

$$= \frac{K_g'}{1+K_g'} \qquad (3.47)$$

For a typical Lundell machine, $K_g' \simeq 1.3$ and so $\frac{\phi_B}{\phi_R} \simeq 0.6$.
and a typical inductor machine, $K_g' \simeq 1.9$ and $\frac{\phi_B}{\phi_R} \simeq 0.7$.

It has been shown by Davies[2,3] that torque is approximately proportional to the cube of the flux. The insertion of these parasitic gaps would therefore reduce the torques to about 20% and 30% respectively. The parasitic gaps thus have a considerable effect on the performance of a machine.

3.3.13.2.3 Low Relative Permeability

In order to calculate the reluctances of the magnetic circuit components, certain physical dimensions must be known. Using figures typical of a small (5kW) coupling it can be shown that for a relative permeability of about 150,

$$S_d + 2(S_p + S_c) \simeq 2\, s_g \qquad (3.48)$$

$$\therefore \quad \frac{\phi_B}{\phi_R} = \frac{4Kg'}{4Kg'+2} \qquad (3.49)$$

For a Lundell machine $\frac{\phi_B}{\phi_R} \simeq 0.7 \quad \frac{T_B}{T_R} \simeq 0.4$

for an inductor machine $\frac{\phi_B}{\phi_R} \simeq 0.8 \; \frac{T_R}{T_R} \simeq 0.5$

This shows that the torque reduction is only about 50% owing to the appreciable reluctance of the iron circuit.

The other point to emerge from these considerations is that the inductor machine is less affected by the conversio to brushless operation. This arises from the different pole arc/pole pitch ratios commonly employed in Lundell and inductor machines, and hence the different Carter's coefficients.

It is not as simple as the above would indicate, to change a rotating coil machine into a brushless one. Other factors must also be considered.

3.3.13.3 Modifications for Brushless Operation

The structural alterations can be seen by comparing outlines of simple couplings of both types, Fig. 3.37. For the same active diameter and length the overall dimensions of the brushless machine must be greater. In this instance a weaker and more complicated rotor results which necessitates an increase in drum length. Other arrangements of brushless machines are possible Figs. 3.38 - 3.40.

The arrangement shown in Fig. 3.39 allows the coil to be mounted externally to the rotor. This permits the coil size to be increased to offset the m.m.f. drop across the parasitic airgaps. The length of the flux path is increased, as is the machine itself.

Mounting the excitation coil outside the drum, Fig.3.40, increases the diameter of the machine and is only feasible in conjunction with an inductor rotor.

The only practicable brushless version of the 'inverted' coupling is shown in Fig. 3.41. It can be seen that virtually no modification is needed. Nevertheless, the performance of this machine is likely to be inferior to that of its rotating coil counterpart. In order to achieve a magnetically smooth parasitic gap the poles have to be flattened and consequently

become less efficient. The parasitic gap must be smooth to prevent the generation of eddy currents in the gap faces. These would cause a drag torque to be produced which would detract from the performance. Alternatively, the gap surfaces could be laminated, but this would be both difficult and expensive.

3.3.13.4 Advantages of Brushless Machines

Summarising, the brushless coupling will be larger, heavier, and less powerful than the rotating coil version with the same active length and diameter. Its principle advantage is that potentially unreliable sliding electrical contacts are dispensed with. In practice the reliability of sliding contacts depends upon the correct selection of materials and sizing of components. Brush lives of 10 000 hours are attainable, representing five years operation for 40 hours per week. In an eddy-current coupling this is a similar life to that of the shaft bearings. For most applications, therefore, the reliability and ease of maintenance of sliding electrical contacts is satisfactory.

Despite the performance disadvantage that the brushless machine suffers, it is a suitable design for large machines, greater than 75 kW. In common with most electrical machines the mechanical power capacity increases as $D^{2+}L$ whereas the cooling area increases as DL. As a result, the major problem with large machines is obtaining adequate cooling, not torque-slip performance. Brushless construction, then, is permissible

in that it is sufficient for the thermal power dissipation capacity of the machine.

3.3.13.5 Brushless Axial Airgap Machines

Broadly similar observations apply to disc machines as those made in the previous section. A similar range of possibilities exists, Fig. 3.42, for brushless disc machines.

3.3.14 Comparison of Drum and Disc Machines

In his work, Davies[2,3] only explicitly discusses drum machines. His methods may nevertheless be straightforwardly applied to disc machines.

Consider a semi-infinite homogeneous conducting material in which the energy loss density caused by the eddy currents is U Watts/m^2. This loss is equal to the work done by a force F travelling at velocity v past the loss member.

In a linear arrangement

$$Fv = UA$$

where A = total area of loss member, m^2.

In a drum machine F is the tangential force and v the peripheral velocity. If the airgap diameter is D and the active length of the machine is L, then,

$$F = \frac{2\pi DLU}{v} = \frac{2\pi DLU}{\omega D/2}$$

or as a torque,

$$T = \frac{2\pi DLU}{\omega} \qquad (3.50)$$

The disc machine is somewhat different in that the elements of force act at different radii,

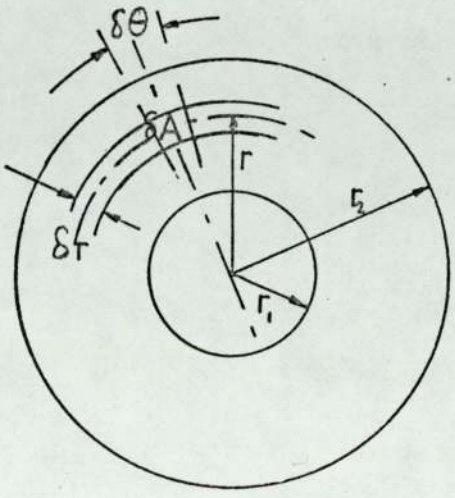

Fig. 3.43 Disc Loss Member

The force acting on the element δA in Fig. 3.43,

$$\Delta F = \frac{U.r\delta\theta.\delta r}{\omega r}$$

hence the element of torque,

$$\Delta T = \frac{Ur\delta\theta.\delta r.r}{\omega r}$$

which by integration yields the total torque,

$$T = \int_0^{2\pi} \int_{r_1}^{r_2} \frac{U}{\omega} r\delta\theta\delta r$$

$$= \frac{2\pi U}{\omega}(r_2^2 - r_1^2) \qquad (3.51)$$

The equations for drum and disc machines become identical if the following relationships are used,

$$D \equiv r_2 + r_1, \qquad (3.52)$$

$$L \equiv r_2 - r_1 \qquad (3.53)$$

i.e. the mean diameter of the swept area of a disc machine is equivalent to the airgap diameter of a drum machine, and the difference of the radii is equivalent to the active length.

It should be noted that this applies to only one region of an inductor machine. If there are two sets of teeth at different mean radii then the normalised torque-slip curve must be used to construct a composite curve. This is necessary because the two sets of inductor teeth act as separate machines of different effective diameters.

It is interesting to note that there can be no such thing as a 'long' disc machine. With a disc machine, the maximum value of $\frac{L}{D} = \frac{r_1 - r_2}{r_1 + r_2}$ is unity. This means that practical disc machines always have significant end-effects (see Section 3.5).

3.3.15 The Loss Member

3.3.15.1 Purpose

The loss member, or induction member as it is sometimes known, has the main function of producing the armature reaction field in the airgap. It must be constructed of an electrically conducting material in order that the eddy currentsmay flow under the influence of the inducing magnetic field. In most machines the loss member also serves to complete the magnetic circuit between poles; in which event it is made of a ferro-magnetic material.

3.3.15.2 The Homogeneous Loss Member

The simplest loss member is constructed from a homogeneous ferromagnetic conducting material. Usually pure iron (Armco) or low carbon steel is employed for this purpose. It has been shown[2] that the resistivity of the loss member only affects the speed at peak torque, n_m, and not the peak torque, T_m, itself. Thus, for a machine to have a low n_m the resistivity must be low. For magnetic reasons it is preferred to have a high permeability, and so materials with a high μ/ρ ratio are desirable.

	Armco	Low Carbon Steel	Aluminium	Copper
μ_r	4000	2000	1	1
$\rho, \Omega m \times 10^{-8}$	10·7	13·9	2·8	1·7
μ_r/ρ	370	140	0·4	0·6

Table 3·2 Properties of Loss Member Materials

The table shows that the ferromagnetic materials are the most suitable in terms of the μ/ρ criterion.

Whilst the homogeneous loss member may be suitable

for most machines, n_m is often found to be higher than desired. Various methods are available to improve this aspect of the performance.

3.3.15.3 End-ring Drums

The first method for reducing n_m is to reduce the effect of the end regions. Low resistivity end rings are electrically connected to the loss member, Fig. 3.44(a) to provide low impedance paths for the eddy currents. The reduction of effective drum resistance significantly reduces n_m Fig. 3.44(b). The subject of end-effects is dealt with more fully in Section 3.5.2.

3.3.15.4 Copper Plated Loss Member

Of the two factors, permeability and resistivity, the former is the more difficult to improve. Few materials possess more suitable magnetic properties than Armco. Resistivity, however, can be effectively reduced by the use of a low resistivity material, plated onto the airgap face of the loss member, Fig. 3.45(a). In this way the eddy currents are able to flow more readily in the copper layer. This results in a lower n_m. Wright[9] investigated this type of loss member and concluded that,

$$n_m \propto \frac{g+d}{d} \qquad (3.54)$$

where g is the airgap length, m

d is the depth of copper plating, m

and

$$T_m \propto \frac{1}{g+d} \qquad (3.55)$$

when the excitation remains constant and saturation effects are not predominant.

The torque-slip curves of drums with different depths of plating, d, but constant magnetic airgap, g+d, are depicted in Fig. 3.45(b). They show that tailoring of the torque-slip curve is easily accomplished by copper plating.

If a machine which operates with a highly saturated magnetic circuit is given a copper plated loss member, the maximum torque will increase despite the magnetic airgap having been increased. Such a machine tends to maintain a constant airgap flux and hence the output rises. Since the physical airgap is largely determined by mechanical tolerances, copper plating inevitably involves increasing the magnetic gap. The actual results of doing so depend upon the state of the machine before plating.

3.3.15.5 Squirrel Cage Drum

A further method of improving the effective μ/ρ ratio of the loss member is to insert low resistivity bars, in the manner of the squirrel cage induction motor, Fig. 3.46(a). Alteration of the number, cross section and resistivity of these bars enables T_m and n_m to be adjusted. Using generalised machine theory it can be shown[28] that the variation of n_m with machine parameters is approximately given by

$$n_m \propto \frac{\rho g p}{D N_s^2} \qquad (3.56)$$

where N_s is the number of slots.

The torque-slip curve of these machines, Fig. 3.46(b), displays a characteristic 'droop' of torque as slip increases beyond n_m. It would appear that armature reaction effects are more marked than in plain loss member machines. Examination of the normalised torque-slip curve reveals that the torque falls away more rapidly on either side of $n/n_m = 1$ when compared with plain iron.

3.3.15.6 Normalised Curves

Normalised torque-slip curves for the various types of loss member are given in Fig. 3.47. If values of T_m and n_m are obtained, the normalised curves may be employed to determine the precise nature of the torque-slip curves for any machine.

3.4 THERMAL FACTORS

3.4.1 Cooling Problems

It is shown in Section 1.2 that the efficiency of eddy-current machines is given by

$$\eta_{p.u.} = 1 - s.$$

The power loss that must take place for non-zero slip must be dissipated by the machine. The loss appears as heat generated by the flow of eddy currents in the loss member. Evidently the temperature of the loss member will rise until thermal equilibrium is attained. The maximum temperature of the loss member is determined by its ability to withstand the operational forces acting upon it. In order to prevent

mechanical failure some heat transfer arrangement must be incorporated in the machine.

It will be shown later in Section 3.5 that the maximum torque from a range of similar machines with the same n_m will vary as $D^{2+}L$. Thus the maximum possible slip power to be dissipated will also vary as $D^{2+}L$. The area of the loss member from which this must be removed will vary as DL and the peripheral velocity as D. The rate of heat transfer will thus vary as $D^{1+}L$. For geometrically similar machines, the difficulty of cooling is given by

$$\frac{\text{Maximum mechanical power}}{\text{Maximum dissipation capability}} = \frac{D^{2+}L}{D^{1+}L} \simeq D$$

i.e. the larger the machine the greater is the difficulty in removing the slip loss.

Although the active length of the machine does not appear in this equation, the ratio of length to diameter, L/D, determines the diameter of the machine for a given mechanical power capacity.

$$\text{Mechanical Power} \alpha D^{2+}L \alpha D^{3+}\frac{L}{D}$$

and $$\text{Dissipation capacity} \alpha D^{1+}L \alpha D^{2+}\frac{L}{D}$$

thus for constant mechanical power

$$\frac{L}{D} \alpha \left(\frac{1}{D}\right)^3 \qquad (3.57)$$

Note, however, that the condition for constant n_m has been violated,

i.e. $$n_m \alpha \frac{1}{D^3} \alpha \frac{L}{D}$$

end effects further complicate matters, as they increase as L/D decreases.

Nevertheless Table 3.3 clearly shows how difficulty of cooling varies with L/D.

L/D	8	4	2	1	1/2	1/4	1/8
Difficulty of Cooling	0·5	0·63	0·79	1	1·26	1·59	2

Table 3·3

In practice this means that above about 75 kW the difficulty of cooling becomes so great that air cooling is inadequate. Liquid cooling is then adopted to overcome this problem.

3.4.2 Air Cooled Machines

The loss member is usually arranged to be the rotating member in a brake or the input member of a coupling. In this way the heat source is always rotating when slip occurs. Fan blades are often attached to the loss member where they both promote air flow and provide additional heat transfer area. Such a configuration is shown in Fig. 3.48. This arrangement is the most likely one for brakes when it yields the best cooling and allows the field assembly and excitation coil to be stationary.

If a low moment of inertia is required to achieve a rapid speed response the loss member is made to be the output.

In this instance cooling air is circulated by a fan mounted on the rotor, Fig. 3.49.

The components most likely to fail owing to overheating are the loss member, the bearings and the excitation coil. The reduction of yield stress with increasing temperature limits the diameter and angular velocity of the loss member. To ensure safe operation of the machine a maximum temperature rise (typically 300^{o} C for Armco) is specified for the back face of the loss drum. This appears on the torque-slip graph as a constant power hyperbola. Continuous operation beyond this limit is not advised and may even be prevented by the use of temperature sensing devices.

If the shaft bearings are allowed to rise above their rated temperature, their life is appreciably reduced. This problem is particularly likely in the arrangements shown in Figs. 3.2 and 3.4. The bearing between rotor and loss member must be cooled by an air flow as it does not have a direct thermal connection to the frame. The mechanical design should ensure that as little of the slip loss as possible is conducted to this bearing.

The excitation coil is both self-heated by resistive losses and heated by the loss member. The permissible temperature rise of the coil is determined by the properties of the interturn insulation. It is usually necessary to arrange an airflow past the coil to remove the excess heat. As with the other cooling problems, the power loss in the coil increases faster than the surface area.

3.4.3 Water Cooled Machines

Above 75 kW cooling problems place a severe restriction upon the performance of self-ventilated air-cooled machines. Whilst forced air cooling and elaborate heat transfer arrangements could be used to extend the range of air-cooled machines it becomes more attractive to resort to liquid cooling.

In the air/water cooled transition zone, otherwise identical machines have three times the power dissipation capacity when water cooled. Thus, for a given application the water-cooled machine will be smaller and cheaper than its air-cooled counterpart, except in that it requires a water supply.

Two possibilities exist with water-cooled couplings - whether to allow the coolant into the airgap region or not. These are known as the wet and dry gap arrangements, with various advantages being apparent for each.

The wet gap method has the advantage that the liquid coolant comes into contact with the surface of the loss member where the heat is generated. Owing to the 'skin effect' the eddy currents flow in a thin layer nearest the airgap surface of the loss member. Cooling this surface minimises the temperature gradient through the loss member, and hence the thermal stresses are kept small. For the same reason the change in airgap due to thermal expansion, the change in resistivity and hence the alteration of T_m and n_m are minimised.

It is, however, the flooding of the airgap that is the principle drawback with this arrangement. Viscous drag caused by shearing of the coolant in the airgap under slip conditions results in a torque being present even at zero excitation. Typically this drag torque is of the order of 5% of the rated torque.

The dry gap system eliminates this viscous drag torque by cooling only the back face of the loss member. This results in a temperature gradient across the loss member which can be undesirable for the reasons given above. Another advantage of the dry gap machine is the absence of corrosion in the airgap region. The short airgap employed in eddy current machines can be bridged by impurities in the coolant and corrosion products, a problem which is avoided by dry gap cooling.

3.4.4 The Effects of Temperature on Performance

Apart from the problems of removing the slip loss from the machine the temperature rise of the loss member can have an appreciable effect upon the performance of the machine. The two prime parameters affected by temperature changes are the airgap length and the resistivity of the loss member material.

3.4.4.1 Length of Airgap

The magnitude of the change of airgap length depends upon whether it is axially or radially disposed. In general, the axial airgap of a disc machine changes little with

temperature as the axial expansion of a thin disc is small. In contrast the radial expansion of a drum type loss member may be as much as the airgap length in an air-cooled machine. Naturally the higher temperatures attained in air-cooled machines make this effect more pronounced than in water-cooled machines.

The change in airgap length for a drum machine is simply given by the change in circumference with temperature,

$$\delta g = \frac{\delta D}{2} = \frac{D.\mathbf{a}.\Delta T}{2\pi} \qquad (3.58)$$

where a is the coefficient of linear expansion, K^{-1} and ΔT is the temperature change.

Assuming that the rotor diameter does not alter appreciably, then the airgap will elongate if the drum surrounds the rotor, and shorten if the rotor is outside the drum.

3.4.4.2 Resistivity

The materials commonly used for the loss member all have positive temperature coefficients of resistivity of the order of 50×10^{-4} K^{-1} at $20^{o}C$.

The change in resistivity is given by the well known formula

$$\rho_T = \rho_o(1 + b\Delta T) \qquad (3.59)$$

where b is the temperature coefficient of resistivity K^{-1}.

3.4.4.3 The Effect of Temperature on Performance

Substitution of the equations 3.58 and 3.59 into Davies expressions for T_m and n_m yields,

$$T_m \alpha \frac{1}{g+\delta g}$$

$$\alpha \frac{1}{g \pm \frac{Da\Delta T}{2\pi}} \qquad (3.60)$$

$$n_m \alpha \rho_T (g + \delta g)^2$$

$$\alpha \rho_o (1 + b\Delta T).(g \pm \frac{Da\Delta T}{2\pi})^2 \qquad (3.61)$$

$\delta g > 0$ for drum outside rotor

$\delta g < 0$ for rotor outside drum.

Equations 3.60 and 3.61 have been evaluated and plotted in Fig. 3.50 for the two drum machines and a disc machine. It can be seen that the disc machine has a constant peak torque and a steadily rising slip speed for peak torque. The machine where the drum surrounds the rotor suffers from a substantial decrease in peak torque and a marked increase of n_m. The only machine where the airgap shortens, the rotor outside drum type, has a reducing n_m and an increasing torque. Care must be taken to ensure that the airgap does not close up completely with this last type of machine.

It must be noted that these curves only indicate the general trend of the changes as no account has been taken of any other parameters. For instance, the airgap m.m.f.

is likely to change with airgap length. Fig. 3.50 does, however, demonstrate the important differences between the three types of machine.

3.5 END EFFECTS

3.5.1 The Analysis of End Effects

Most theories which apply to the electromagnetic aspects of eddy-current machines deal with end effects by assuming that the eddy currents flow axially along the drum in the active region, forming closed loops in the end regions. The additional impedance presented by these end regions is the end effect.

Gibbs accounted for end effects by considering them simply to raise the resistivity of the loss member material. He assumed a semi-infinite, resistance limited end region from which a resistivity multiplier was obtained by the use of Schwarz-Christoffel transformations. This multiplier is of the form

$$\rho_{eff} = r.\rho$$

where $$r = 1 + f_1.\frac{\lambda}{L} \qquad (3.62)$$

using $f_1 \simeq 0.2$ good results can be obtained in many circumstances. This approach fails when used on small machines with small overhanging regions of the loss member. Since it is precisely these machines which are most end effect dominated, a less simplistic method must be employed.

Russell and Norsworthy, in their paper on screened

rotor induction motors, derive relationships for the power loss in a non-magnetic, conducting sheet in the airgap of an induction motor. They assume purely axial current density in the active region and peripheral current density in the end region. They obtain power correction factors which compare the power loss in overhanging shells with and without endplates, with the loss in a shell with no overhang and zero resistance end plates.

For an open ended homogeneous shell the following is obtained,

$$P = P_o \left| 1 - \frac{\tanh \frac{p\ell}{a}}{(\frac{p\ell}{a})(1+\lambda)} \right| \qquad (3.63)$$

where p = pole pairs

a = shell radius

2ℓ = shell length

λ = overhang coefficient = $\tanh\frac{p\ell}{a} \tanh \alpha \frac{p\ell}{a}$

$\alpha\ell$ = overhang length

Care must be exercised if equation 3.63 is to be applied to eddy-current machines as it was derived for the case of a thin, non-magnetic shell subjected to a radial magnetic field. End effects in such a shell are not frequency dependent. The use of iron, with variable permeability, will introduce frequency effects.

The extra analytical problems associated with the use of iron are considered by Woolley and Chalmers. Using a similar approach to Russell and Norsworthy, but applied to

the solid-rotor induction motor, Woolley and Chalmers obtain similar power reduction factors for rotors with and without end effects.

For example, a rotor with endplates and no overhang,

$$P = P_o \left\{1-\left(\frac{a}{p\ell}\right) \frac{\tanh \frac{p\ell}{a}}{1 + k \tanh\frac{p\ell}{a}}\right\} \qquad (3.64)$$

where P_o is the power loss with endplates of zero resistivity,

and $$k = \frac{t_e \rho_c}{t_c \rho_e}$$

where t_e is the thickness of the endplate

t_c is the thickness of the rotor shell

ρ_e is the resistivity of the endplate

and ρ_c is the resistivity of the shell.

The values of the thicknesses, t_e and t_c are chosen with regard to the skin depth of the material. This depth in turn depends upon both frequency and flux density.

An alternative approach to the estimation of end effects is given by Wright. He rejects the usual model of eddy-current paths as being unrealistic, instead postulating that cross-pole currents occur in the active region as well as in the end regions. In his work on the copper-faced eddy-current coupling, Wright obtains an expression for the fundamental eddy-current loss where

$$P = f n \left\{\frac{1}{1+\left(\frac{\lambda}{2L}\right)^2}\right\} \qquad (3.65)$$

where λ is the pole wavelength

L is the active length.

This, again, shows that the end effect depends upon the ratio of wavelength to active length.

3.5.2 Practical Considerations

At first sight it might appear that end effects cause a reduction in torque at all slip speeds. James' work shows that this is not so. His results demonstrate that upon fitting a solid iron drum with copper end rings, T_m is slightly increased and n_m is appreciably decreased. At low slip speeds the endring machine yields more torque for a given excitation but at higher slips ($n/n_{m\ solid} > 1$) the torque is lower than the original machine, Fig. 3.44(b).

3.5.3 Disc Machines

End effects are more significant in disc machines owing to the impossibility of achieving a large L/D ratio (Section 3.3). In addition, the physical problems associated with providing endrings on disc loss members, generally militates against the choice of axial airgap construction for small machines ($\frac{pL}{D} < 3$).

3.6 THE EFFECT OF MACHINE SIZE UPON PERFORMANCE

3.6.1 Method of Estimation

In this section use is made of two key equations due to Davies[3] to investigate the effect of diameter on torque-slip performance. The two equations are,

$$T_m \propto \frac{pDL}{g} F_g^2 \qquad (3.66)$$

and

$$n_m \propto \frac{\rho g^2 p^{4m-1}}{F_g^{4-4m} D^{4m}} \qquad (3.67)$$

where m is the index giving the degree of saturation of the loss member iron.

Equations 3.66 and 3.67 are used to scale up and down from the machine used by Wright in his investigation of transient performance. Equation 3.66 is used to obtain the values of the scaled parameters. The criterion used is that n_m remains constant as diameter is varied, which would be desirable in a homologous series of machines.

Care must be taken when using equation 3.67. Rearranging in terms of m, the following is obtained,

$$n_m \propto \left(\frac{p.F_g}{D}\right)^{4m} \quad \text{(all parameters constant, save m)}$$

Now in a typical medium sized coupling,

$F_g \simeq 200A$,

$p \simeq 5$ pole pairs

$D \simeq 0.2m$

i.e. $n_m \propto (5000)^{4m}$

This means that n_m is highly dependent on m. When using this equation to predict absolute value of n_m, great care must be taken to ensure that the correct value of n_m is obtained. A small error in m can lead to a large error in n_m

$$e.g. \frac{n_m(m=0.77)}{n_m(m=0.75)} \simeq 2$$

When, however, equation 3.67 is being used for scaling of n_m from known values, the choice of m is not so crucial. The indices change relatively little over the range of interest $0.8 > m > 0.75$ and so the effects of changing p, F_g and D can be clearly seen. Nevertheless, this procedure is only strictly applicable to machines having the same loss member material in the same state.

Davies states that for a solid iron loss member $m = 0.77$ at n_m. Substituting this value in equation 3.67 yields,

$$n_m \propto \frac{\rho g^2 p^{2.08}}{F_g^{0.925} D^{3.08}}$$

In the interests of simplicity it is best to round the indices to the nearest integer, but remembering the above warning,

$$n_m \propto \frac{\rho g^2 p^2}{F_g D^3} \qquad (3.68)$$

Next, decisions must be made about the dependence of the variables upon D. It has been assumed that ρ is constant, that is to say the material and temperature of the loss member are the same for all diameters. The length of the airgap is assumed to vary as the diameter. Neglecting end effects for the moment, equation 3.68 becomes,

$$n_m \propto \frac{p^2}{F_g D}$$

The m.m.f. per pole, F_g, varies as a function of both p and D for a salient pole rotor and only as D for an inductor or Lundell type.

Salient pole $F_g \propto \frac{D^2}{p}$

Lundell $F_g \propto D^2$

3.6.2 Salient Pole Machines

Considering the salient pole type first, substitution for Fg with equation 3.68 yields,

$$n_m \propto \frac{p^3}{D^3}$$

and so for constant n_m,

$$p \propto D$$

using this result in equation 3.66 yields,

$$T_m \propto D^3L \quad \text{(c.f. } D^{2+}L \text{ in Section 3.4.2)} \qquad (3.69)$$

This function has been evaluated for diameters changing by a factor of $\sqrt{2}$, Table 3.4. Examination of the calculated results shows that under these conditions the pole wavelength remains constant. The airgap flux density also remains constant as both F_g and g increase in proportion. In turn this means that the flux per pole per unit axial length remains constant. In practice this causes problems with magnetic circuit losses as the machine becomes smaller. In order to carry the flux the loss member thickness will be kept constant, and so the overall diameter of the machine will not reduce as fast as the active diameter.

Likewise the space occupied by the end turns will not diminish at the same rate as the diameter. If the same L/D

ratio is employed this means that the total length of the machine is less efficiently utilised the smaller it becomes.

The length of the leakage paths between poles remains substantially constant with constant wavelength. Since, however, the airgap length increases with diameter, the ratio of leakage to airgap permeances will increase.

3.6.3 Lundell and Inductor Rotors

The most notable difference with this type of rotor is the independence of m.m.f. per pole and number of poles. Following the same procedure adopted in Section 3.6.2 the following are obtained,

$$p \alpha D^{3/2}$$

and hence,

$$T_m \alpha LD^{11/2} \qquad (3.70)$$

The large index for the diameter in equation 3.70 results from the assumption that the airgap m.m.f. increased as the square of diameter. This in turn means that airgap flux density must increase as the diameter. Given the characteristics of all commonly used magnetic materials, this is clearly impossible. Airgap flux densities in excess of 1.5T are exceedingly difficult to attain. Thus, although the coil m.m.f. per pole may increase as D^2, the useful airgap m.m.f. per pole will at best increase as D once the saturation flux density has been reached.

Using this assumption the results turn out to be the

same as for salient pole rotors.

3.6.4 End Effects

The importance of end effects in an eddy-current machine is largely determined by the size of the machine. It is generally acknowledged that the magnitude of the end effects is a function of pole wavelength to active length. Accordingly, as machines become larger the active length increases, the pole wavelength tends to remain constant and so end effects diminish. In addition, the L/D ratio is likely to increase with diameter, for cooling reasons (Section 3.4.1).

For most purposes, when scaling machines, the use of Gibbs' end-effect factor, equation 3.62, is sufficient except for small machines. Especial care must be taken then.

3.6.5 Long Rotors

Eddy-current machines rarely have an active length which exceeds the airgap diameter, typically $D/L \simeq 3$ for a 15 kW machine. The reasons for this are both mechanical and electromagnetic. Shaft stiffness and whirling problems discourage the adoption of high L/D ratios unless centrifugal stresses are predominant. High-speed machines tend to be long if of the radial airgap type, or utilise unconventional materials[12] if axial airgap.

The torque capability of a machine varies as $D^{2+}L$. Thus, for a constant volume the L/D ratio should be as low

as possible to maximise the torque.

Should it be desired to build a machine with an L/D ratio greater than 1 it would be necessary to employ a salient pole or distributed winding rotor. The absence of axial flux in these rotors means that they can be elongated without detriment to their performance. The Lundell and inductor rotors, however, will suffer from saturation problems as the pole face area increases faster than the core area. Beyond a certain point, m.m.f. drops in the rotor would offset any increase in active length. The only satisfactory way of obtaining a long Lundell machine would be to use tandem rotors of more conventional proportions. These rotors with their three dimensional flux paths cannot effectively be elongated beyond one half of their diameter.

CHAPTER 4

4. THE CONTROL OF EDDY-CURRENT MACHINES

4.1 Introduction

In this chapter the means by which eddy-current machines are controlled, and the manner in which they respond are enumerated and discussed. It will be shown that depending upon the application of the machine, various control systems from a simple constant voltage source to a digitally controlled closed loop system may be required.

Firstly it is necessary to examine the relationships between the machine parameters, torque, slip and excitation current, and time.

4.2 STEADY-STATE CONTROL

Under steady-state conditions all elements of the machine are subject to constant or cyclically varying conditions whereby properties do not vary in the long term. There is then a time-independent relationship where,

$$T = f(s, i)$$

where s is the per unit slip

and i is the excitation current.

Owing to the magnetic non-linearity of iron an exact analytic expression for this function is not available. There is however, an expression for the relationship between fundamental flux, slip and torque due to Davies[3],

$$\phi_{ac} \propto \frac{T^{\frac{2m-1}{2m}}}{s^{\frac{1}{4}m}} \qquad (4.1)$$

At constant slip and m ≃ 0.77 equation 4.1 becomes

$$T \tilde{\alpha} \phi_{ac}^{3} \qquad (4.2)$$

The relationship between fundamental flux and excitation current is not so precise. Saturation of the magnetic circuit greatly complicates matters. Under low slip conditions, say $n/n_m < 0.1$, the fundamental flux is near its standstill value and so a considerable proportion of the coil m.m.f. may be dropped across the rotor iron. At $n/n_m = 1$, ϕ_{ac} is approximately half the standstill value. In virtually all machines this will mean that the magnetic circuit will no longer be saturated. With a constant excitation m.m.f., the airgap m.m.f., F_g, must increase as ϕ_{ac} decreases. Davies' theory then only strictly applies to machines where saturation effects are negligible.

The effect of rotor saturation can be visualised in block diagram form, Fig. 4.1, where a varying proportion of F_ϕ, the flux produing m.m.f., is subtracted from the coil m.m.f.

This diagram introduces the quantity F_ℓ, the m.m.f. dropped across the rotor reluctance. If F_ϕ is the fundamental flux producing m.m.f. then,

$$\phi_{ac} = \frac{F_\phi}{S_g}$$

where S_g is the airgap reluctance.

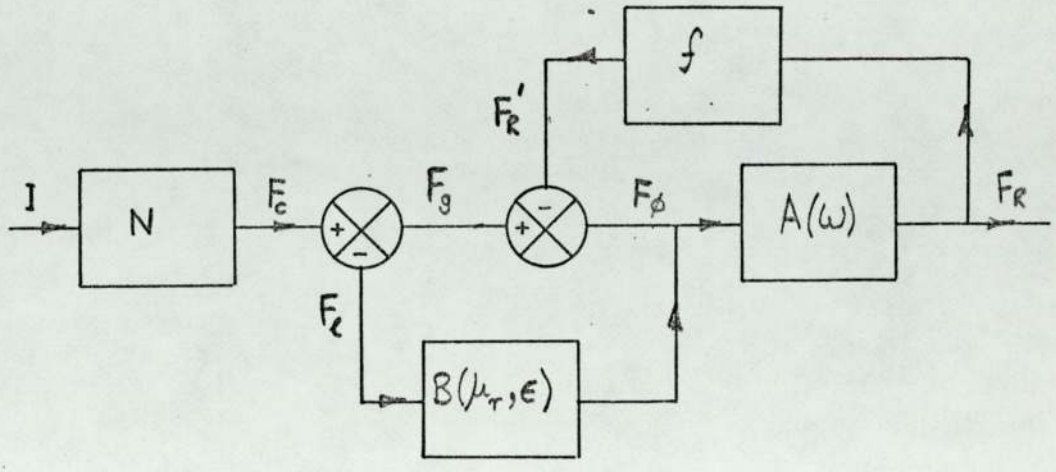

Fig. 4.1. Block Diagram of m.m.f.s.

$$\therefore \qquad \phi_t = \frac{F_\phi}{S_g} \cdot \frac{1}{\varepsilon}$$

and so

$$F_\ell = \frac{F_\phi}{S_g \varepsilon} . S_\ell \qquad (4.3)$$

where S_ℓ is the rotor reluctance and is a function of ϕ_t. From the block diagram the airgap m.m.f. is given by,

$$F_g = F_c - F_\ell$$

Hence from 4.3

$$F_g = N_i - \frac{F_\phi S_\ell}{S_g \varepsilon} \qquad (4.4)$$

Unfortunately, the substitution of equation 4.4 for F_g in Davies' theory leads to non-linear equations.

Fig. 4.1 does not lead to an analytic method of solving the problem of magnetic saturation. It is only, therefore, given as an aid to the understanding of the problem.

4.3 TRANSFER FUNCTION

When time dependence is also considered it becomes necessary to know the transfer function of the machine.

In his thesis Wright[9] tackles the problem of obtaining the transfer function of an eddy-current machine at constant slip speed when subjected to an excitation voltage step. He considered a two-dimensional machine and, by making the usual idealising assumptions, obtains a block diagram of the form of Fig. 4.2.

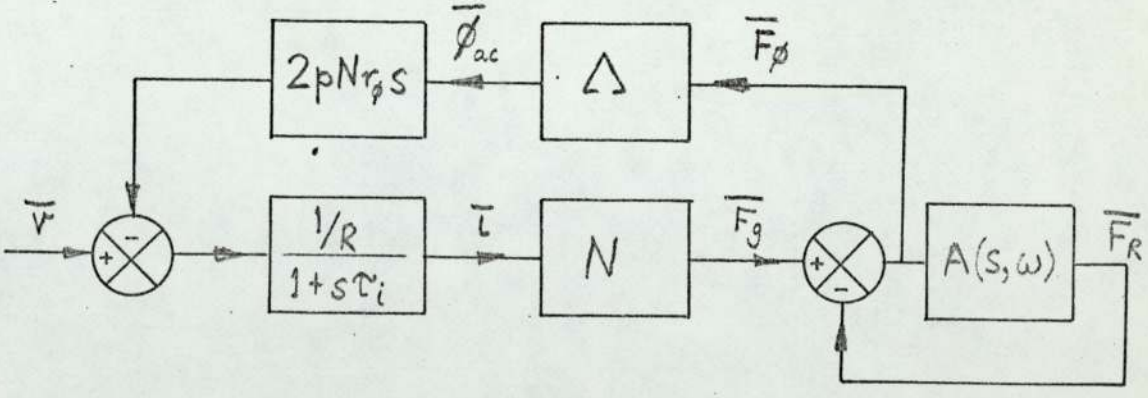

Fig. 4.2 Complete Block Diagram of E.C.M.

Where $$A(s,\omega) = \left(\frac{\lambda}{2\pi}\right)^2 \frac{\mu_o}{g} \left(\frac{1}{\mu\rho}\right)^{\frac{1}{2}} (s^2+\omega^2)^{\frac{1}{4}} \qquad (4.5)$$

and s is the Laplace operator.

In order to make equation 4.5 analytically useful Wright introduced the approximation that motional induction is more important than transformer induction in the loss member. This implies that $\omega >> S$ and so equation 4.5 becomes

$$A = \left(\frac{\lambda}{2\pi}\right)^2 \frac{\mu_o}{g} \frac{1}{(\mu\rho)^{\frac{1}{2}}} \omega^{\frac{1}{2}} \qquad (4.6)$$

He further simplifies the problem by the discovery that drum damping is negligible in most machines, a result verified by the use of laminated and solid loss members. The dominant time constants are those of the field winding and the eddy-current damping in the rotor structure; thus, in order to obtain the maximum speed of response to a changing excitation both of these must be minimised.

Wright demonstrated the difference between a salient pole and a partially interdigitated rotor by comparative tests. These showed, Fig. 4.3, that although each rotor had a substantially similar peak torque, the times taken to reach 63% of the steady state torque were 0.1s and 0.8s respectively. The principal cause of this difference was the field winding time constant, being 55.2 ms for the laminated salient pole rotor and 430 ms for the p.i. rotor at 100 rev/min slip speed. Furthermore, at the same slip speed, the rotor damping time constant of the p.i. rotor is double that of the salient

pole rotor.

The foregoing considerations lead to the prediction of the time response of ϕ_{ac}. In order to obtain the torque response it is necessary to employ equation 4.1. It can be seen that this procedure requires knowledge of the value of m, the magnetisation coefficient of the loss member iron. In most instances a value of m = 0.77 is correct, the exception being at low slip speeds and excitations. The use of experimentally obtained values[3] is suggested here.

The existence of redundant flux increases the response time of the machine. Both a low value of ε and a large proportion of leakage flux will effectively delay the change in active flux. Lamination of the rotor would reduce the eddy-current damping present in solid rotors. Such lamination is only practicable in rotors with effectively two-dimensional flux paths such as the salient pole rotor. Alternatively, the use of powder metallurgical techniques to produce sintered rotors would have the same effect. In this manner the complex shapes required for Lundell rotors could be made having a high relative permeability combined with high resistivity.

4.4 THE BALANCE BETWEEN STEADY-STATE AND TRANSIENT PERFORMANCE

It can be shown[10] for a given peak torque, that the winding time constant is inversely proportional to the power loss in the field coil. A balance must therefore be made between the speed of response of the machine and the size and cost of the controller. In practice, it is found that a

field coil designed to fit into the space available yields an acceptable transient response from a field power of 1 to 2% of the power rating of the machine.

4.5 CONTROL SYSTEMS

4.5.1 Open-Loop Control

With this type of control, the excitation coil of the machine is supplied from an adjustable d.c. source, commonly a variable auto-transformer and rectifier or lead-acid accumulators. For a given setting of the excitation supply the machine will be constrained to operate along the corresponding torque slip curve. Open-loop control is normally limited to applications where a high degree of accuracy is not required. The torque-speed characteristic must also be suitable to achieve a stable operating point. Normally only certain pump drives and braking systems are controlled in this way.

4.5.2 Closed-Loop Control

4.5.2.1 General

Closed-loop control is employed when it is necessary accurately to maintain a set condition in the system. Whilst it is normally the speed or torque of the machine that is controlled, any variable whose value depends upon the excitation can be controlled. Such control is effected by a system like that in Fig. 4.4. Here a reference signal is compared with the controlled variable by means of an error detector. Any

difference between reference and control variable is then amplified and used to modify the excitation so as to reduce the error. In this way the variable is held within certain limits. The accuracy with which the reference value can be maintained depends upon the type of control system, i.e. whether analogue or digital signal processing is used.

4.5.2.2 Analogue Control

In an analogue system the accuracy is limited to about ± 0.1% of the maximum signal. Thermal drift, noise, non-linearity and ageing of components prevent better accuracies being achieved without disproportionate expense and complexity. This level of accuracy is quite adequate for a large number of eddy-current machine systems. The block diagram in Fig. 4.2 is typical of a simple analogue controller.

The main source of inaccuracy in this type of controller is the small signal levels employed. The type of transistor circuitry commonly in use operates on signals over a 20V range. This means that in order to achieve ± 0.1% accuracy the sum of all spurious signals must be less than 10 mV. If the controller is operating over a 20 : 1 signal range errors of ± 2% will be present at the lower end.

Superior performance is available by the use of digital signal processing.

4.5.2.3 Digital Control

Digital techniques allow better accuracies to be achieved owing to the higher immunity to spurious signals that such

systems possess. Digital circuits operate according to whether a signal is present or absent. As long as the signal is above a certain threshold voltage the presence of noise or thermal drift is unimportant. Likewise, in the absence of a signal, all voltages below a certain level have no effect. By using such circuits to operate upon trains of pulses of varying repetition rates a control system may be built. A simple system is depicted in Fig. 4.5. As can be seen by comparison with Fig. 4.4, the initial signal processing is performed digitally. The digital error signal is then converted into analogue form and used to control the power stage as before.

The limitation on the accuracy of the digital system is the D.A.C. (digital to analogue converter) which is limited by the number of bits (binary digits) that it can handle. For instance, an 8 bit D.A.C. is accurate to 1 in 2^8 or 0.4%. In order to obtain an accuracy comparable with the best analogue system 10 bits would be required.

Whilst there is no theoretical limit to the size of the D.A.C. that may be employed, the expense and complexity of a purely digital, high accuracy controller may be prohibitive. A satisfactory blend of analogue and digital techniques can then be adopted.

4.5.2.4 Hybrid Control

If two control loops are nested the overall error is given by the product of the two individual loop errors. By

using an analogue system to cope with gross differences between the desired and actual values of the control variable, a digital loop encompassing the steady-state error range of the analogue system will then provide further accuracy. In this way an 8 bit D.A.C. can be utilised to obtain very high accuracy and stability of control[29].

4.6 POWER CONTROL ELEMENTS

4.6.1 Power Control Devices

Two types of power semiconductor device are commonly used in eddy-current machine controllers, the transistor and the thyristor.

The transistor is mostly used in low power controllers for machines up to 3 kW, with the thyristor being used for the remaining machines.

4.6.2 Transistor Controllers

As the transistor is a d.c. device, it must be operated from a d.c. supply. Whilst this makes it highly suitable for controlling machines from lead-acid accumulators, the a.c. mains must be transformed to a low voltage and rectified.

The principle limitations of the transistor are its relatively low voltage capability and high power consumption. The former constraint means that direct-on-line operation is not feasible in the U.K. as transistors capable of operating at 300V and tolerating mains-borne transients are not yet readily and inexpensively available. The latter constraint

limits the transistor to low power operation as it may be called upon to dissipate a similar power to that needed by the excitation control when operated as a linear amplifier.

For higher power P.W.M. (pulse width modulation)[30] may be used whereby the transistor is used as a switching device supplying variable width voltage pulses to the excitation coil. The mean voltage output is proportional to the ratio of ontime to cycle time with a resistive load. Since the transistor is either switched fully on or fully off the dissipation is low (< 10%). Even though the P.W.M. controller is more efficient than the class A amplifier, the required heatsink area makes controllers very bulky for machines in excess of 10 kW.

4.6.3 Thyristor Controllers

The thyristor or S.C.R. (silicon controlled rectifier) operates as a controlled rectifier. When a voltage is applied to the gate the thyristor will allow current to flow in the forward direction. Once triggered this current will continue to flow irrespective of conditions at the gate. The thyristor will only return to its blocking state if the current drops below a value known as the holding current. These characteristics are illustrated in Fig. 4.6. This ability to change from blocking to conducting states is particularly useful when the supply voltage is alternating. By synchronising the gate pulses to the supply voltage, and altering the point at which they are applied, the mean

voltage applied to the load may be varied. This is known as phase controlled rectification and may be achieved by applying the error signal to a voltage controlled delay pulse generatcr.

There are various possible configurations of thyristors and diodes in controlled rectifiers, five of which are depicted in Fig. 4.7. That shown by 4.7(a) is the half-wave rectifier with a flywheel diode. The diode is required to provide a path for the current during the non-conducting half cycle. With an inductive load it ensures continuity of the current flowing in the load thereby reducing the harmonic content. Figs. 4.7(b) and (c) are known as half-controlled full-wave bridges. The flywheel diode again ensures continuity of load current during the non-conducting periods of the thyristors. In addition it ensures that control is not lost should the firing pulses fail. As an alternative, extra pulses may be applied to the thyristors at the end of each half cycle to ensure that they are switched off. The remaining two arrangements, Figs. 4.7(d) and (e) are full-wave, fully controlled rectifiers. Neither requires a fly-wheel diode as the load current recirculates via the supply. They have the additional feature that the supply can be effectively connected in reverse across the excitation coil to force the current rapidly to fall to zero. This process, known as inversion, enables unloading of the machine to be achieved two to three times faster than the natural time constant of the excitation coil would permit.

The full-wave rectifiers have a lower ripple factor than the half wave. This is a desirable feature as the harmonics in the excitation current contribute little to the torque transmission but do increase the thermal losses in the excitation coil.

4.7 RESUMÉ

For most applications of eddy-current machines a simple analogue controller with a half-wave thyristor power stage is adequate. The accuracy with which steady-state conditions are maintained depends almost entirely upon the controller and associated transducers. On the other hand, the time constants of the machine itself dominate the transient response.

It is a fortunate feature of the eddy-current machine that the control power is low. This means that suitable control systems can be realised more easily and cheaply than with alternative machines.

5. FUTURE TRENDS IN EDDY-CURRENT MACHINES

5.1 INTRODUCTION

The foregoing chapters contain information about the uses and nature of eddy-current machines. It is hoped that the work contained therein, by drawing together the results of other authors, will create a better understanding of the strengths and weaknesses of eddy-current machines.

The purpose of this chapter is to suggest ways in which real machines might be improved in order to increase their competitiveness with alternative form of mechanical-power absorbers and transmitters.

5.2 COUPLINGS

The eddy-current coupling finds most frequent application as an industrial variable-speed drive. In this field it is amongst small and medium sized couplings (up to 10 kW) that competition is most fierce. The eddy-current couplings available at present are predominantly general purpose machines. That is to say at a given power level one machine is required to function with a variety of different loads. Whilst this makes sense from a manufacturing point of view, it means that the coupling can never be optimal for a particular load. Recalling from Chapter 2 the difference in torque speed requirement of the winder and pump loads, it would seem sensible to be able to tailor the coupling performance better to suit the load. It is here that the options discussed in Chapter 3

are important. As a general rule, it is the loss member which determines the shape of the torque slip curve for a given peak torque, and the field member which determines the peak torque itself. If, then, a standard frame and configuration were offered with a choice of loss and field members, each application could be more satisfactorily fulfilled.

Another area where a significant improvement might be wrought is the power to weight or power to volume ratio. The adoption of rotating coil rather than brushless excitation would furnish great benefits here. Since these small and medium sized machines do not suffer unduly from cooling problems the resultant performance improvements could be effectively utilised.

It is considered that even the largest machines could be improved in many respects, by first identifying their weaknesses in the context of the concept of optimal performance, and then using currently available methods to overcome them.

5.3 OTHER MACHINES

Whilst the remarks of the previous section also apply to retarders, brakes and dynamometers, there is another good reason for the improvement of these machines. Recent and likely future legislation in the fields of vehicle safety and atmospheric pollution by prime movers will provide an enlarged market, of which eddy-current

machines are well suited to take a substantial proportion. A reappraisal of the eddy-current machine in these roles would be both timely and rewarding.

5.4 CONCLUSION

5.4.1 General

Chapter 2 described the factors which are frequently important in selecting an eddy-current machine for a particular application. Chapters 3 and 4 covered the means available to tailor the characteristics of a machine. Using the information contained therein, the designer should be able to choose suitable components and techniques to obtain an optimal machine.

Whilst no hard and fast rules can be stated concerning the optimality of the various types of rotors, loss members etc., some general trends are apparent. The following comments should not be taken as rigid rules but as guidelines which will be true in many instances.

5.4.2 Rotors

The salient pole rotor is characterised by yielding a high torque for a given volume. This makes it particularly suitable for machines where a high specific performance is required, e.g. vehicle retarders. By using a small pole number a torque-slip curve can be obtained which is suitable for pump drives (Fig. 2.11). The facility with which it can be made from laminations

makes the salient pole rotor very suitable for machines where good transient performance is required. The major disadvantage of this rotor is the high manufacturing cost.

The Lundell and partially interdigitated rotors are commonly used in small and medium size machines (up to 75 kW). Their performance is mid-way between the salient pole and unductor rotors. Their cheapness and their suitability for brushless operation make them a common choice for general purpose eddy-current couplings and brakes.

It is when torque is not the primary consideration that the inductor rotor is often employed. Despits its poor torque transmitting ability, the inductor rotor is used in high power machines (greater than 75 kW) where cooling is the biggest problem. Another virtue of the inductor rotor is its robustness, this makes it suitable for high speed and large diameter machines where centrifugal forces are significant. The inductor rotor also finds application where a steadily rising torque slip curve is required, such as that for a constant power load (Fig. 2.15). Here a large pole number is used ($p > 15$) to achieve a high n_m.

5.4.3 Loss Members

The most commonly adopted loss member is the plain

type, Armco iron being used for small machines or where high performance is required, progressing through low carbon steel to cast iron as performance becomes less important. The use of copper plating or end-rings is ncecessary where a low n_m is required.

The squirrel cage loss member is a relatively unusual choice in eddy-current machines. It may well become popular for pump drives where it can provide a suitable torque-slip curve when used with a Lundell rotor. There are, however, two potential disadvantages, both caused by the slotting of the airgap surface, pole face losses and noise. These two problems are not normally encountered in eddy-current machines, and it may be that they outweigh the performance advantage of the squirrel cage loss member.

5.4.4 Construction

The choice between axial and radial airgap, and the layout of the machine depend upon so many factors that no guide can be given here. It is sufficient to say that most existing machines are of the radial airgap type, and that the position is unlikely to change in the future.

5.4.5 Conclusion

In conclusion it must be said that development of eddy-current machines has been slow in the last two decades. It is hoped that the facets of eddy-current machines covered in this thesis will stimulate the design of new machines.

REFERENCES

1. GIBBS, W.J. : The Theory and Design of Eddy-current slip couplings. BEAMA Journal 1946, 10, pp 123, 172, 219.

2. DAVIES, E.J. : An Experimental and Theoretical Study of Eddy-current Couplings and Brakes. IEEE Trans. P.A.S. 1963, 67, p.401.

3. DAVIES, E.J. : General Theory of Eddy-current Couplings and Brakes. Proc. IEE, 1966, 113, p.825.

4. DAVIES, E.J., James, B., Wright, M.T. : Experimental Verification of the Generalised Theory of Eddy-current Couplings, Proc. IEE 1975, 122, p.67 and Proc. IEE 1976, 123, p.171.

5. DAVIES, E.J., Wright, M.T., Johnson, R.C. : Transient Performance of Eddy-current Couplings, Proc. IEE 1975, 122, p.1128.

6. JAMES, B. : A Study of Eddy-current Couplings with and Without Endrings, M.Sc. Thesis, University of Aston in Birmingham, 1969.

7. RUSSELL, R.L., Norsworthy, K.H. : Eddy Currents and and Wall Losses in Screened Rotor Induction Motors, Proc. IEE 1958, 105 Part A, p.163.

8. WOOLEY, I., Chalmers, B.J. : End Effects in Unlaminated-Rotor Induction Machines, Proc. IEE 1975, 120, p.641.

9. WRIGHT, M.T. : Steady-state and Transient Performance of Eddy-current Couplings, Ph.D. Thesis, University of Aston in Birmingham, 1972.

10. DAVIES, E.J., James, B., Wright, M.T. : High Performance, Low Cost, Simple Eddy-Current Couplings, IEE Conference Publication, Oct.1972,p.42

11. BAHLER,W.and VAN DER HOEK, W. : Eddy-current Coupling as a Variable Speed Drive, Philips Technical Review, 1966, 27, p.15.

12. JACKSON, P.N. : High Speed Eddy-current Couplings and Dynamometers, Ph.D. Thesis, University of Aston in Birmingham, 1975.

13. LAITHWAITE, E.R. : Electrical Variable Speed Drives, Part II. Engineers Digest, 1964, 25(10), p.111.

14. BLOXHAM, D.A. and WRIGHT, M.T. : Eddy-current Coupling as a Variable Speed Drive, Proc. IEE 1972, 119(8), p.1149.

15. BLOXHAM, D.A. and WRIGHT, M.T., : Economic Aspects of Eddy-current Coupling Variable Speed Drives, IEE Conference Publication.

16. FLACK, R.F., GRANT, W.T., PARKER, C. : Applications for Eddy-current Couplings, Electrical Times 1969, 155(16), p.52.

17. WRIGHT, M.T. : The Economics of Eddy-current Couplings Applied to Pump Drives, Part I, Power 1976, p.101.

18. REED, J. : Electric Retarders, I. Mech. E. Conf. Publication C79/72, p.45.

19. SCHARFF, T.E. : Gearbox Retarders for Heavy Trucks, Automotive Engineer, 1976, 1(2), p.22.

20. REVERDIN, D., BORIONE, J. : The Electric Retarder Today and its Future, I. Mech. E. Conf. Publication, 1976, C2/74, p.9.

21. BRETON, P., : The Principles of Electro-magnetic Retarders, Revue Ingenieurs de l'Automobile, 1975.

22. ADBY, P.R., DEMPSTER, M.A.H. : Introduction to Optimisation Methods, Chapman and Hall, First Edition, 1974.

23. KINGSHOT, A.L. : Investment Appraisal, Ford Business Library, First Edition, 1967.

24. CAMERON, A.L. : Principles of Lubrication, Longmans, 1st Edition 1966, p.277.

25. CRC Handbook of Mathematical Tables

26. WALKER MILES, : Specification and Design of Dynamo-Electric Machinery, Longmans, 1915.

27. GLAZENKO, T.A. : Some Problems in the Design of an Asynchronous Clutch with a Monolithic Rotor, Automation and Remote Control, V19, 1958, p.783.

28. WRIGHT, M.T. : The Design of Squirrel Cage Eddy-Current Couplings, Heenan Drives Ltd., (unpublished).

29. HAURYKIEWICZ, J.M., : Digital Velocity Lock Control System, IEE Conference Publication, MSAC^2 1976, p.239.

30. JANSSON, L.E., : A Survey of Converter Circuits for Switched-Mode Power Supplies, Mullard Technical Communications, 1973, 12 (119), p.271.

31. SCR Applications Handbook, International Rectifier. First Edition, 1974.

32. BAILLIE, T.C. : A Diagram of Correction Coefficients for Air-Gap Reluctances, The Electrician, January 8th 1909, p.494.

33. POHL,R. : The Magnetic Leakage of Salient Poles, JIEE, 1914, 52, p.170.

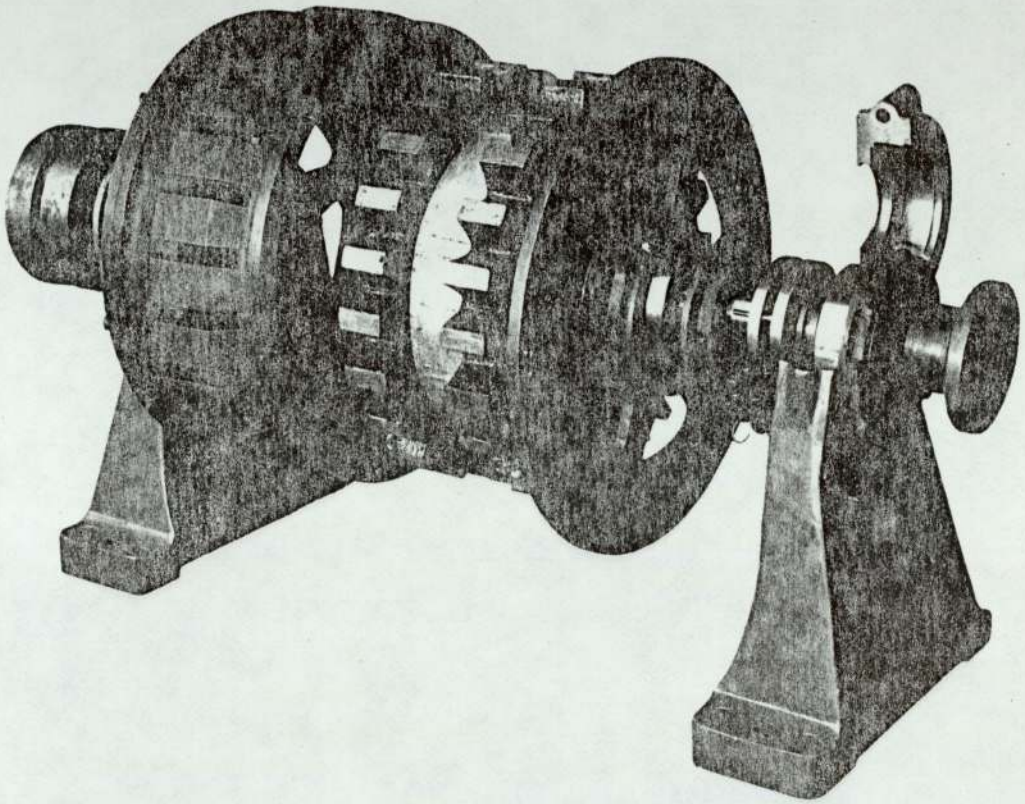

Plate 1 Air-Cooled, Inductor Rotor, Rotating Coil Eddy-Current Coupling. Circa 1945.

(Photo - Heenan Drives Ltd.)

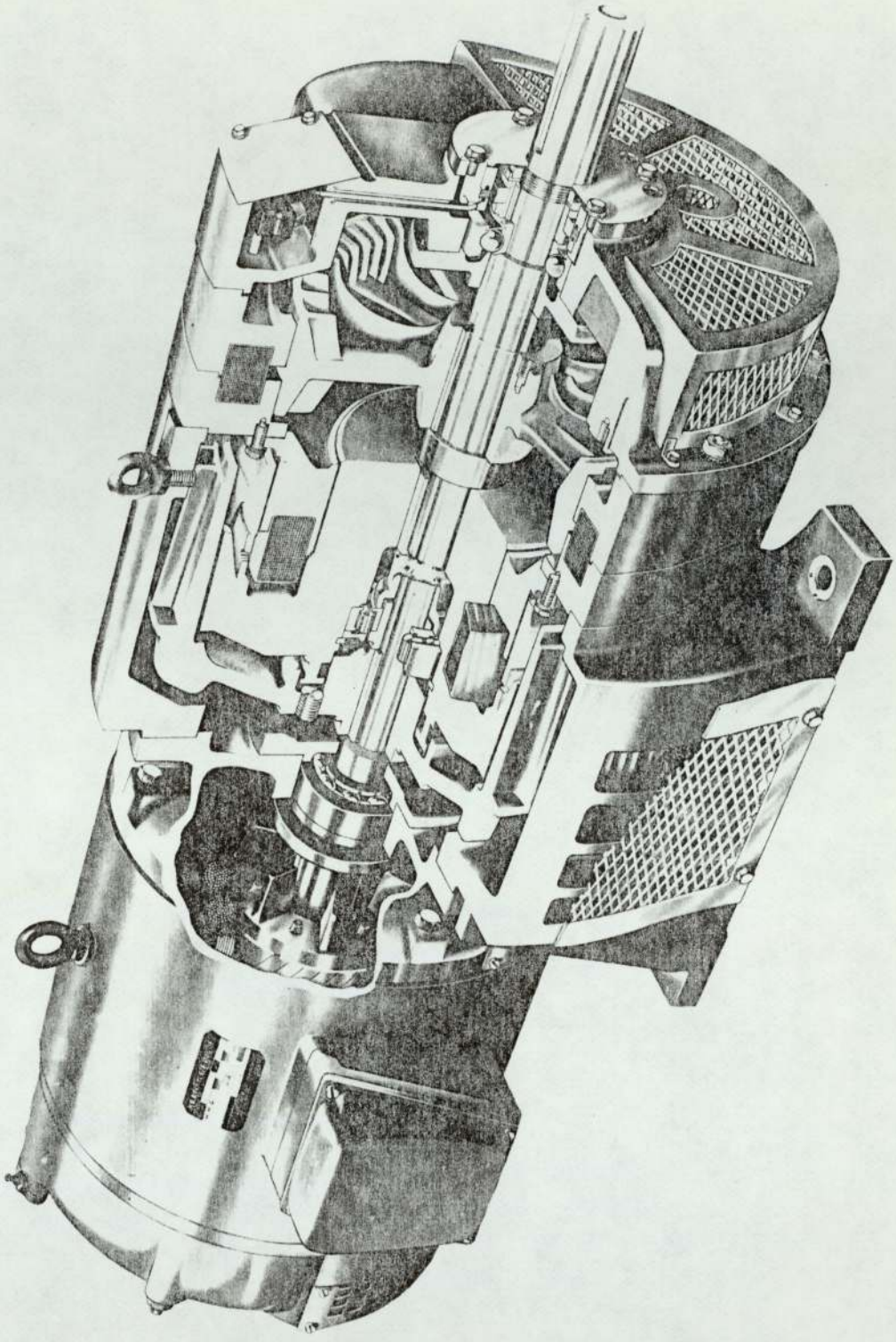

Plate 2 Air-Cooled, P.I. Rotor, Stationary Coil Eddy-Current Coupling with Integral Brake. Circa 1963.

(Photo - Heenan Drives Ltd.)

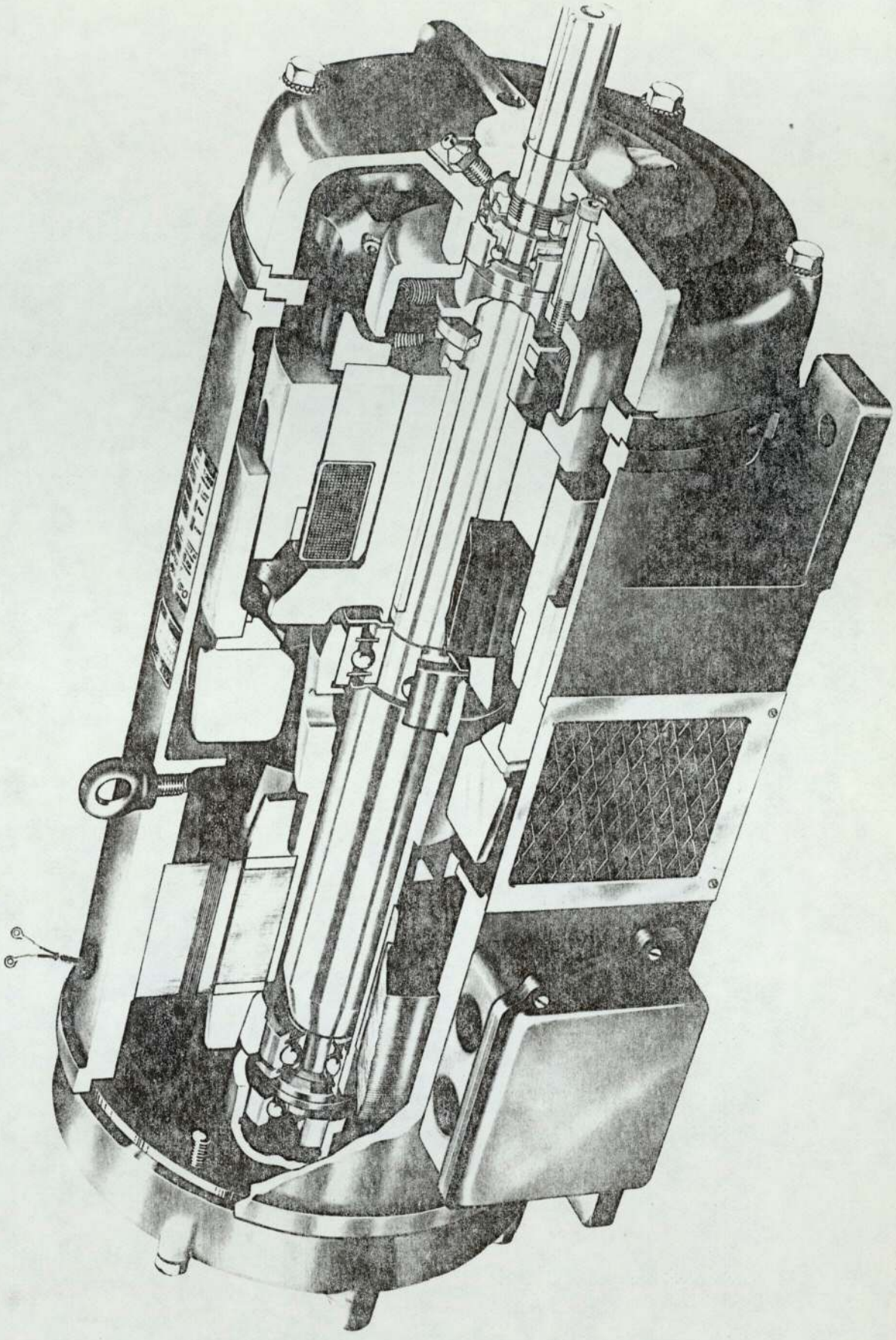

Plate 3 Air-Cooled, P.I. Rotor, Stationary Coil Eddy-Current Coupling with Integral Drive Motor. Circa 1963.

(Photo - Heenan Drives Ltd.)

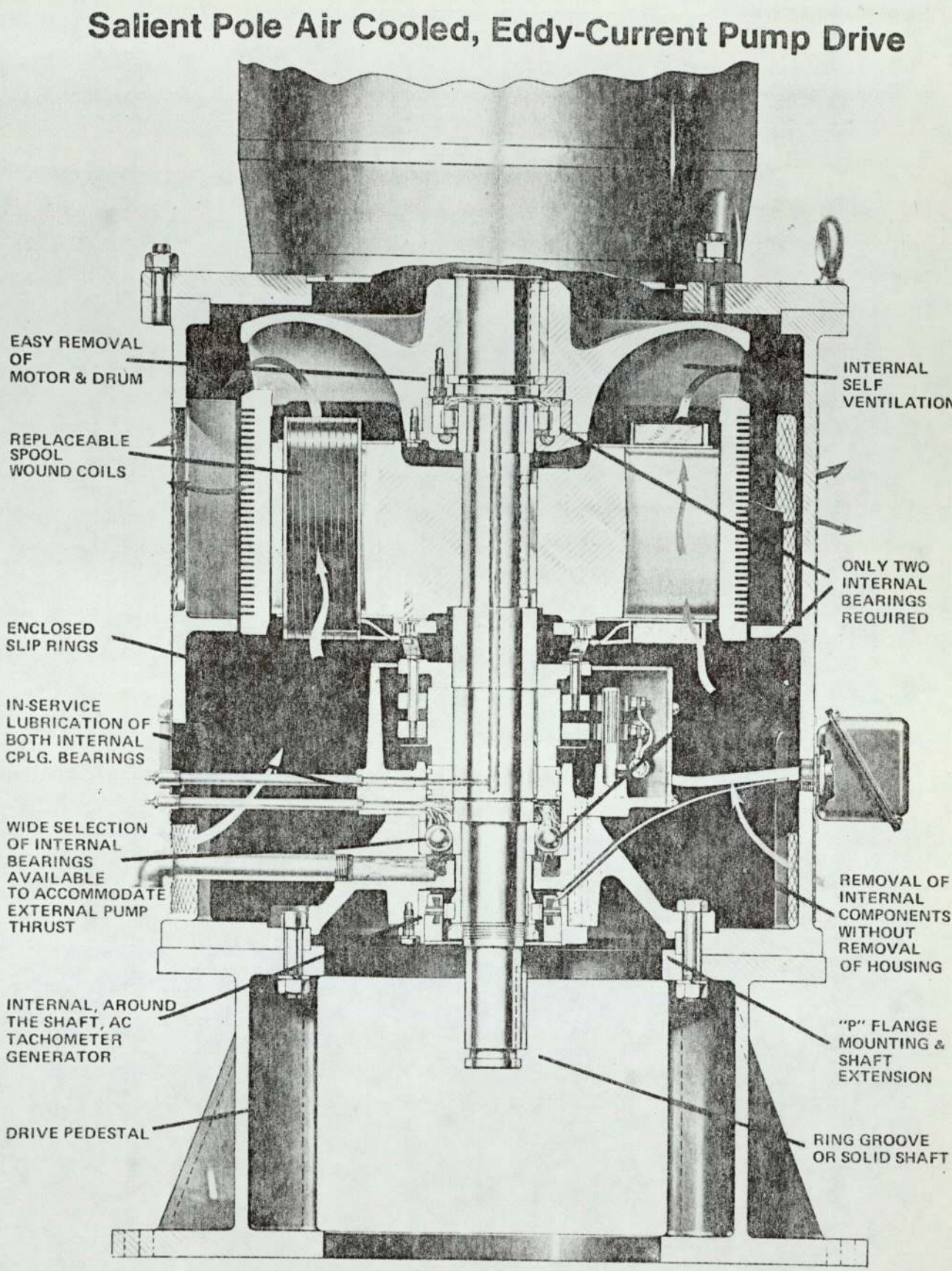

Plate 4 Salient Pole, Air-Cooled, Eddy-Current Coupling. Circa 1973.

(Photo - Eaton Corporation)

FIGURES FOR CHAPTER 1

Fig. 1.1

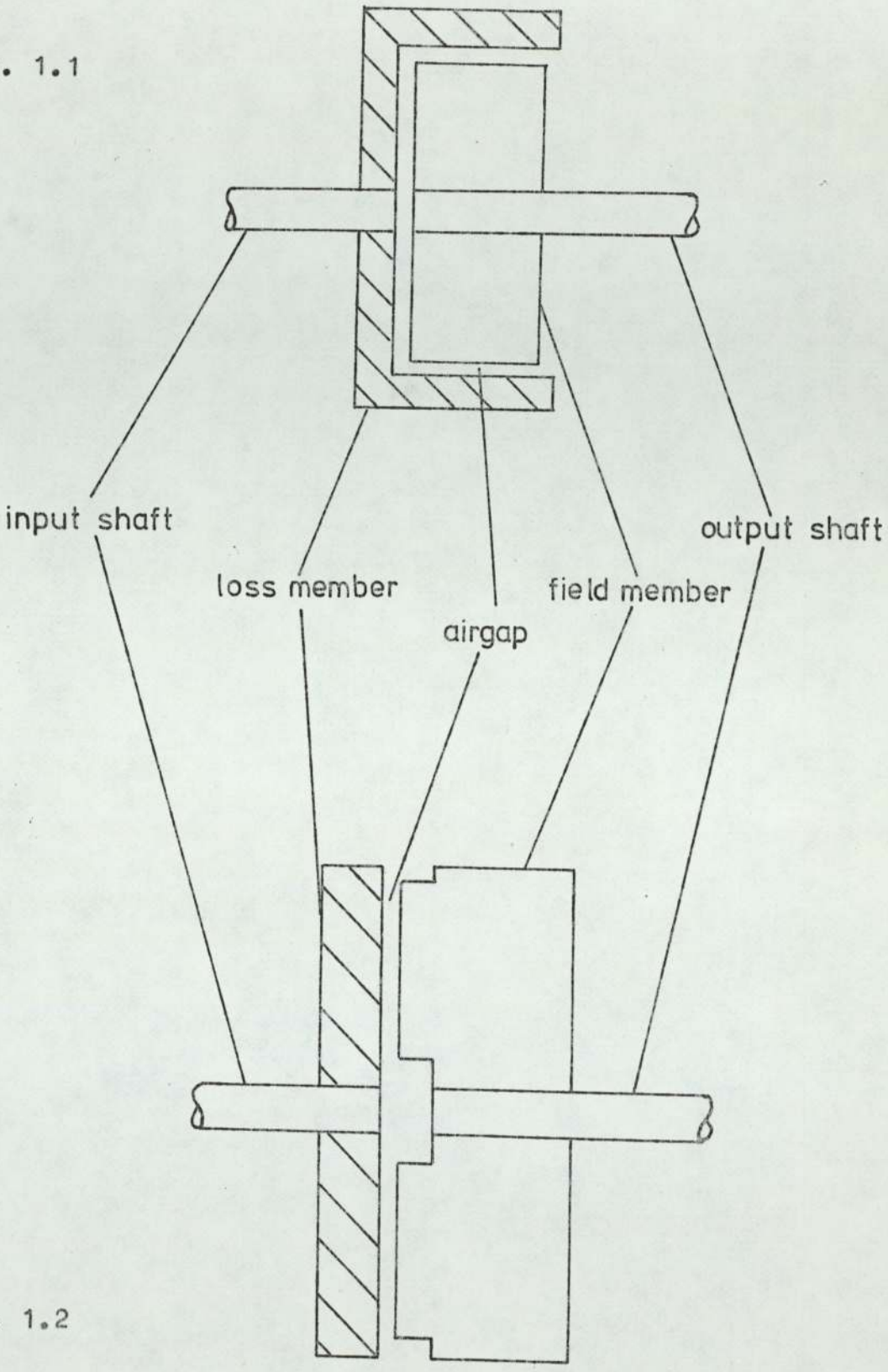

Fig. 1.2

Simple Eddy Current Couplings

FIGURES FOR CHAPTER 2

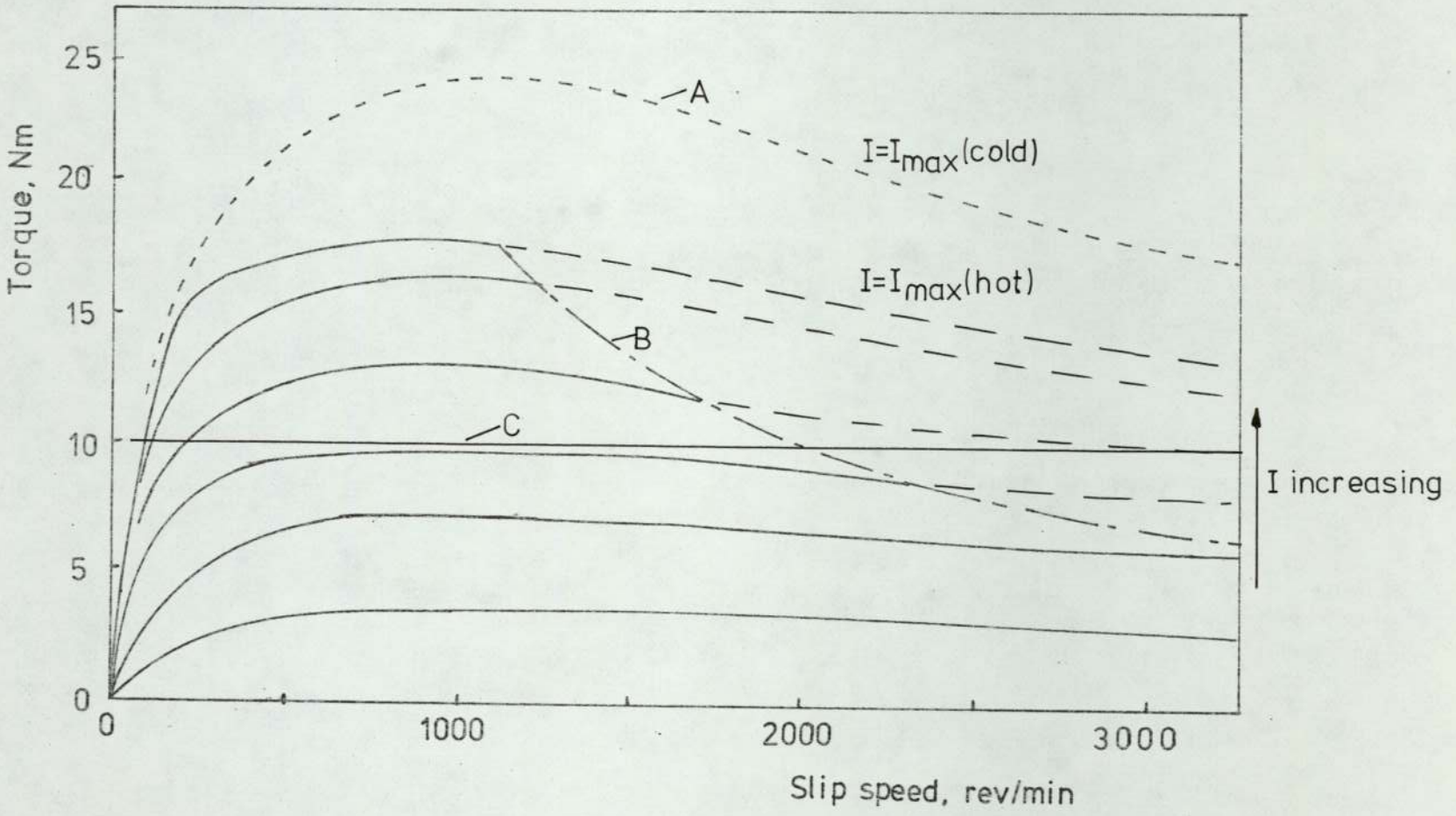

Fig. 2.1 Typical Family of Torque-Slip Curves.

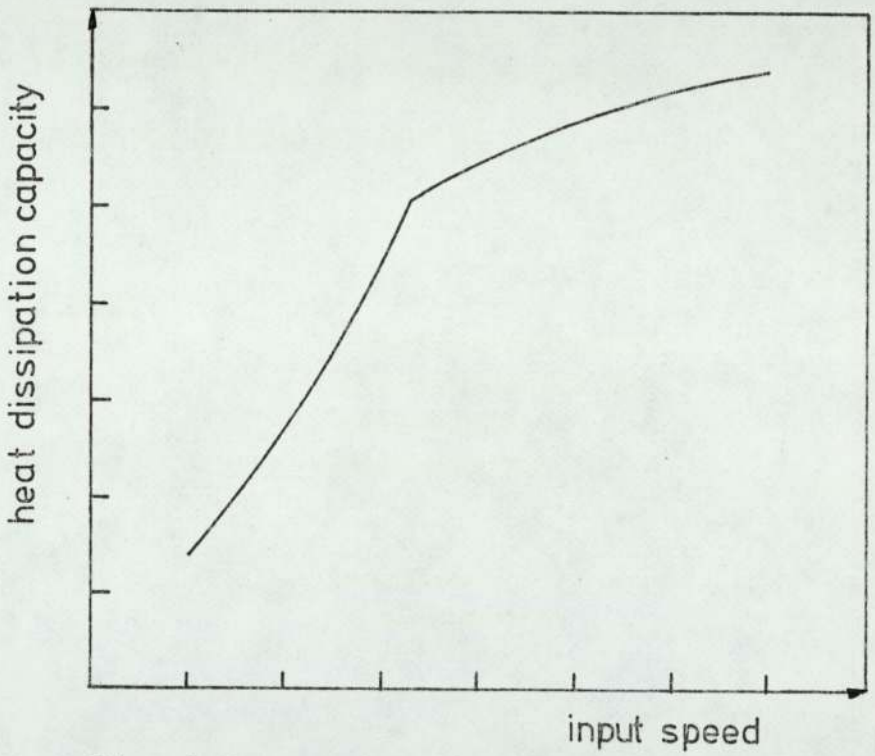

Fig. 2.2 Typical Variation of Cooling Capacity with Speed.

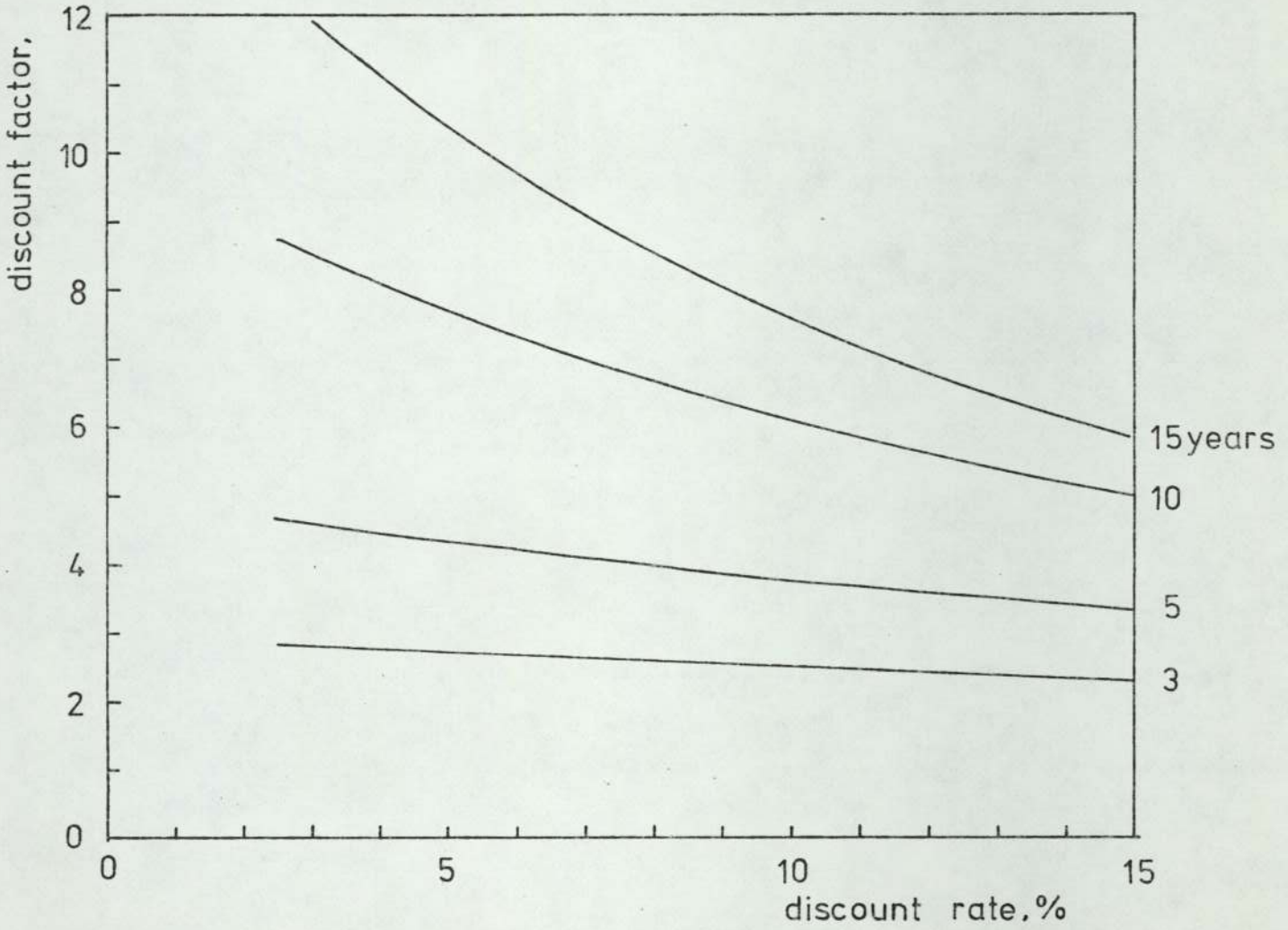

Fig. 2.5 Discount Factor vs. Discount Rate for Various Periods.

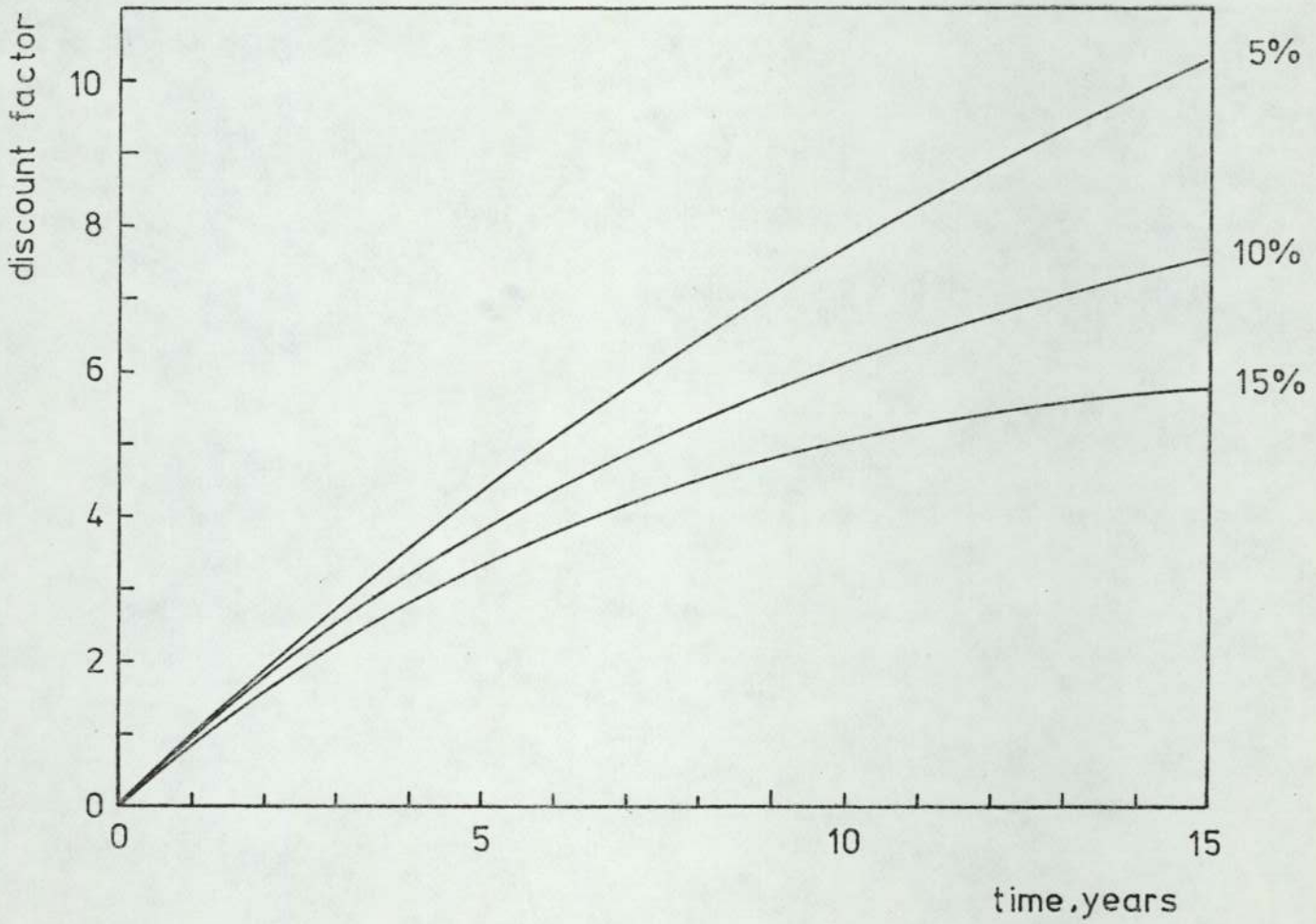

Fig. 2.6 Discount Factor vs. Period for Various Discount Rates

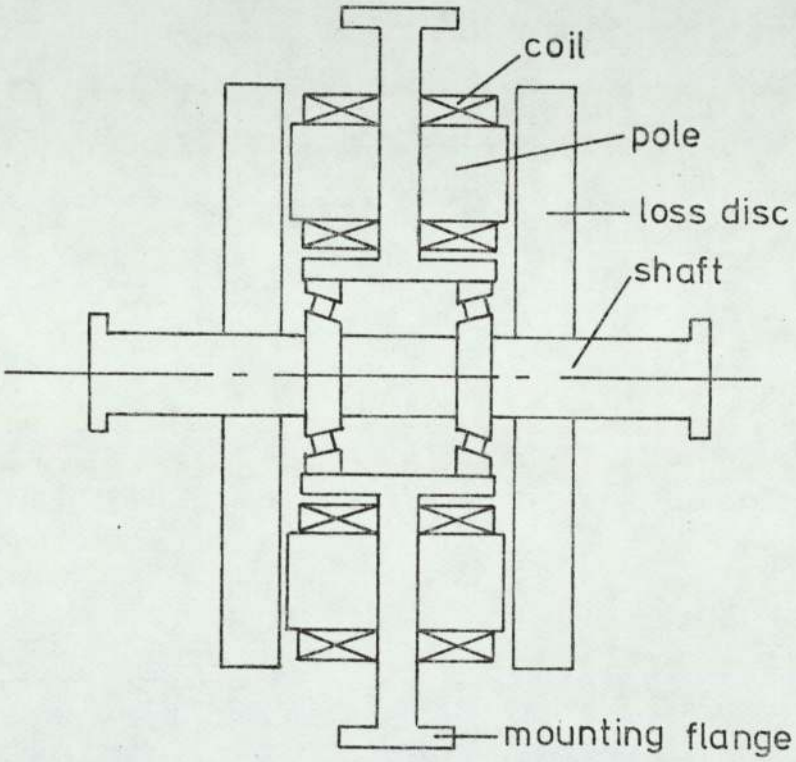

Fig. 2.8 Eddy-Current Retarder

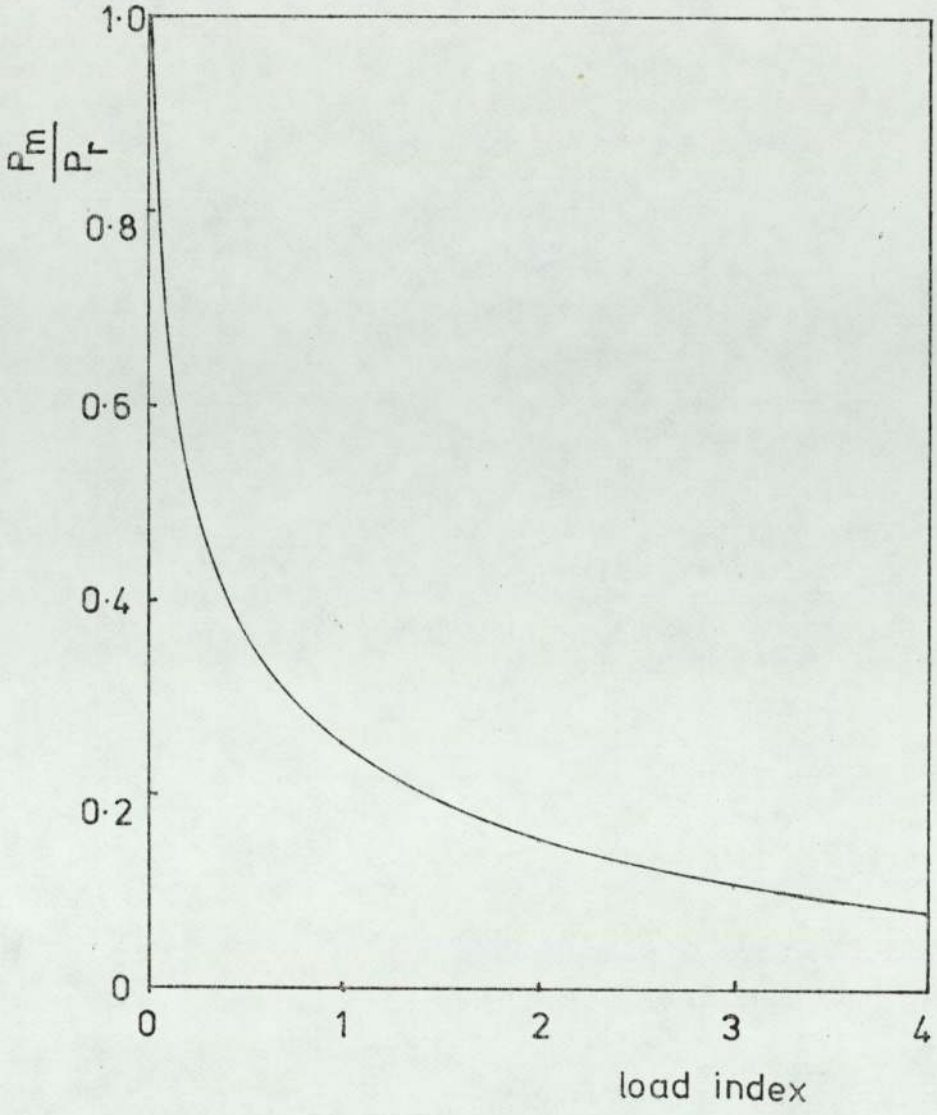

Fig. 2.9 Maximum Loss-Rated Power Ratio vs. Load Index

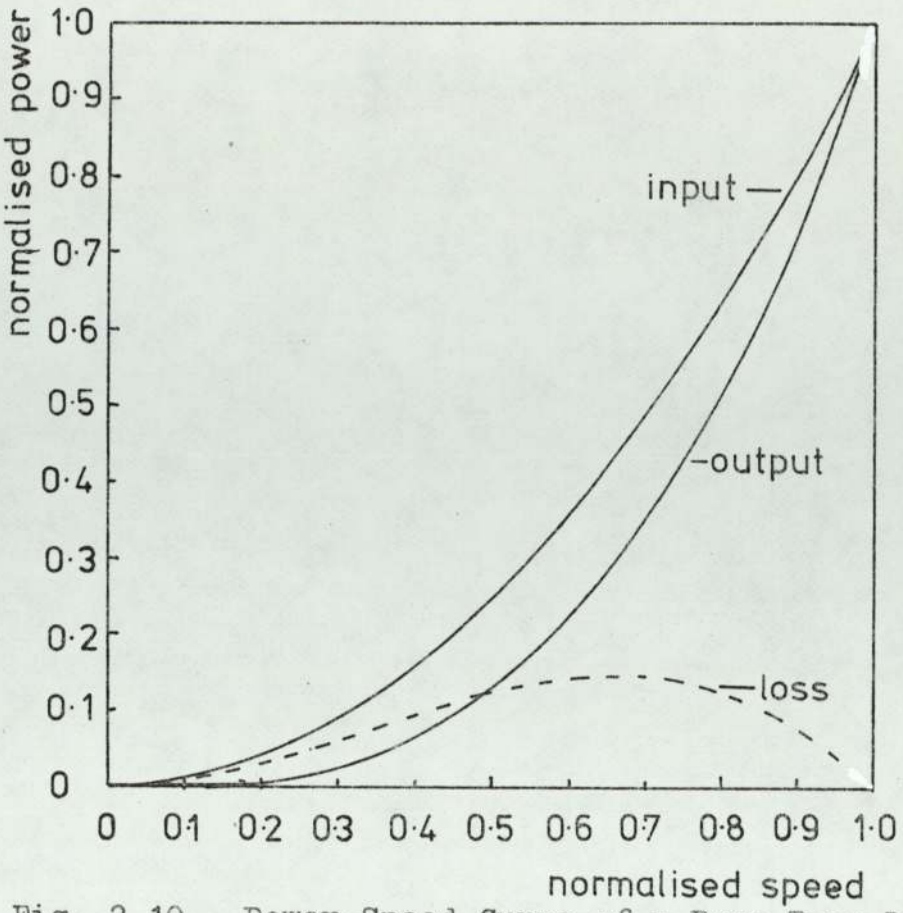

Fig. 2.10 Power-Speed Curve of a Pump-Type Load

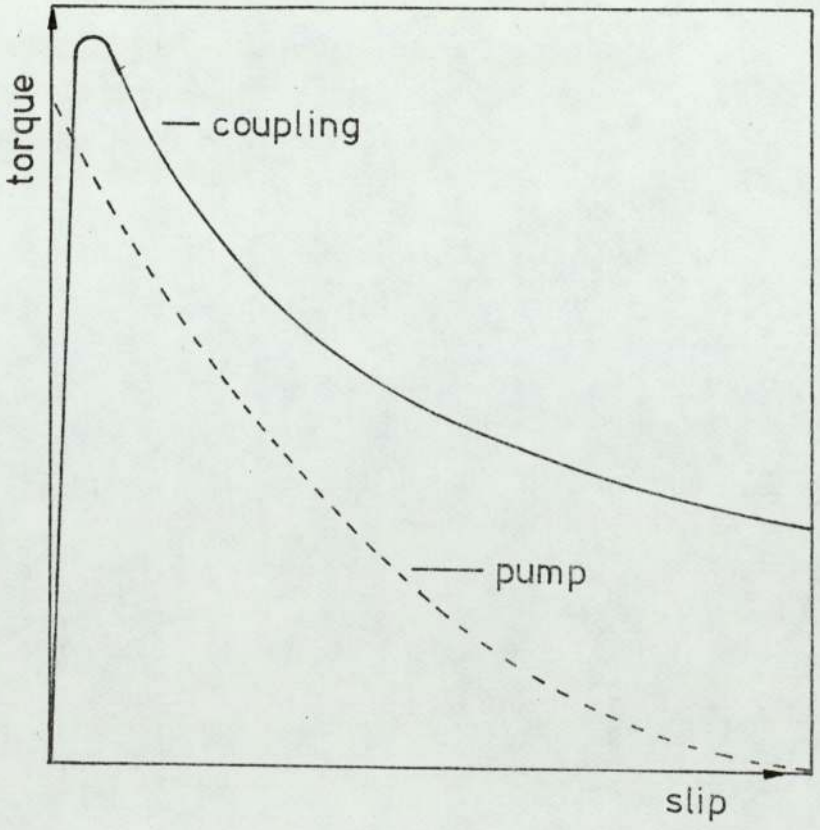

Fig. 2.11 Torque-Slip Curve Suitable for a Pump Load.

Fig. 2.13 Radius & Inverse of Radius vs. Time (Centre Driven Winder).

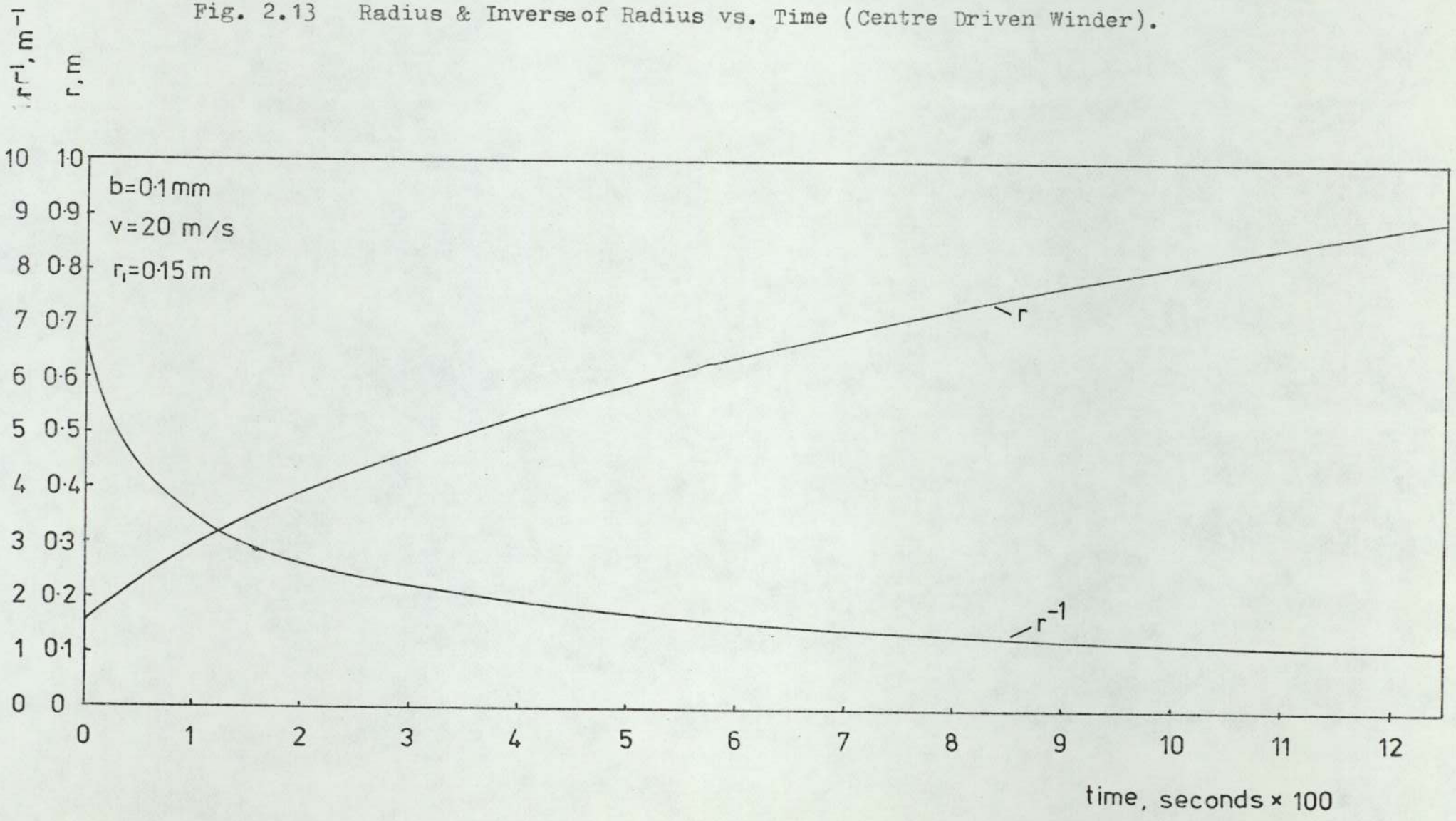

Fig. 2.14 Efficiency Ratio vs. Build Up Ratio (Centre Driven Winder).

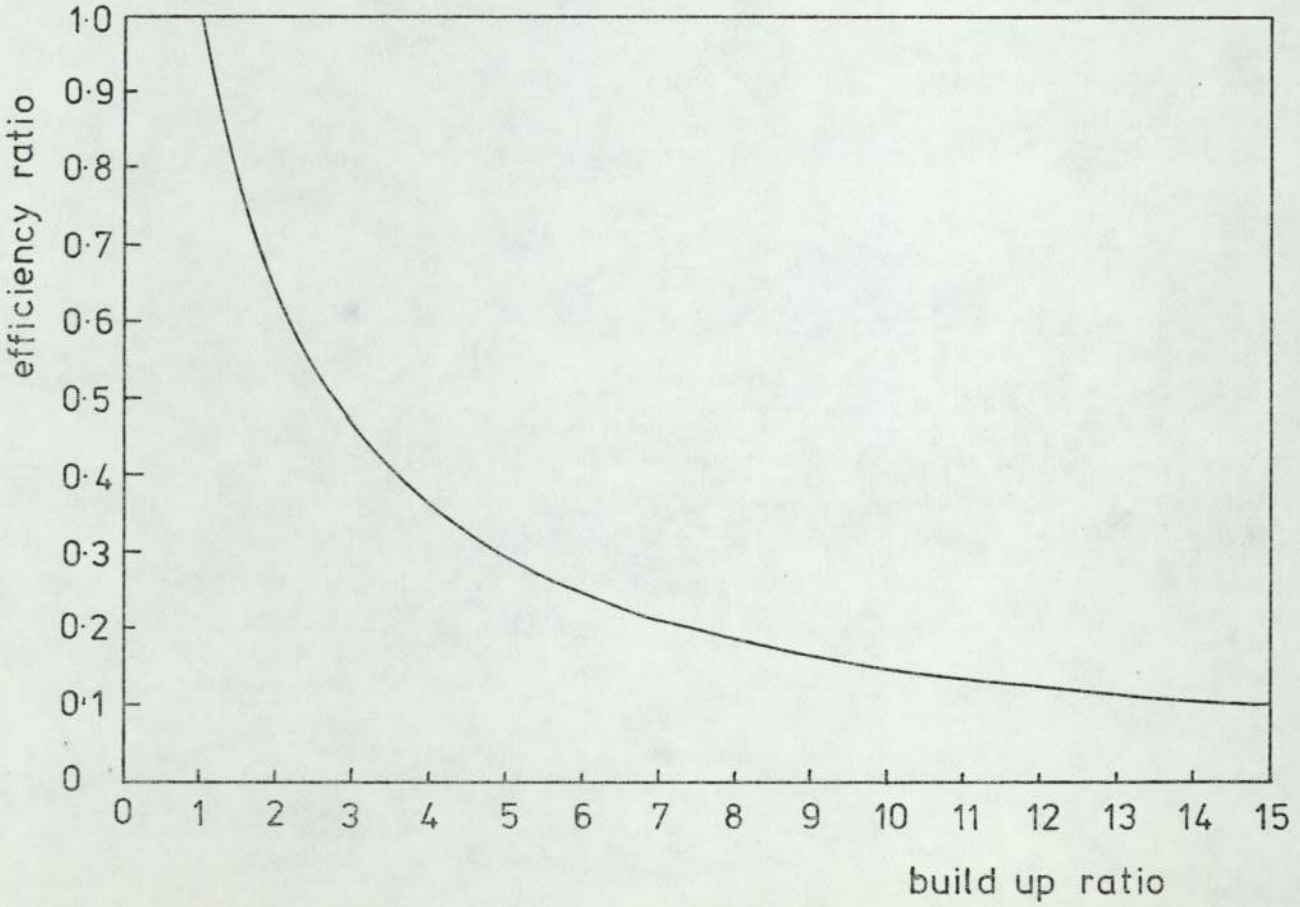

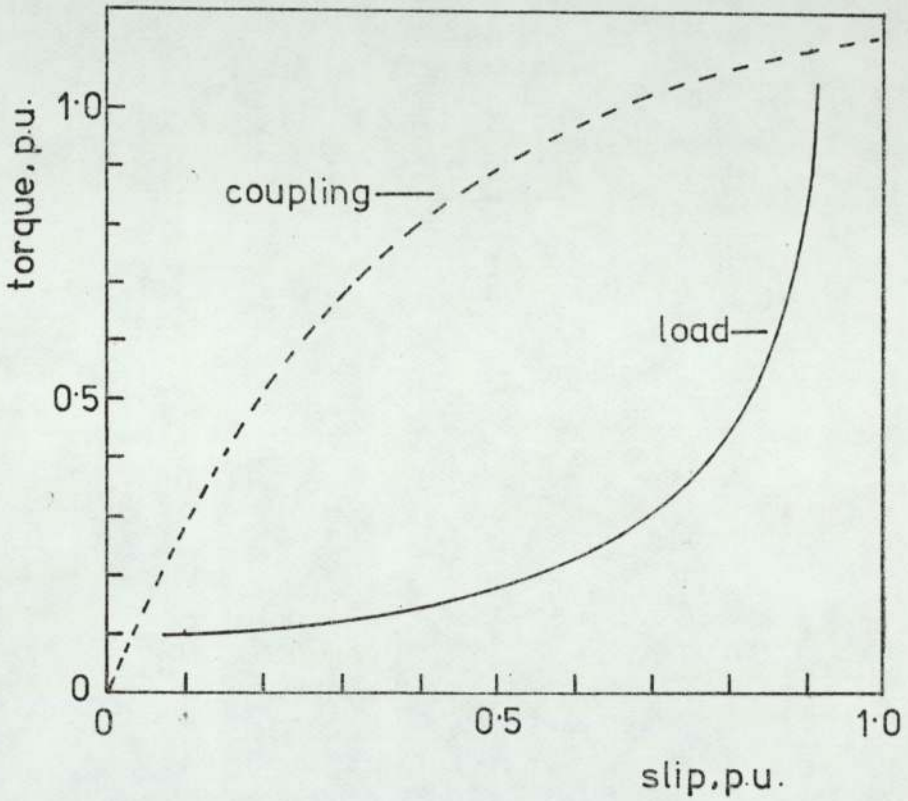

Fig. 2.15 Torque-Slip Curve Suitable for a Constant Power Load.

FIGURES FOR CHAPTER 3

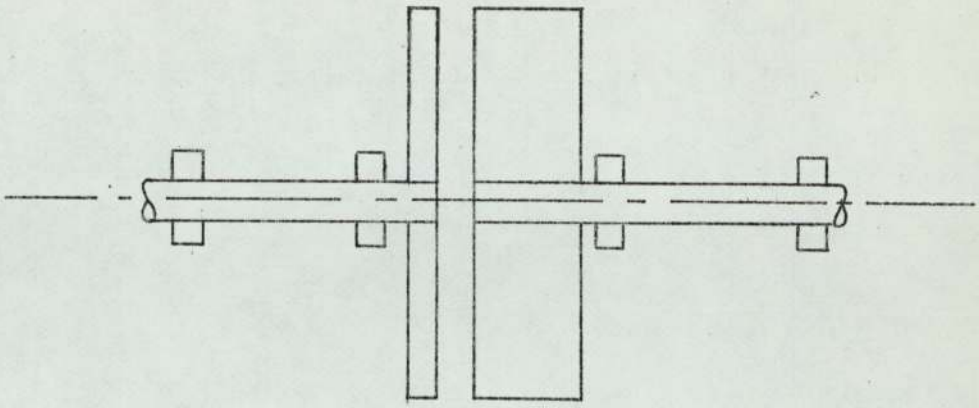

Fig. 3.1 Primitive Disc Machine

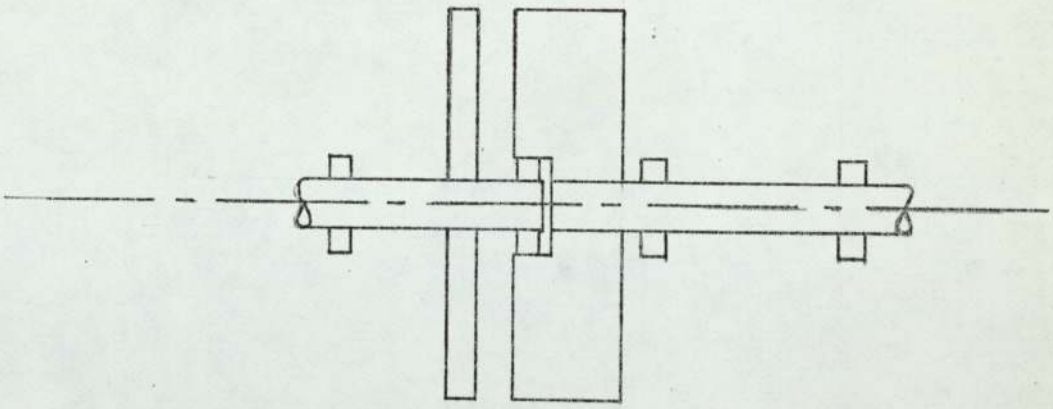

Fig. 3.2 Primitive Disc Machine with Pilot Bearing

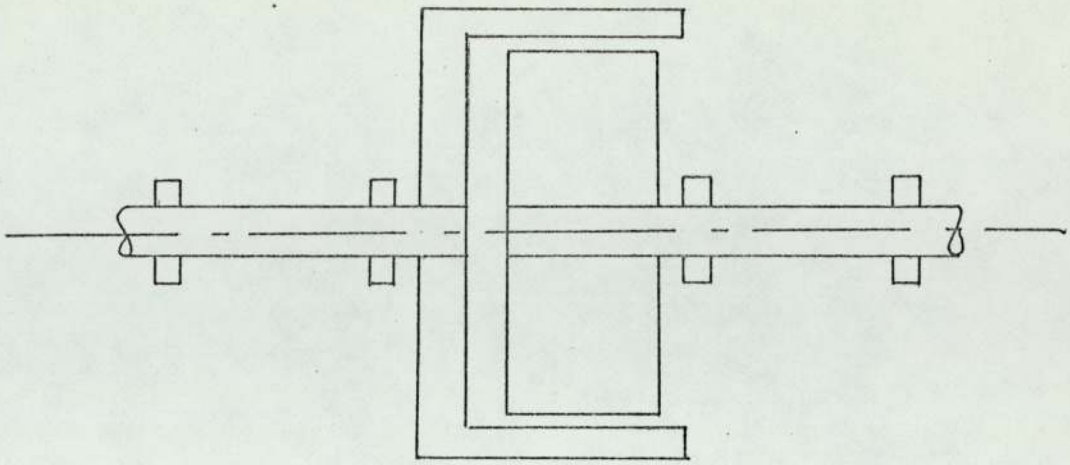

Fig. 3.3 Primitive Drum Machine

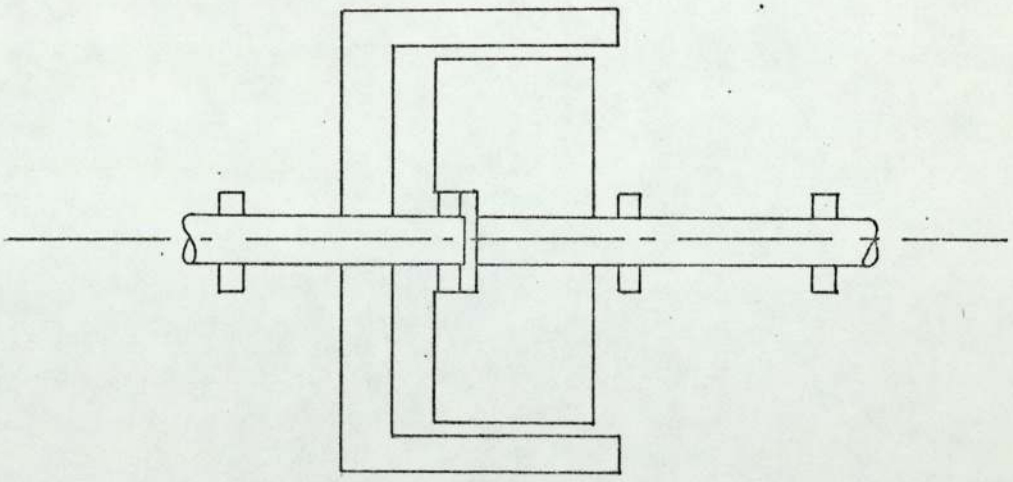

Fig. 3.4 Primitive Drum Machine with Pilot Bearing

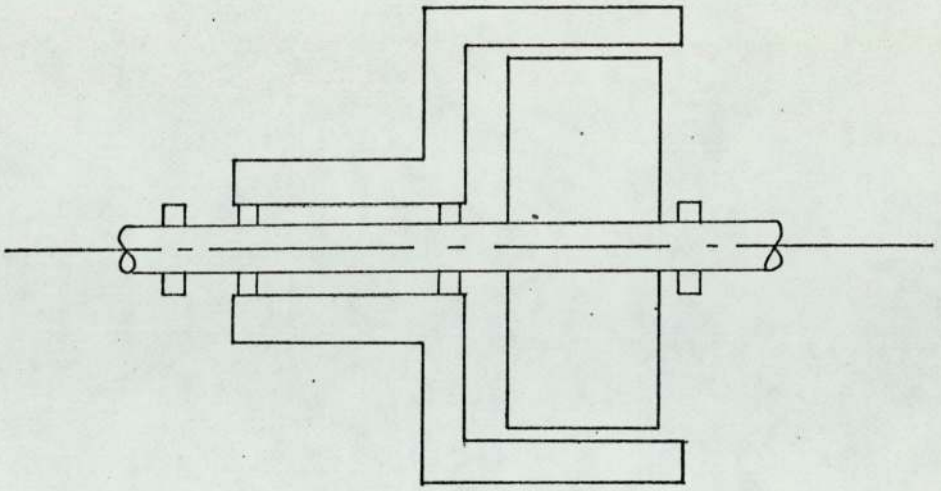

Fig. 3.5 Drum Coupling with Quill Shaft

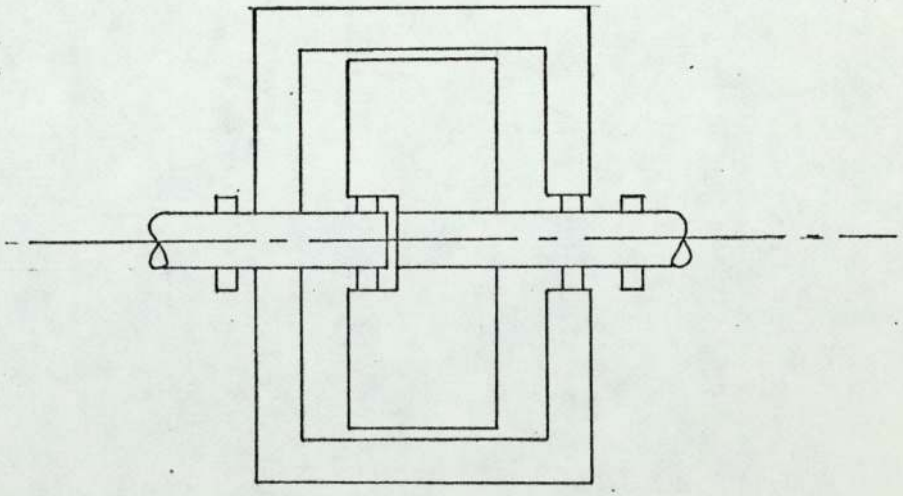

Fig. 3.6 Doubly Supported Drum Machine

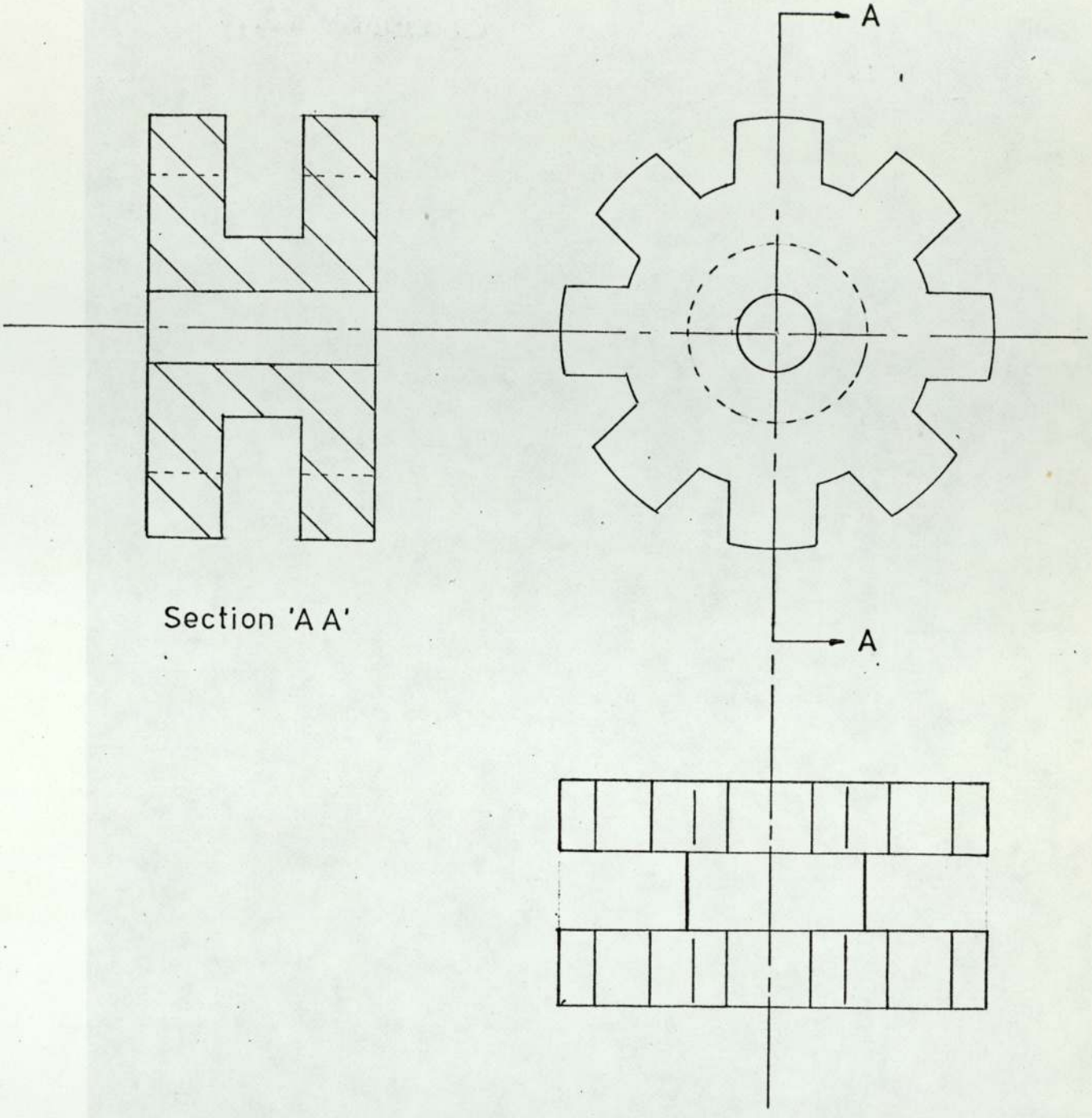

Fig. 3·7 Inductor Type Rotor

Fig. 3.9(a) Total and Fundamental Flux vs. Tooth Width/ Tooth Pitch Ratio.

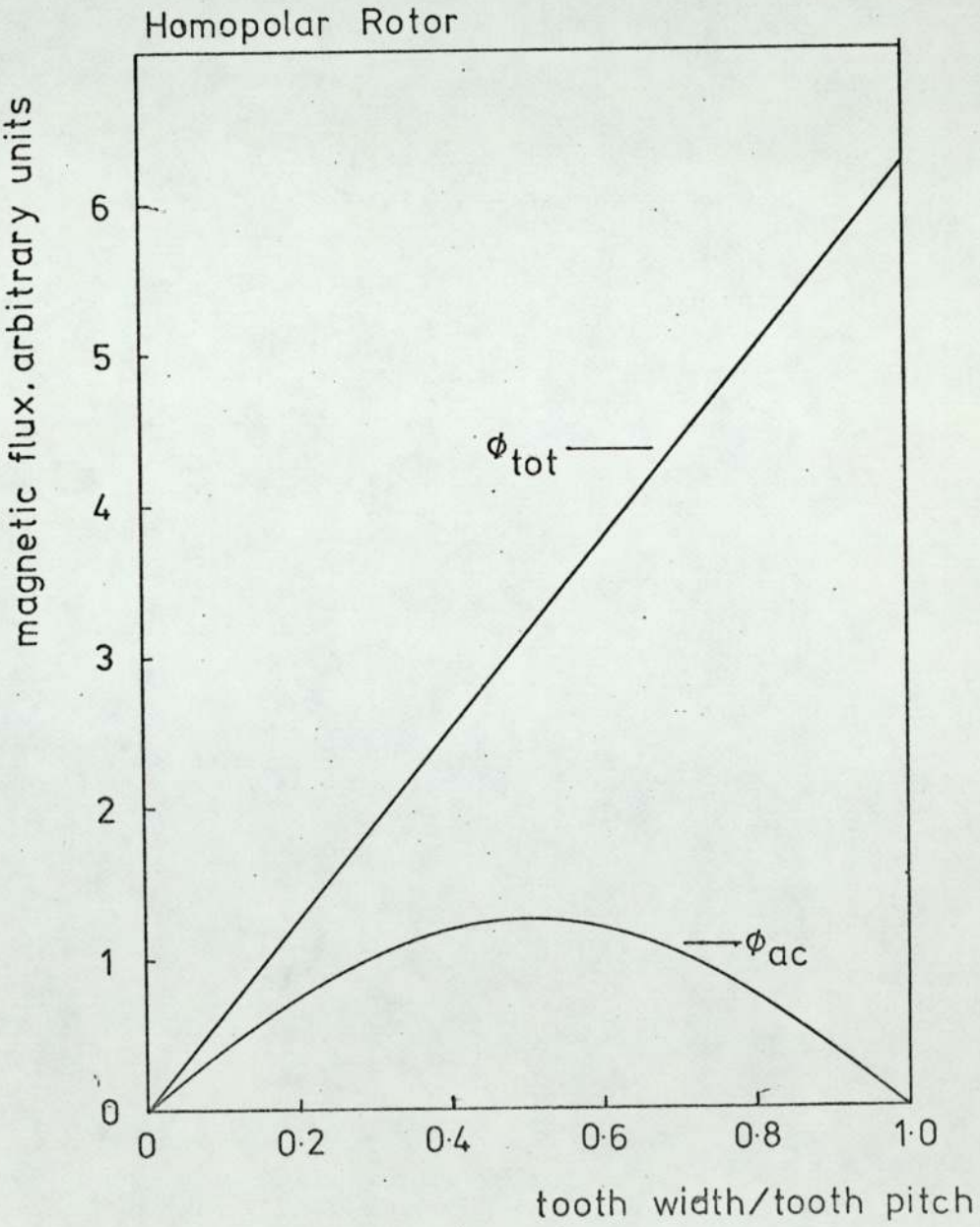

Fig. 3.9(b) Flux Utilization Coefficients for Different Slot Depth-Airgap Length Ratios.

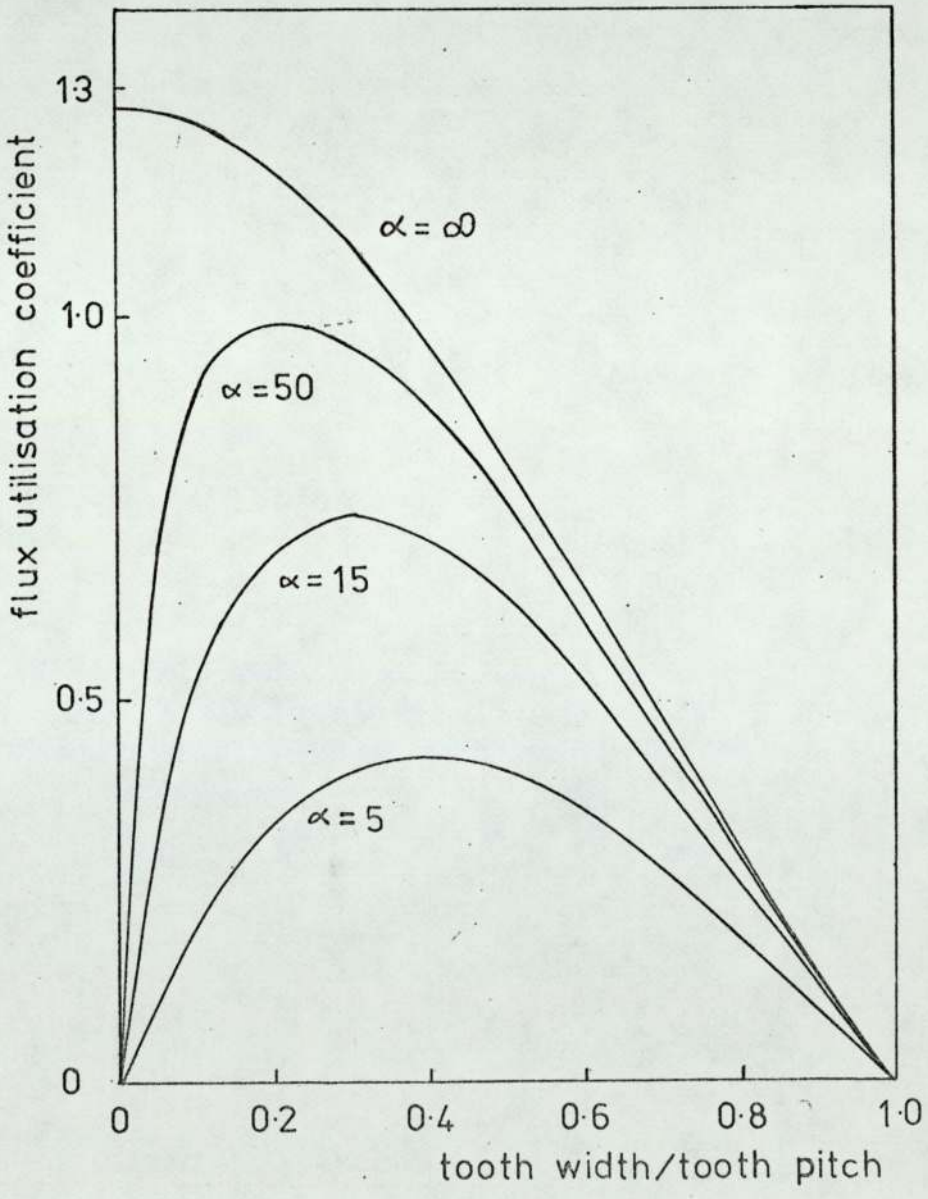

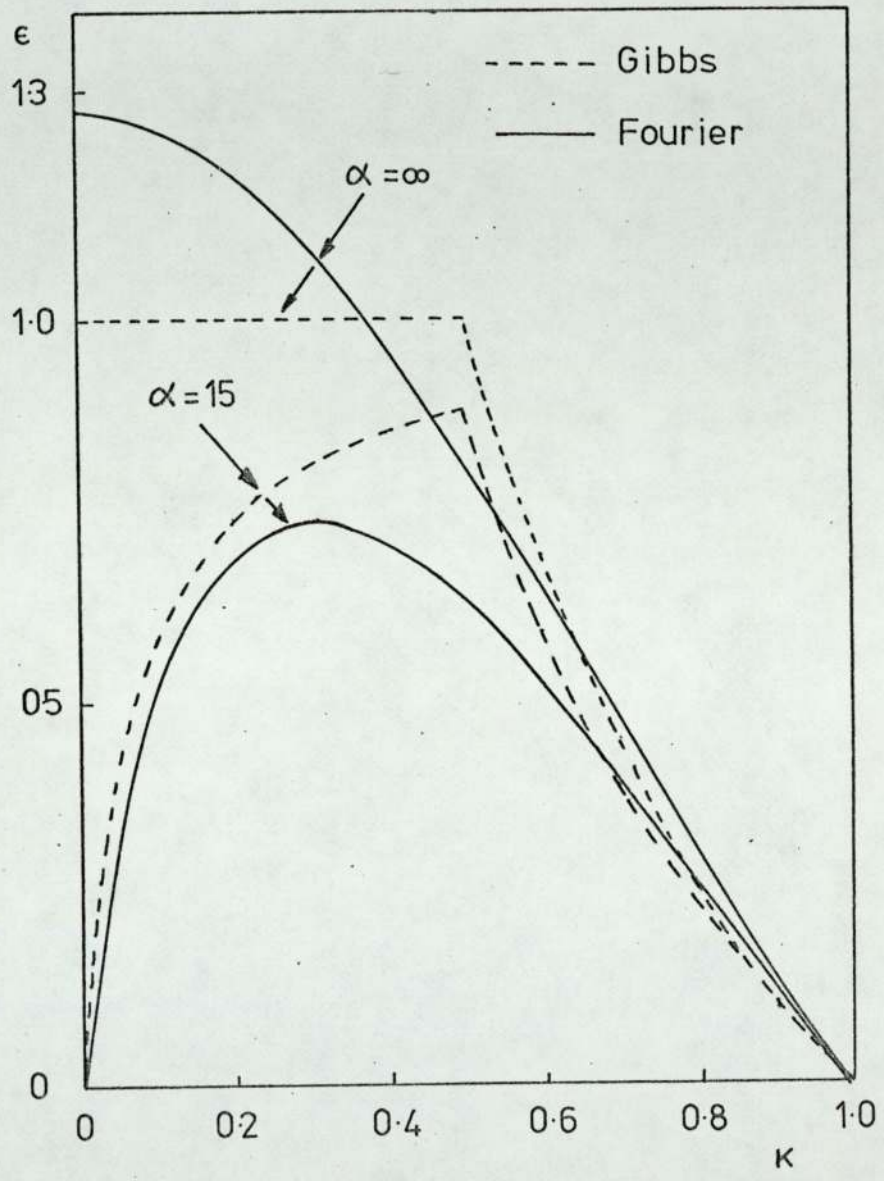

Fig. 3.11 Alternative Flux Utlization Coefficients

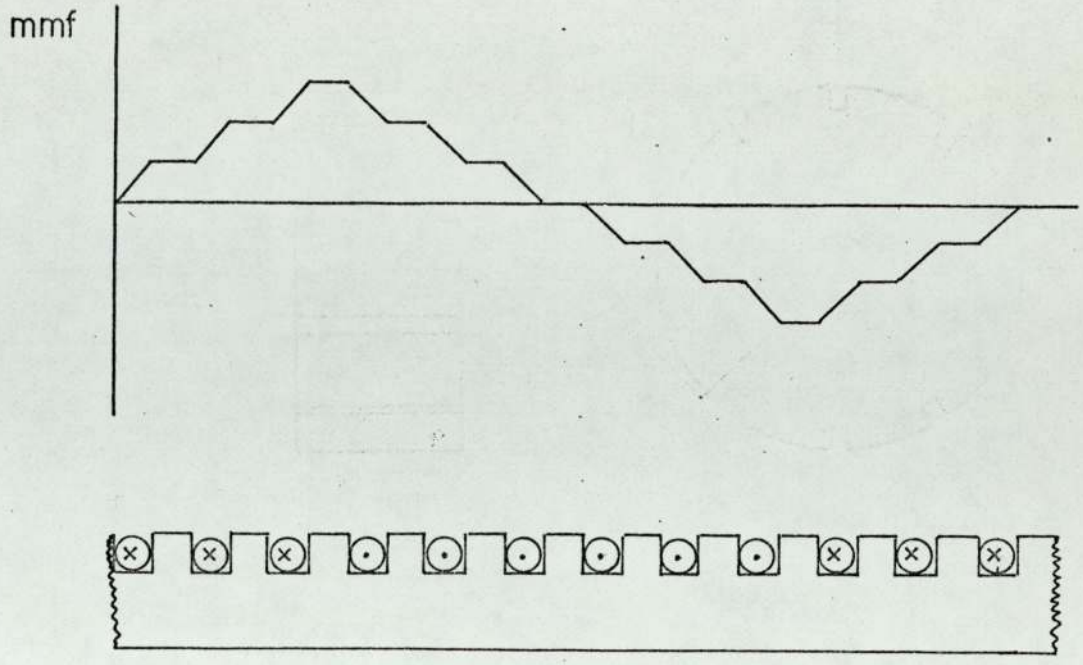

Fig. 3.12 Distributed Winding Rotor;
MMF Wave and Developed View of Rotor Slots.

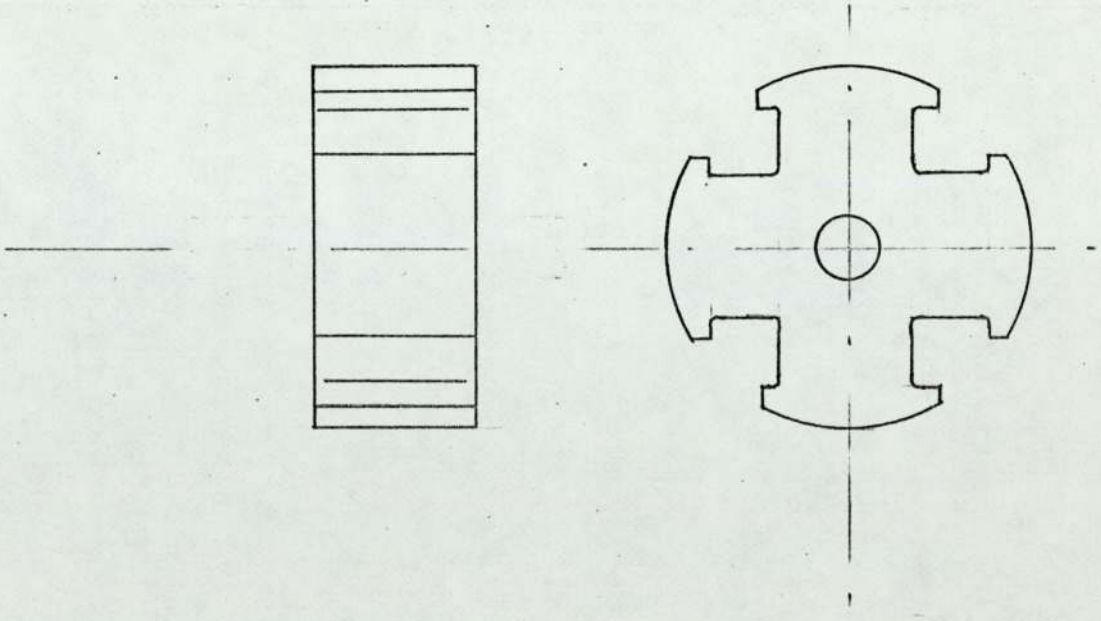

Fig. 3.13 Salient Pole Rotor.

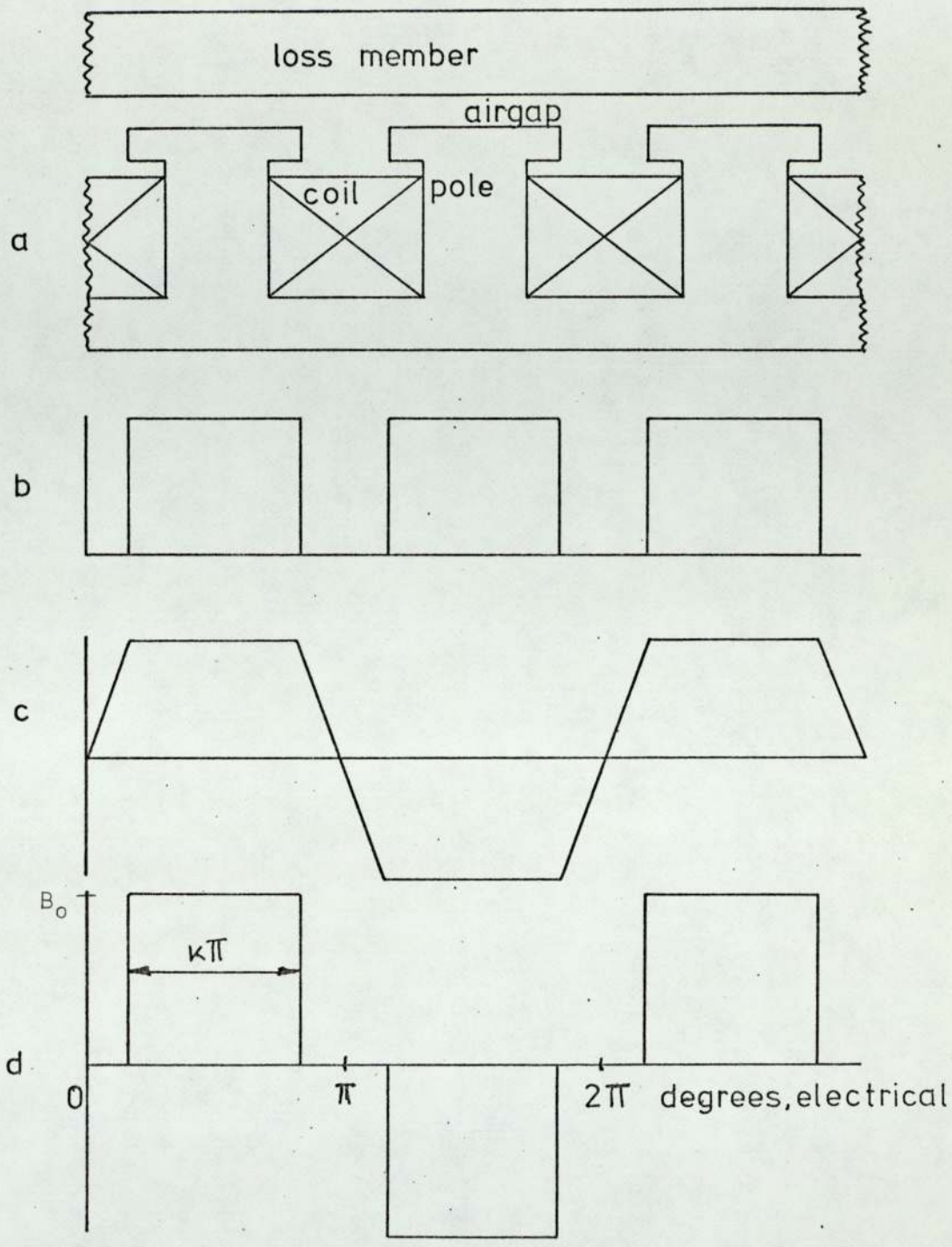

Fig. 3.14 Salient Pole Rotor

(a) developed airgap region

(b) permeance wave

(c) m.m.f. wave

(d) flux density wave

Total and Fundamental Flux

and Flux Utilisation Coefficient (ϵ)

variation with

Pole Arc - Pole Pitch Ratio

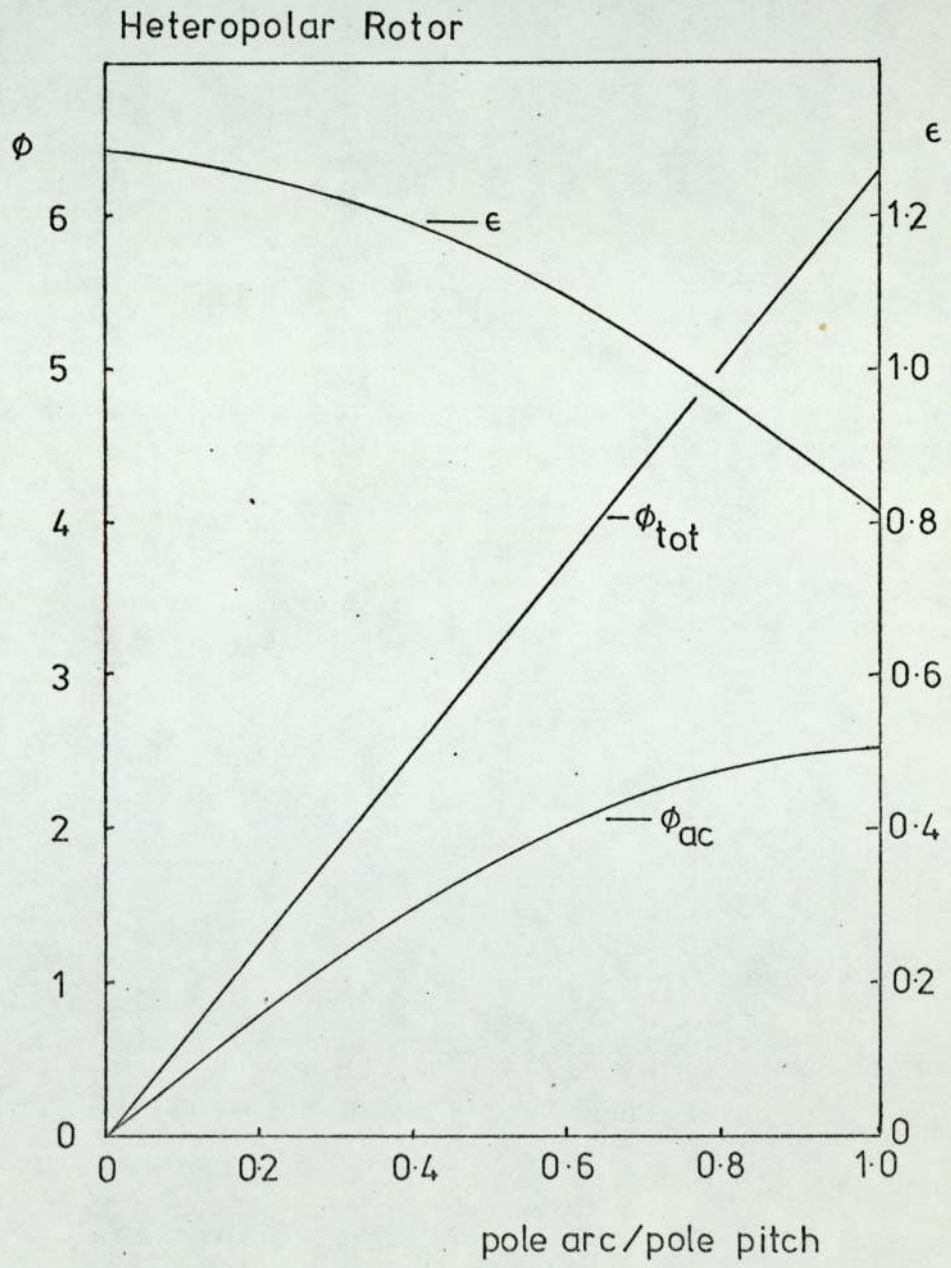

Fig. 3·15

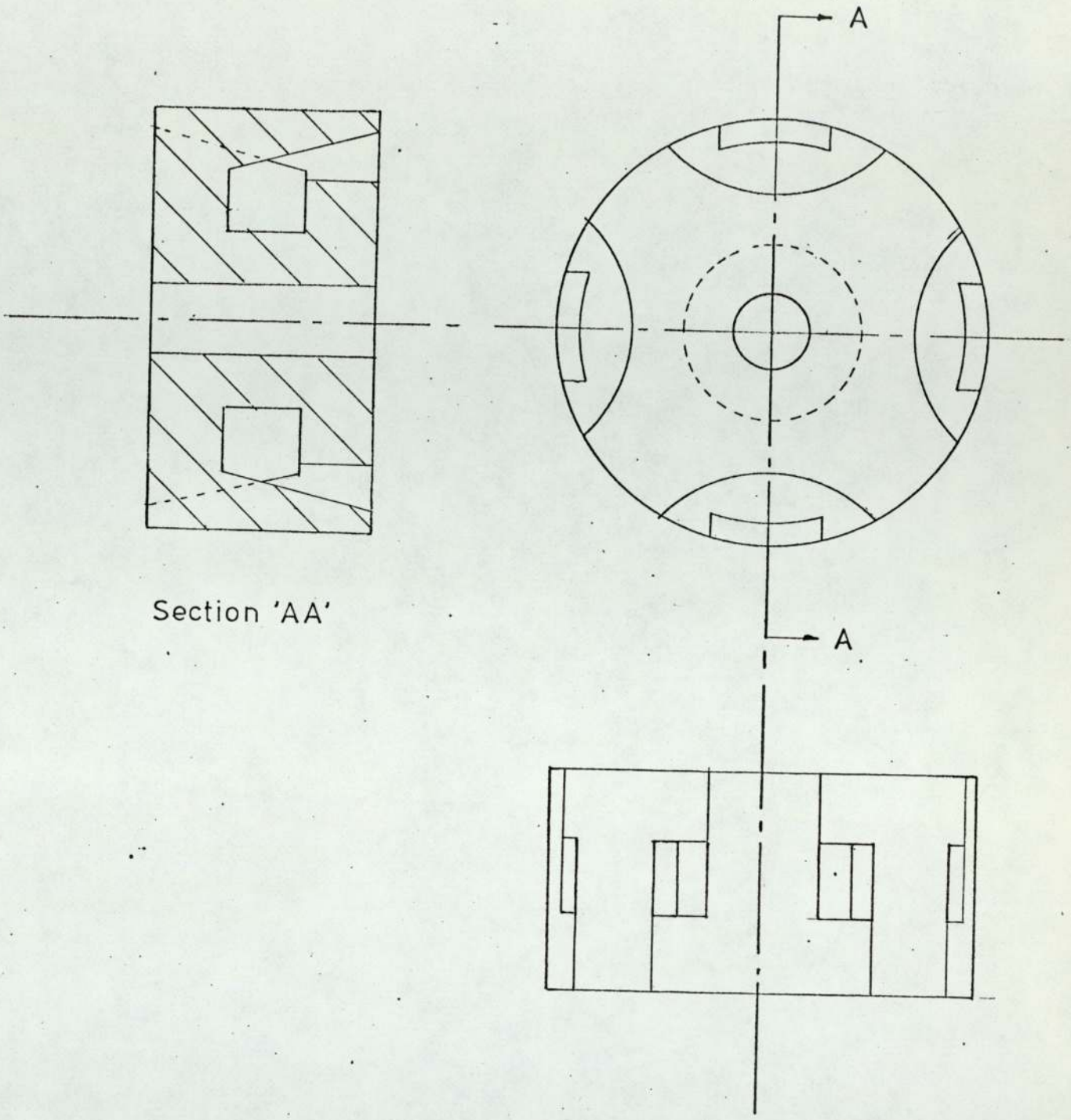

Fig. 3·16 Lundell Rotor

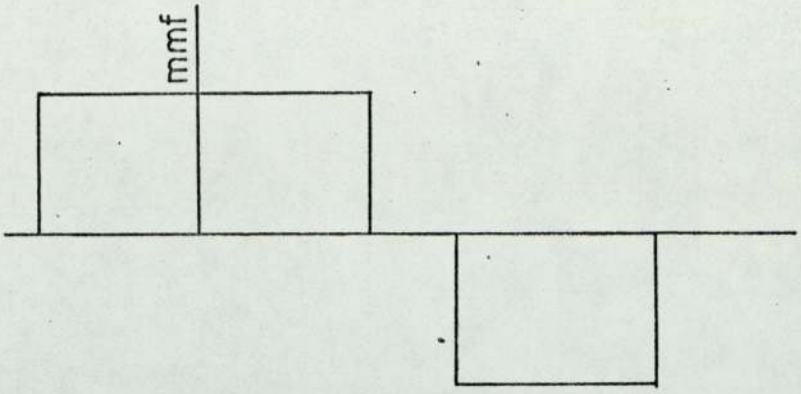

Fig. 3.17 Unbalanced M.M.F. Wave

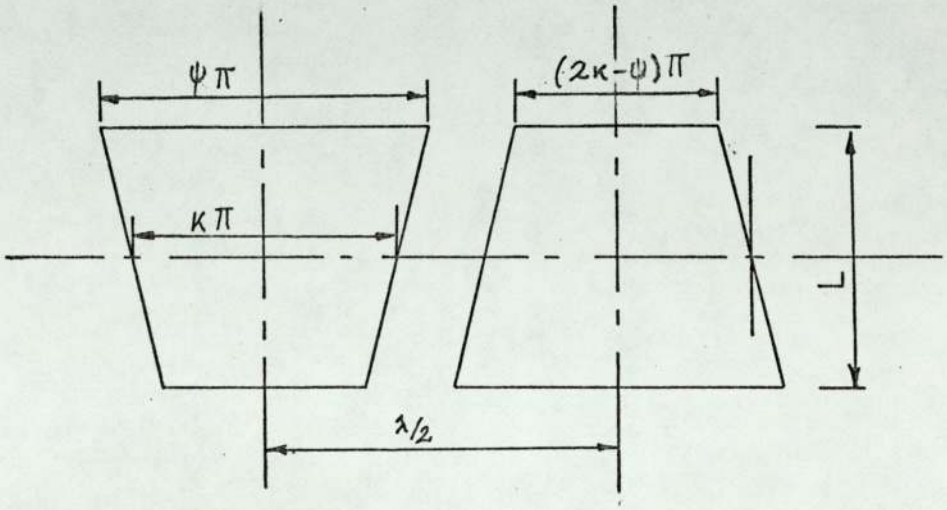

Fig. 3.18 Tapered Poles

ψ	ϵ	$\epsilon_{p.u.}$	$T_{p.u.}$
0·7	1·03	1·0	1·0
0·8	1·02	0·99	0·97
0·9	1·00	0·97	0·91
1·0	0·96	0·93	0·80
1·2	0·83	0·82	0·53
1·4	0·66	0·64	0·26

for $\kappa = 0{\cdot}7$

Fig. 3.19 The Effect of Tapering the Poles

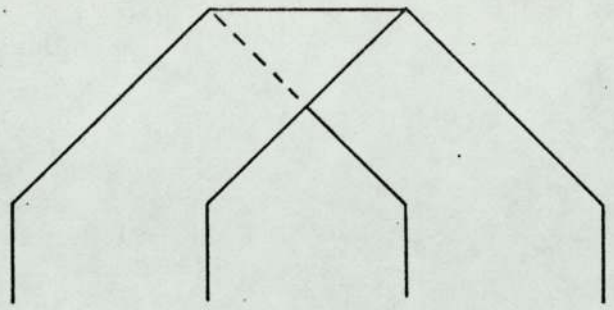

(a)

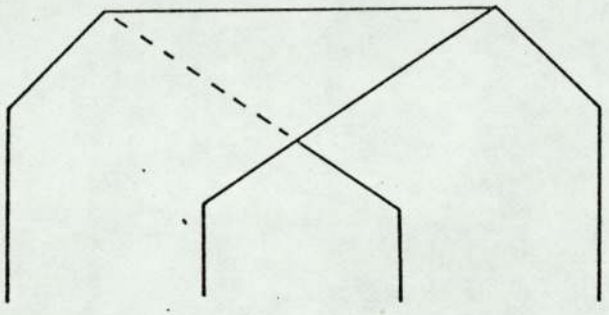

(b)

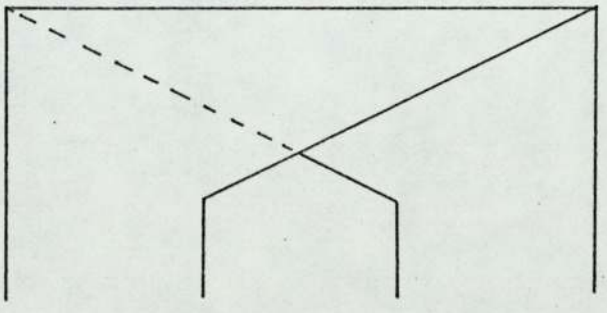

(c)

Fig. 3.20 Lundell Rotor Pole Shapes.

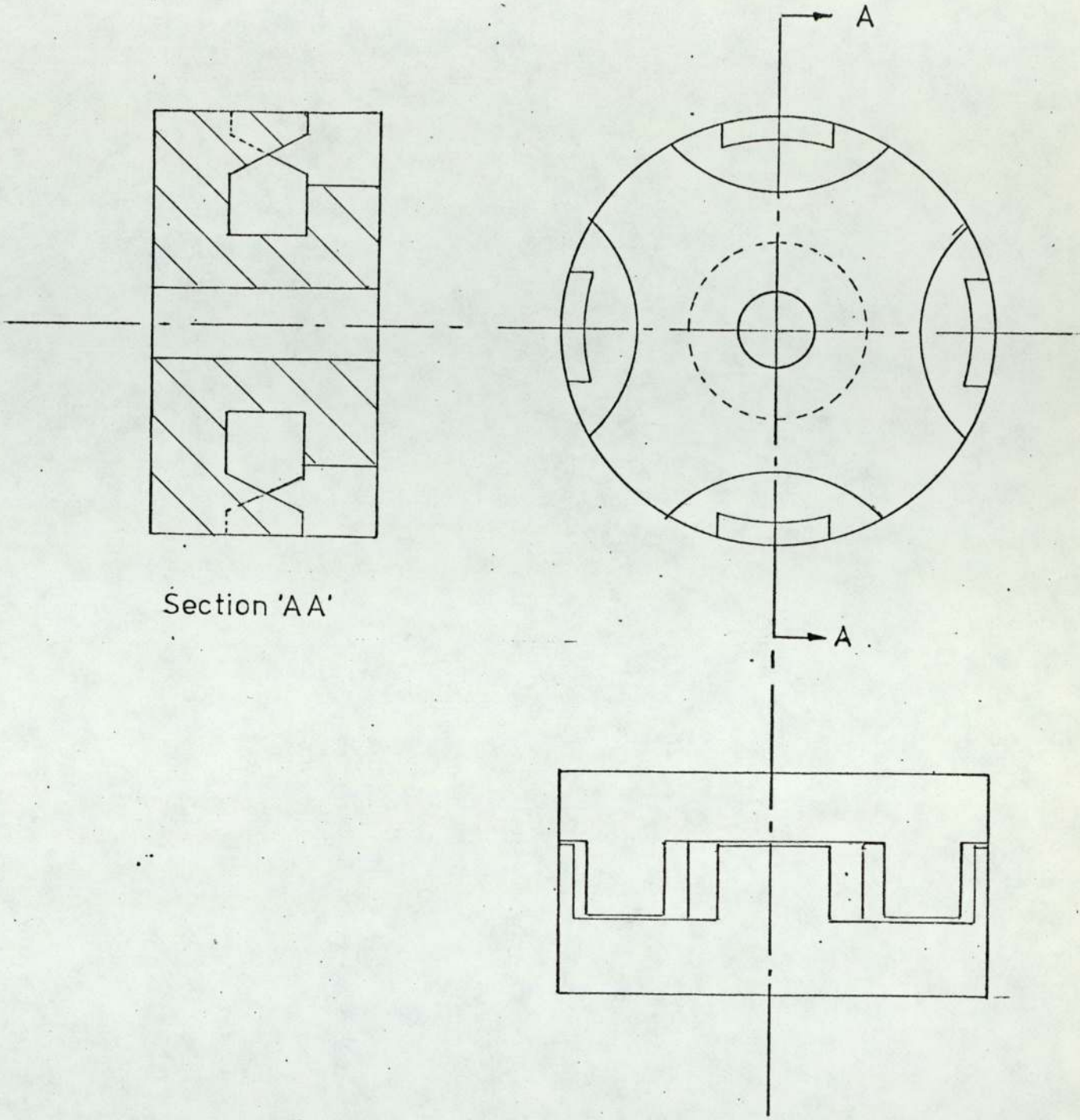

Fig. 3·21 Partially Interdigitated Rotor

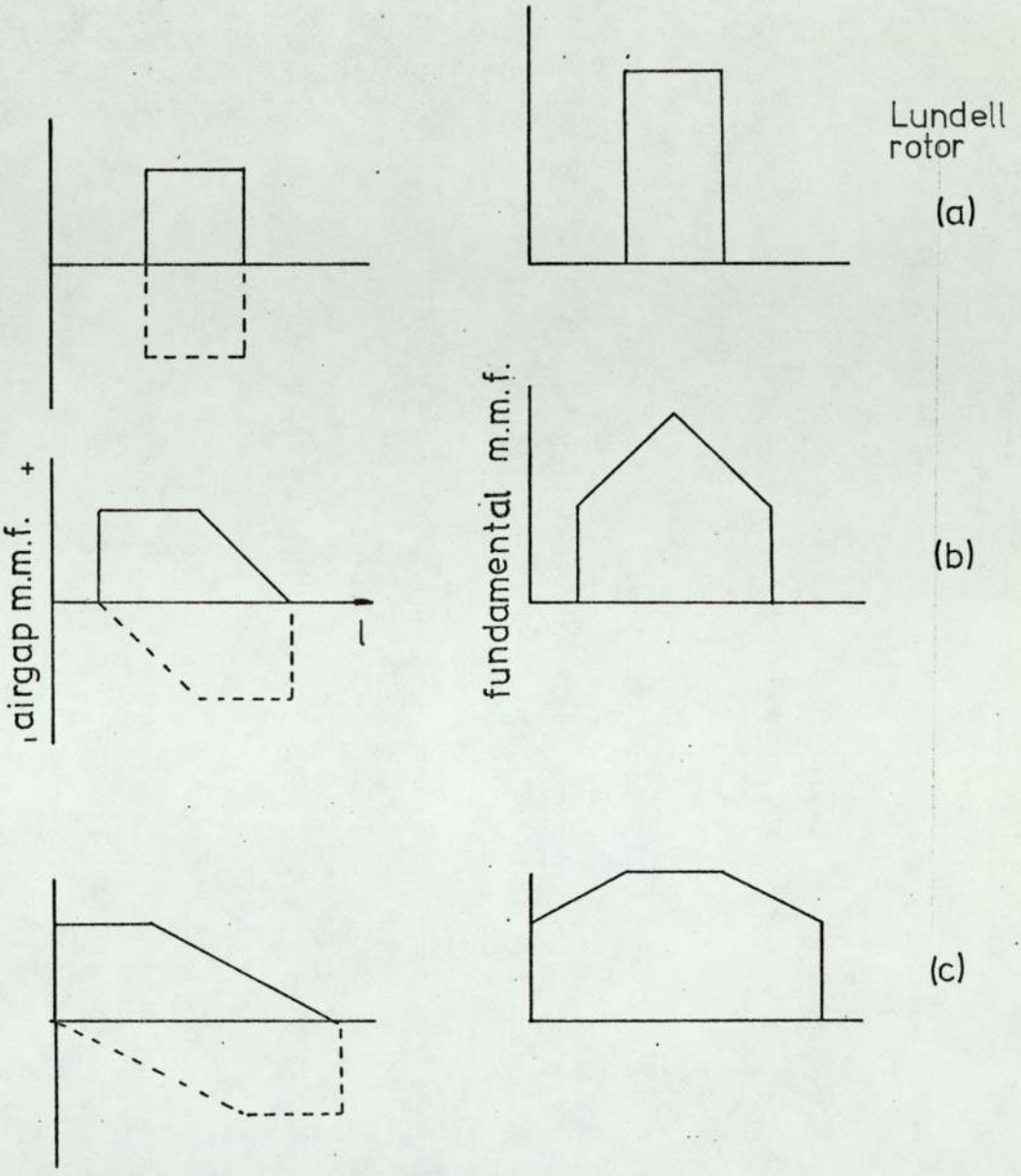

Fig. 3.23 Assumed Axial M.M.F. Distribution
(Lundell Rotor)

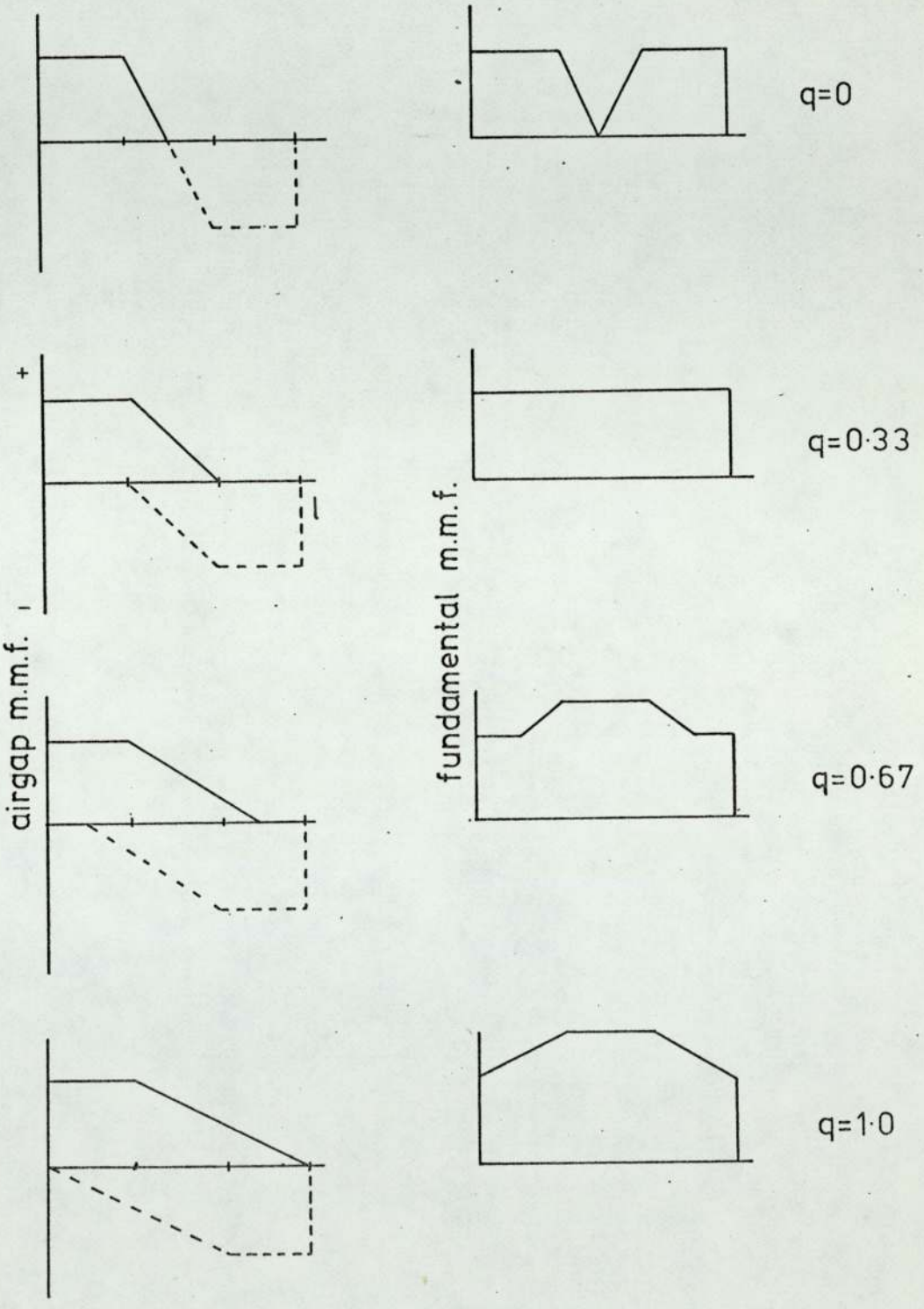

Fig. 3.24 Assumed Axial M.M.F. Distribution (P.I. Rotor)

MAX. TORQUE vs. DEGREE OF INTERDIGITATION OF P.I. ROTOR

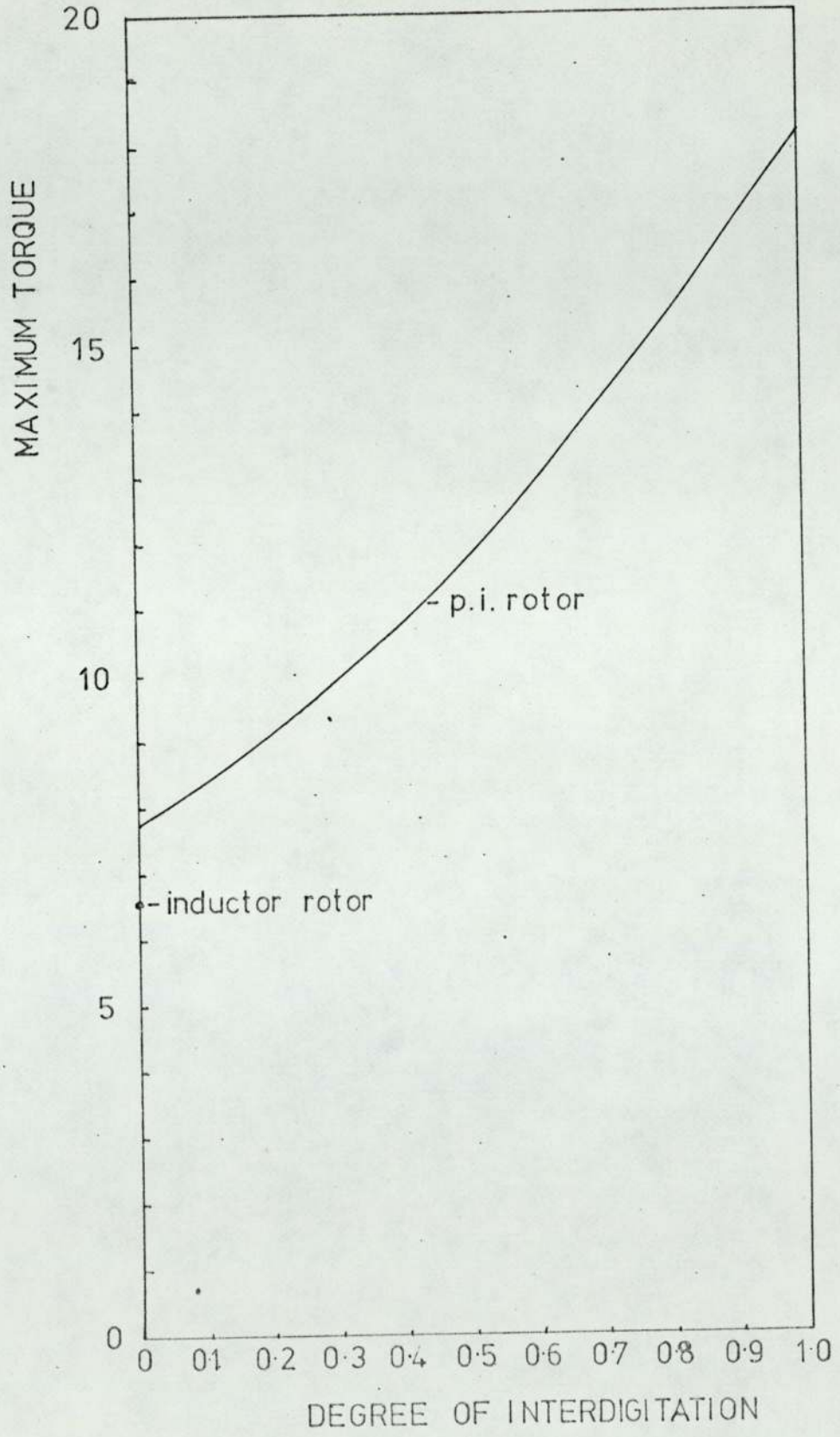

FIG. 3.25

Airgap & Leakage Permeances vs. κ

Salient Pole Rotor

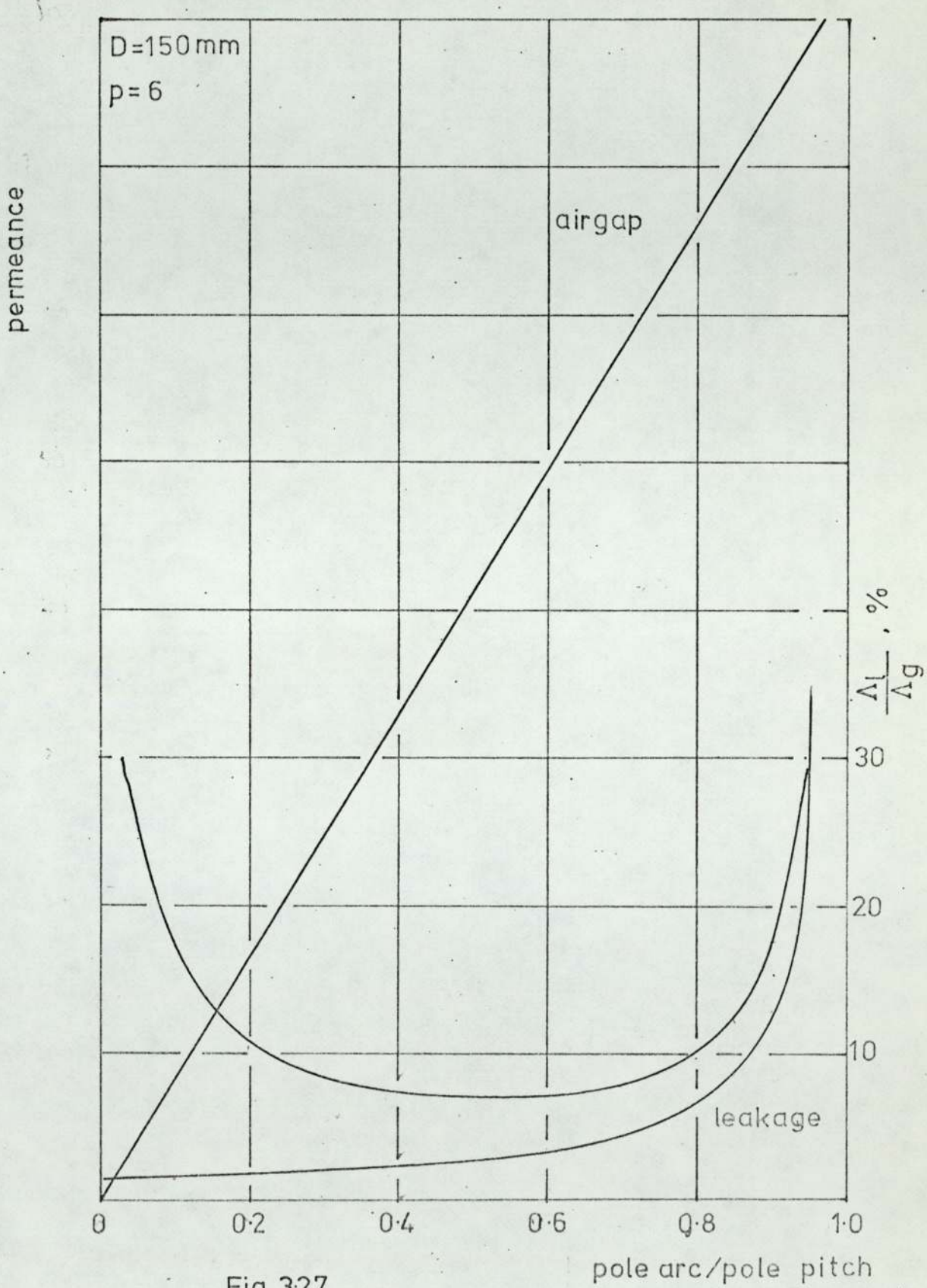

Fig. 3·27

Airgap & Leakage Permeances

Lundell Rotor

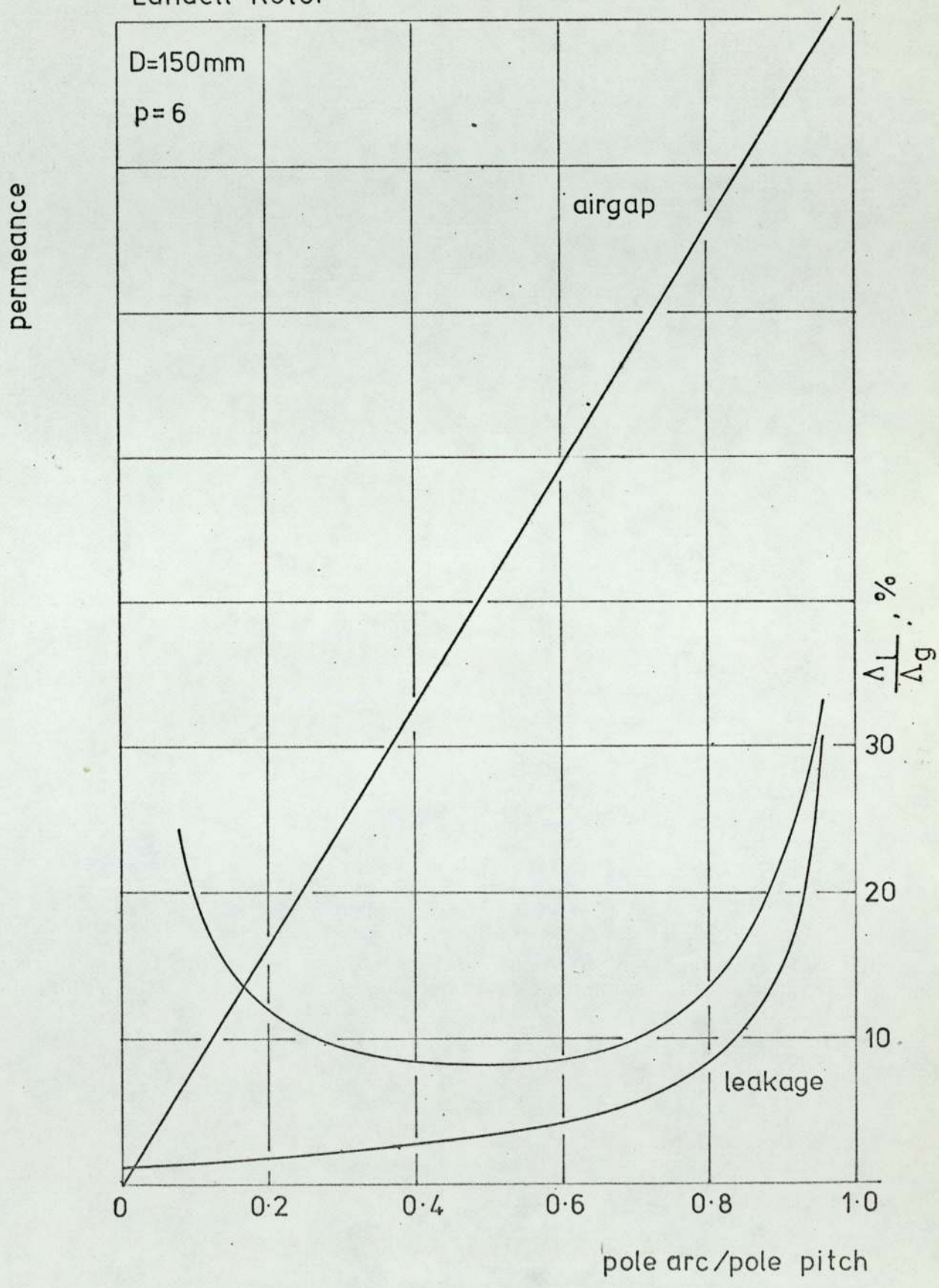

Fig. 3·30

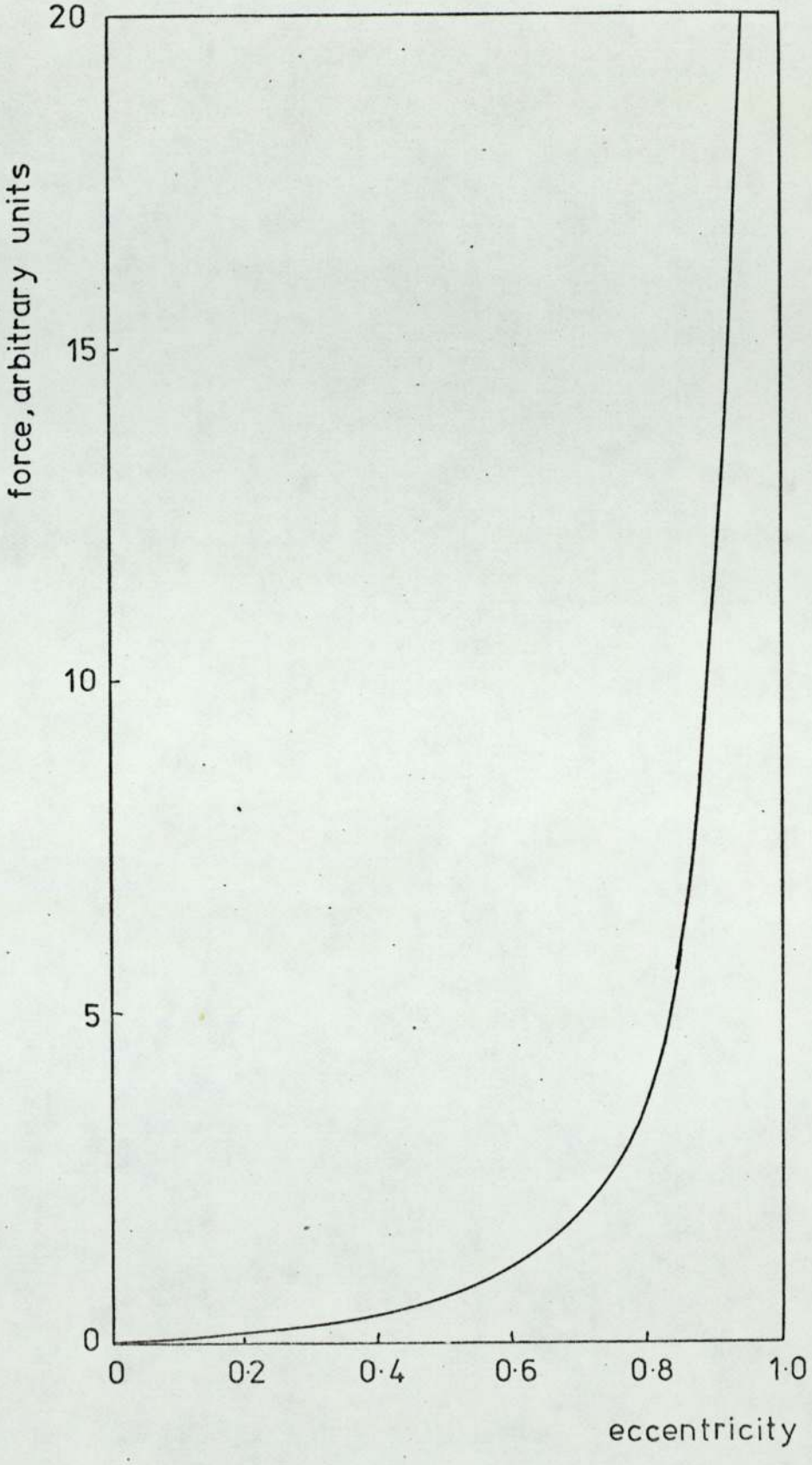

Fig. 3.32 Unbalanced Magnetic Pull vs. Eccentricity

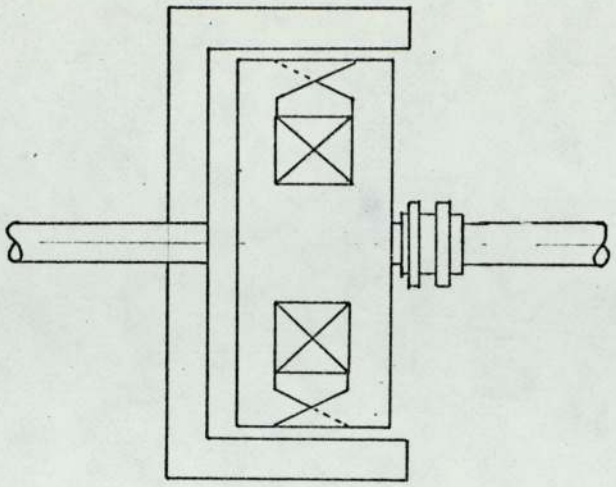

Fig. 3.33 Simple Rotating Coil Machine

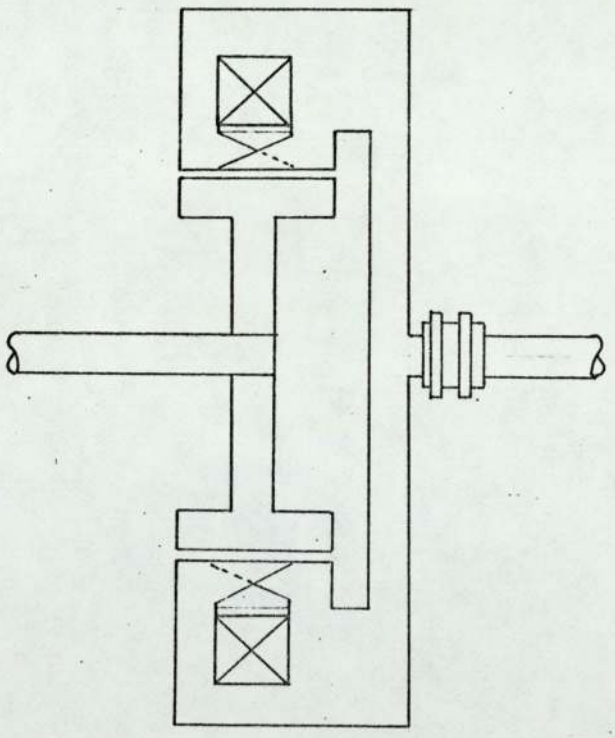

Fig. 3.34 Simple Rotating Coil Machine

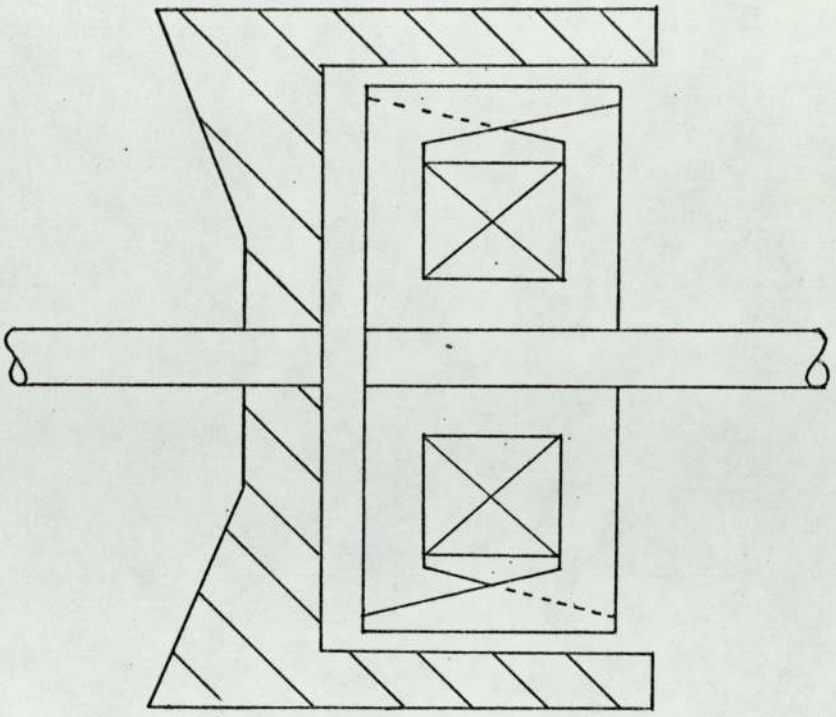

(a) rotating coil coupling

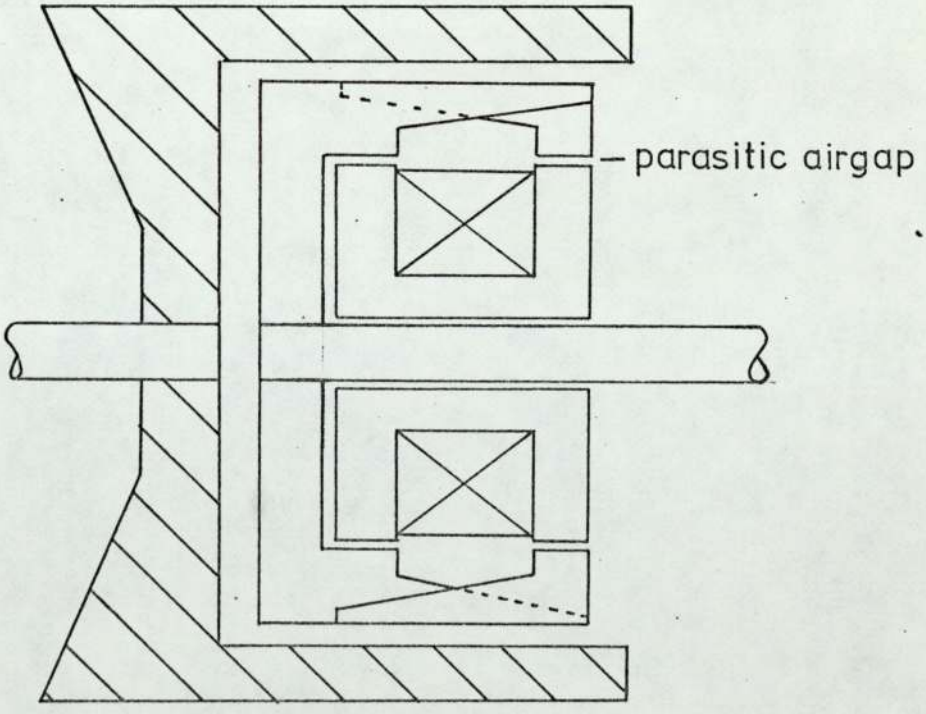

(b) brushless coupling

Fig. 3.37 Couplings with Identical Active Dimensions.

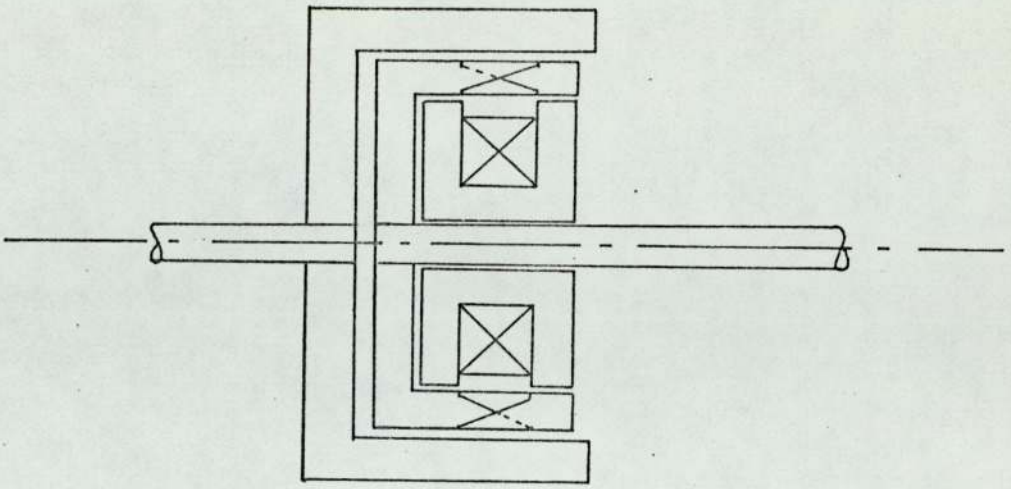

Fig. 3.38 Simple Brushless Coupling

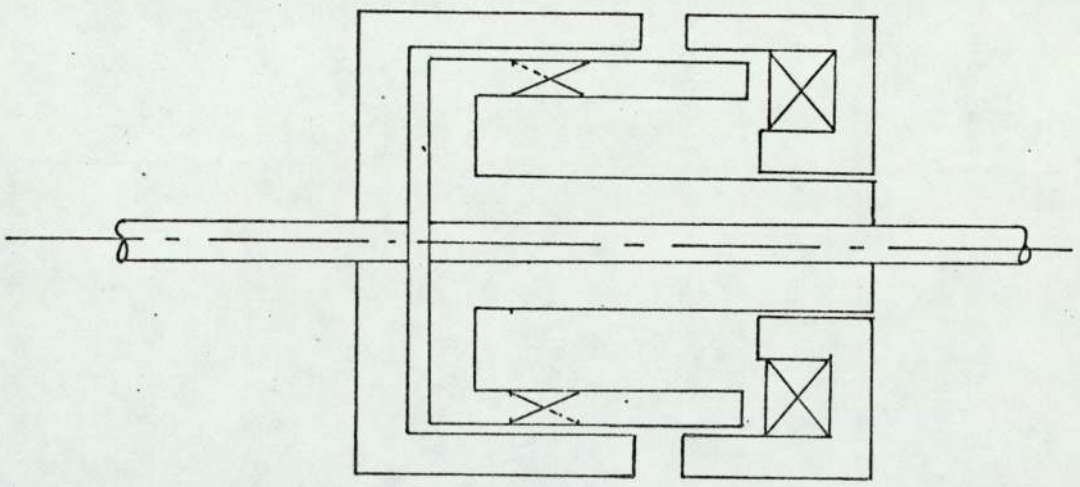

Fig. 3.39 Quill Type Brushless Coupling

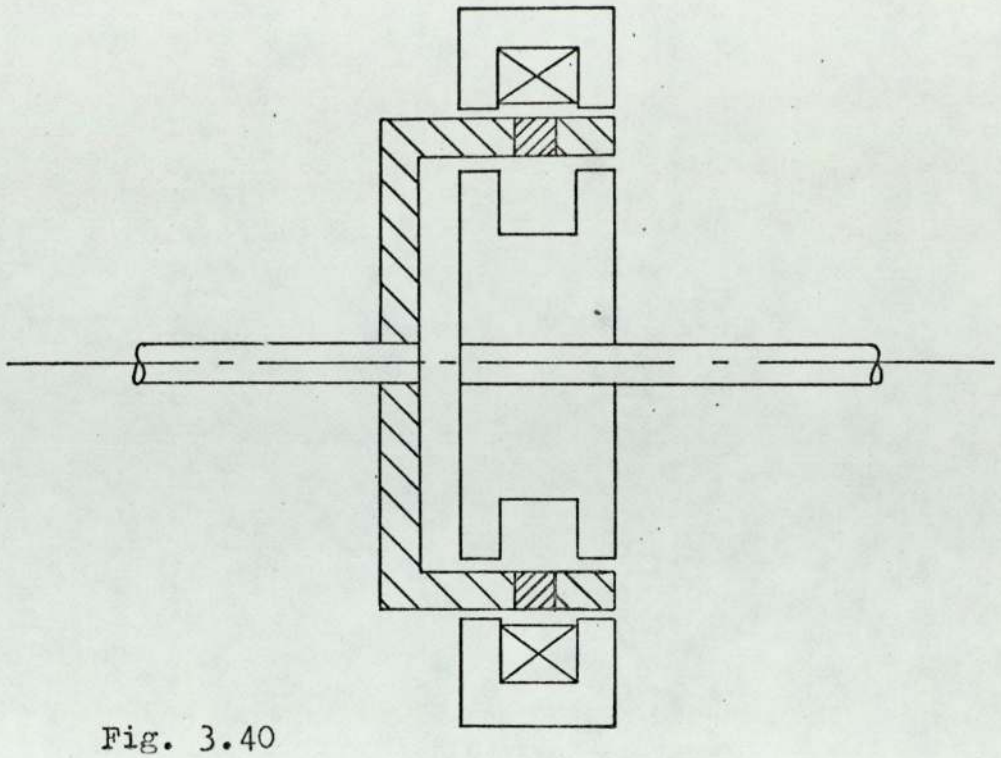

Fig. 3.40

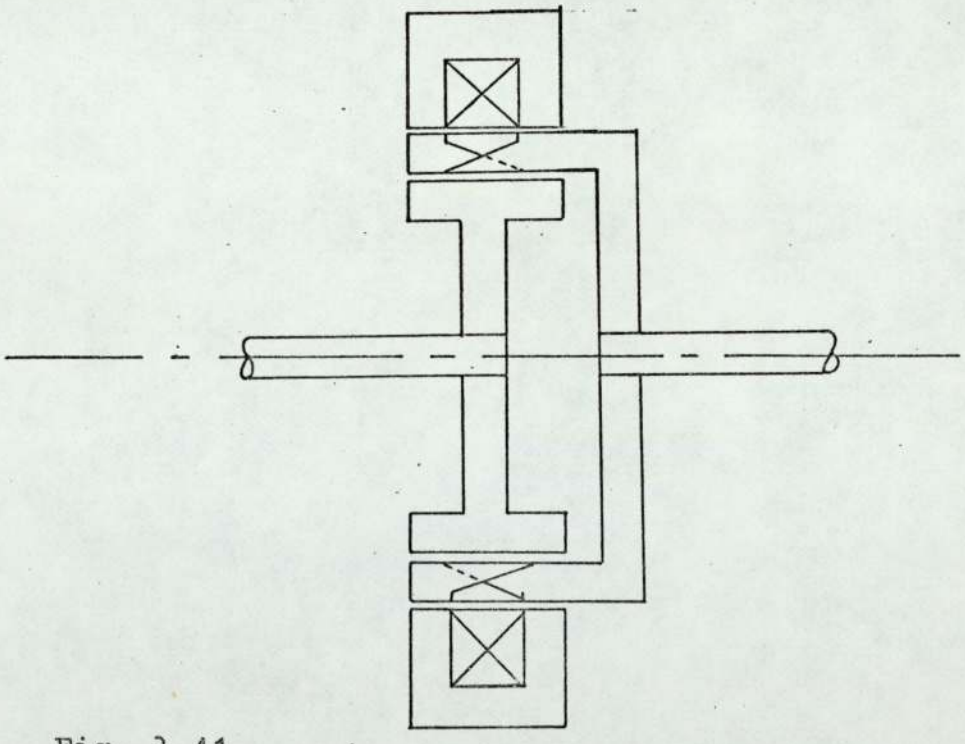

Fig. 3.41

Alternative Brushless Coupling Configurations.

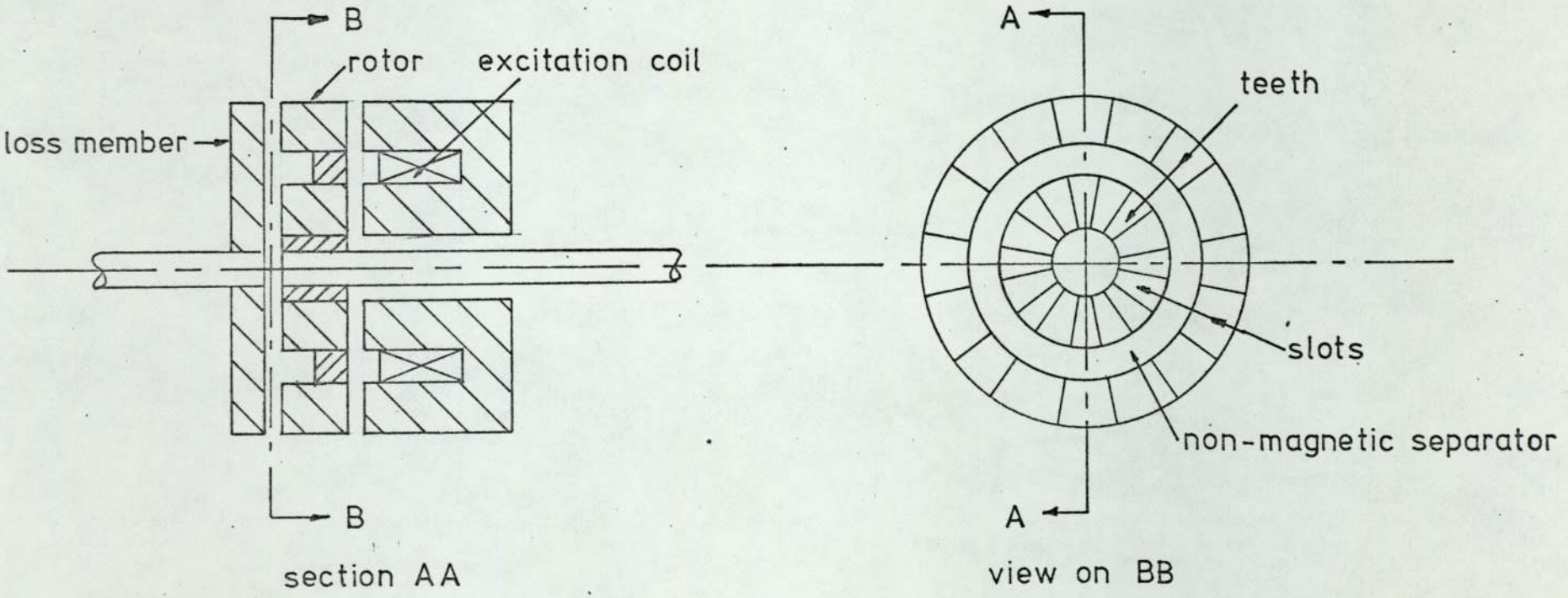

Fig. 3·42 Brushless, Inductor Type, Disc Coupling

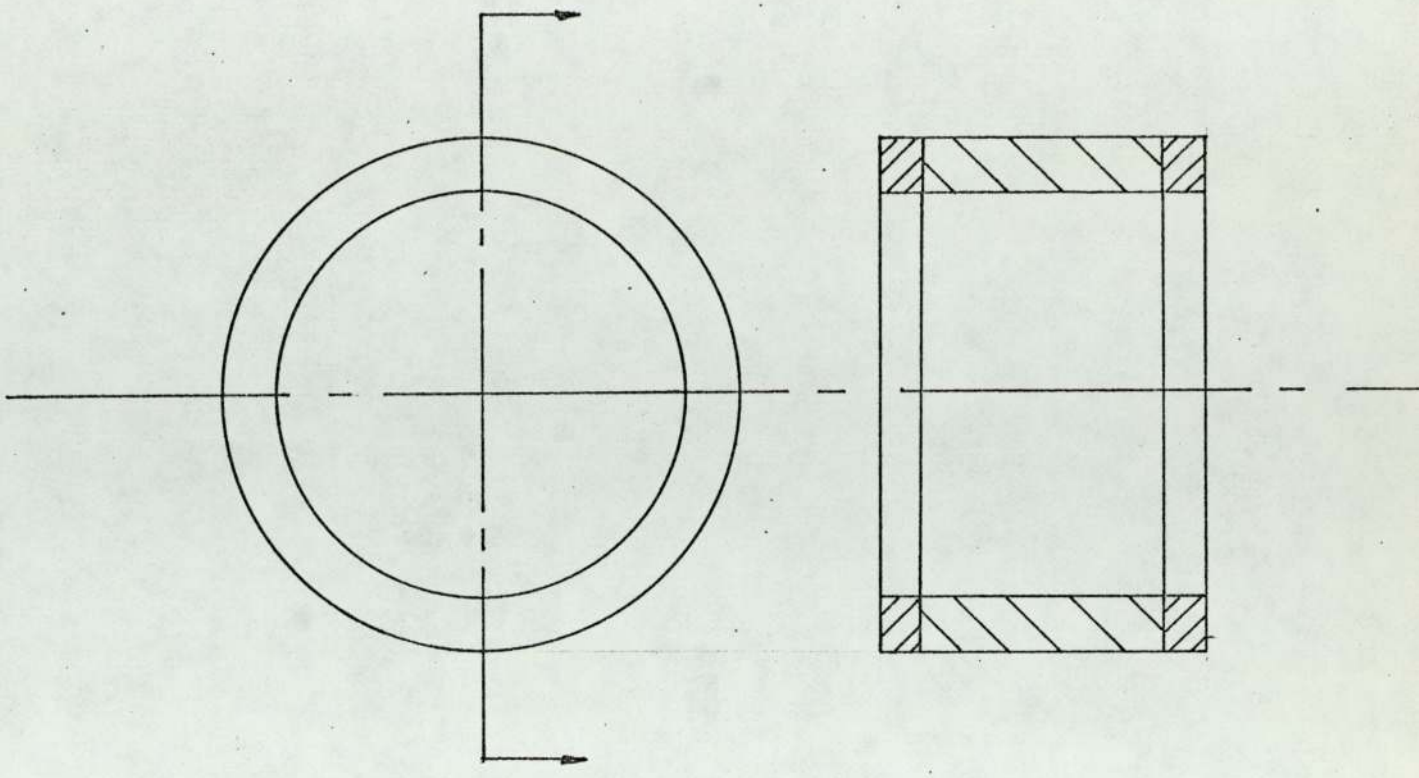

(a)

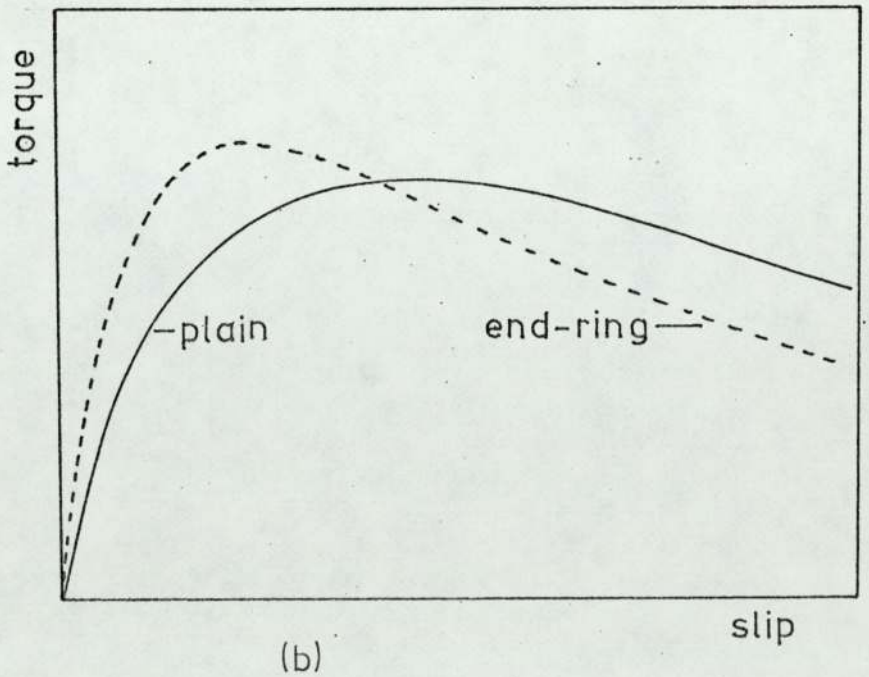

(b)

Fig. 3.44 End-Ring Loss Member

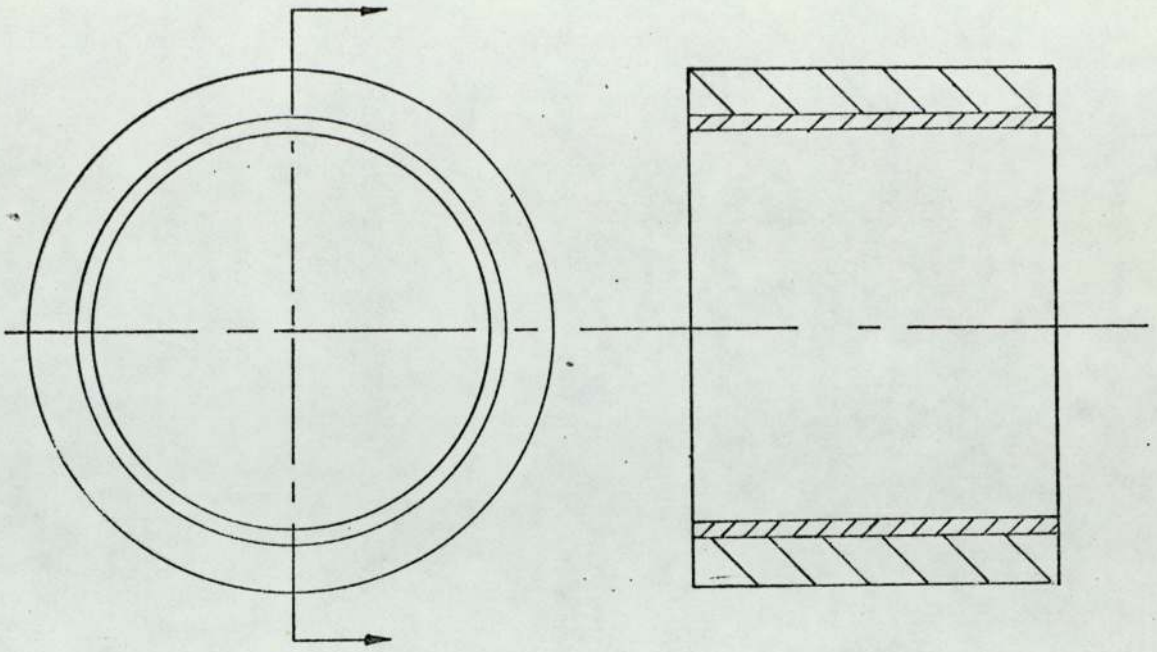

Copper Plated Loss Member

(a)

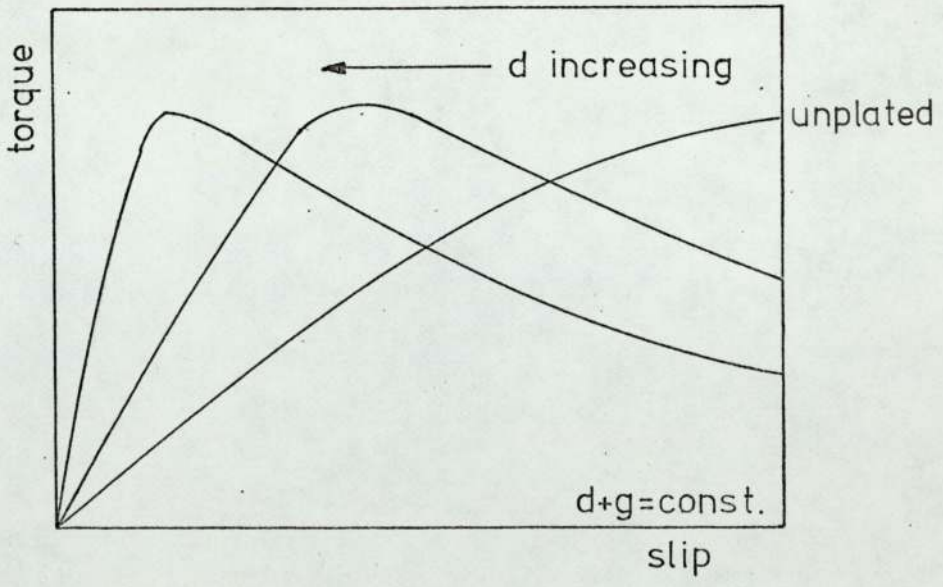

Effect of Copper Plating on Torque-Slip Curve

(b)

Fig. 3.45

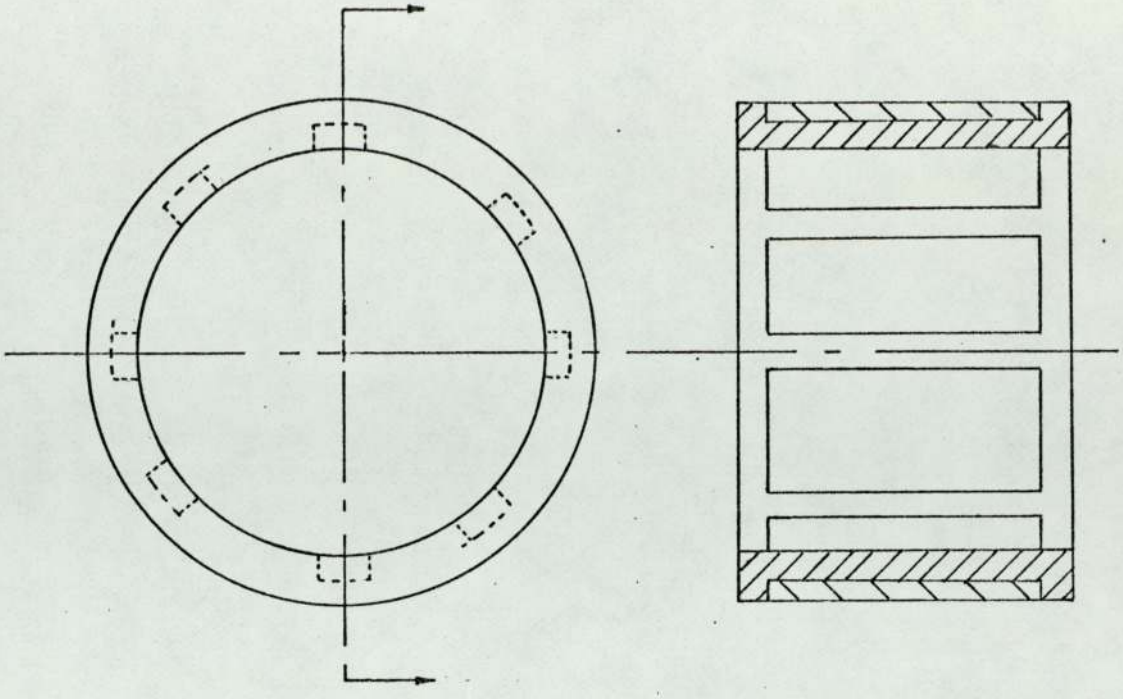

(a)

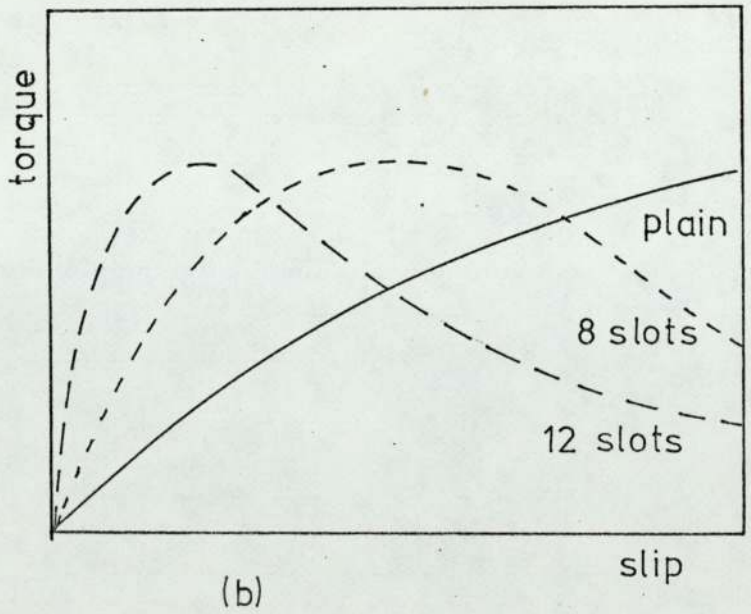

(b)

Fig. 3.46 Squirrel Cage Loss Member

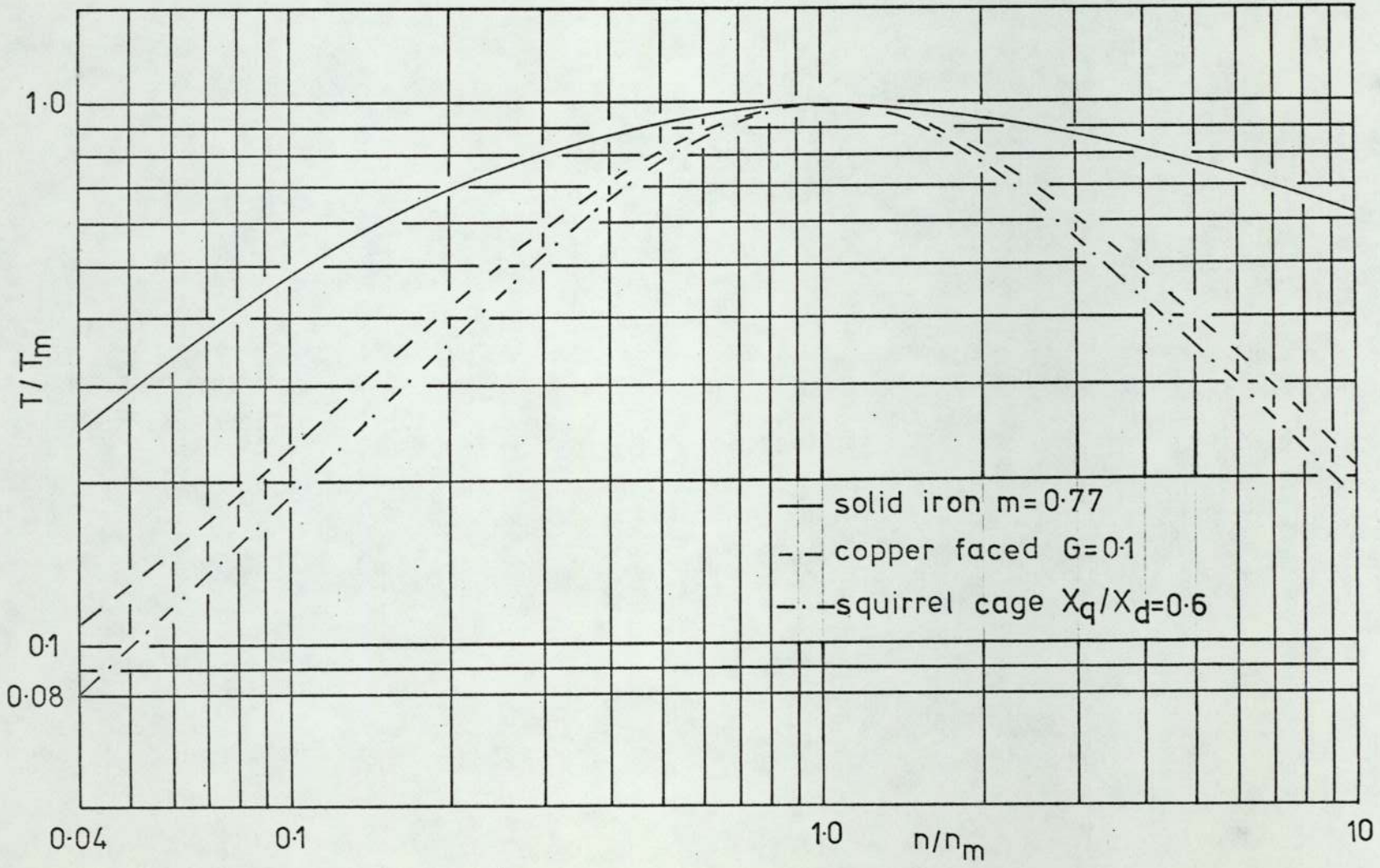

Fig. 3.47 Normalised Torque Slip Curves for Different Loss Members.

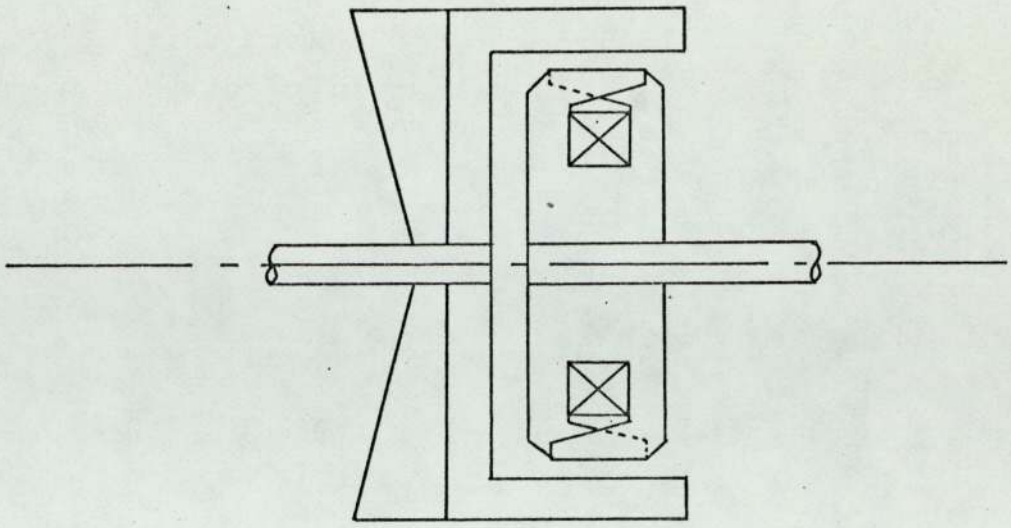

Fig. 3.48

Air Cooled Machine with Fan on Loss Member

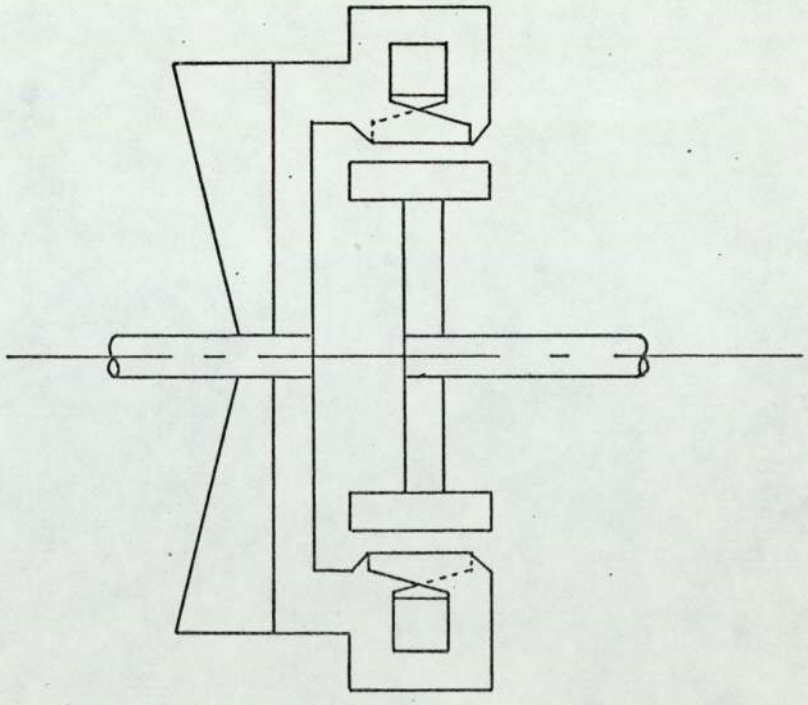

Fig. 3.49

Air Cooled Machine with Fan on Field Member

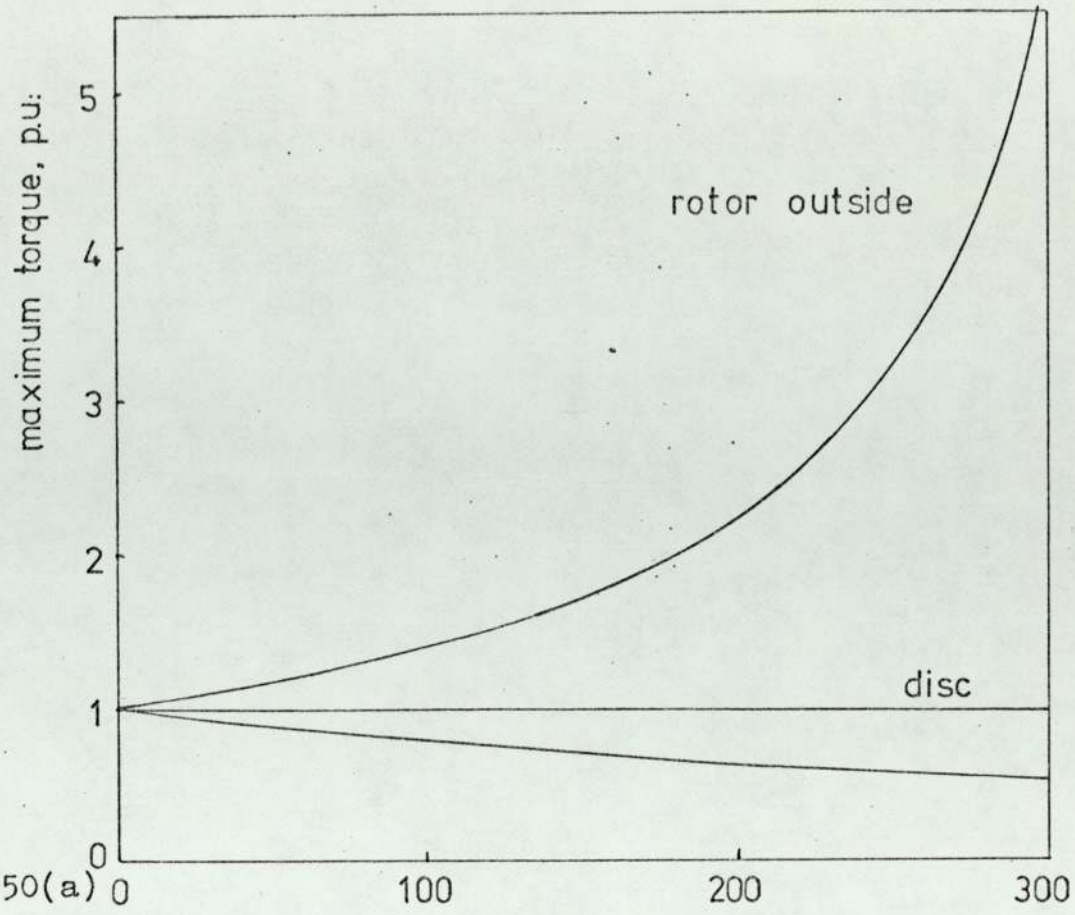

Fig. 3.50(a)

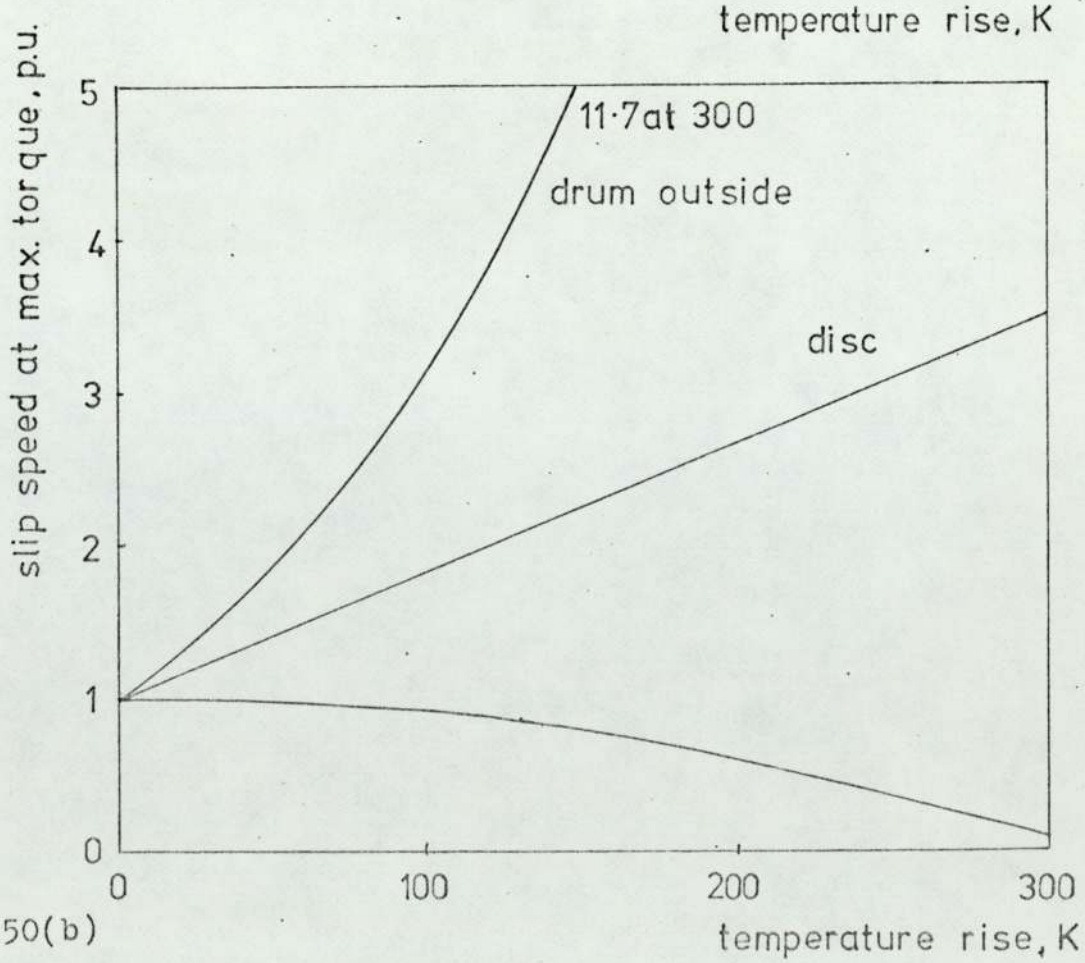

Fig. 3.50(b)

The Effect of Temperature upon Performance

Diameter mm	Airgap mm	Pole Pairs	λ mm	Torque per unit
140	0·23	4	109	0·25
200	0·32	6	105	1
280	0·45	8	109	4
400	0·64	12	105	16
560	0·91	16	109	64
800	1·28	24	105	256

Table 3·4 Variation of Prime Parameters with Size for Constant n_m

FIGURES FOR CHAPTER 4

Fig. 4.3 Comparative Torque-Time Response at Constant Slip.

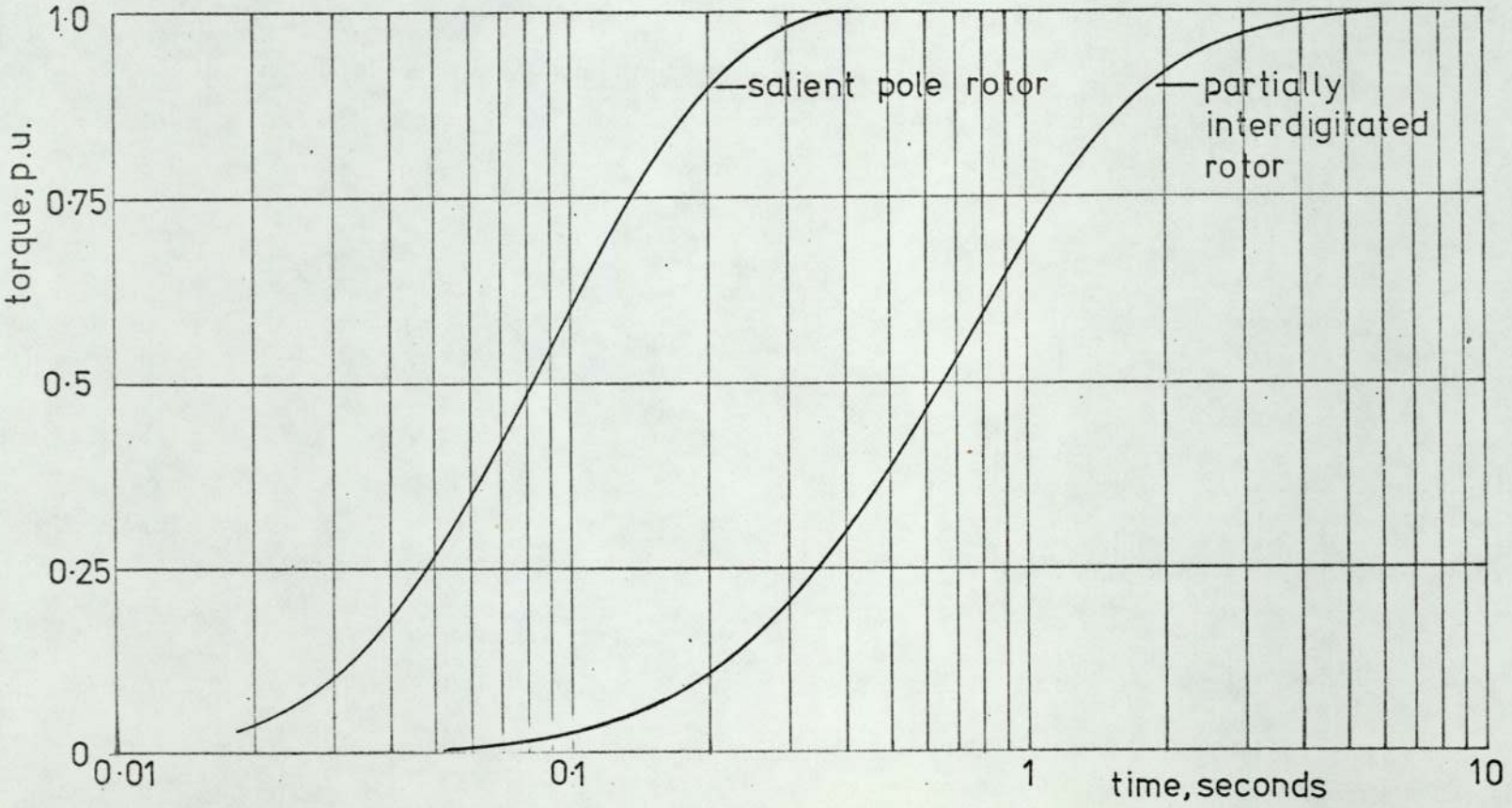

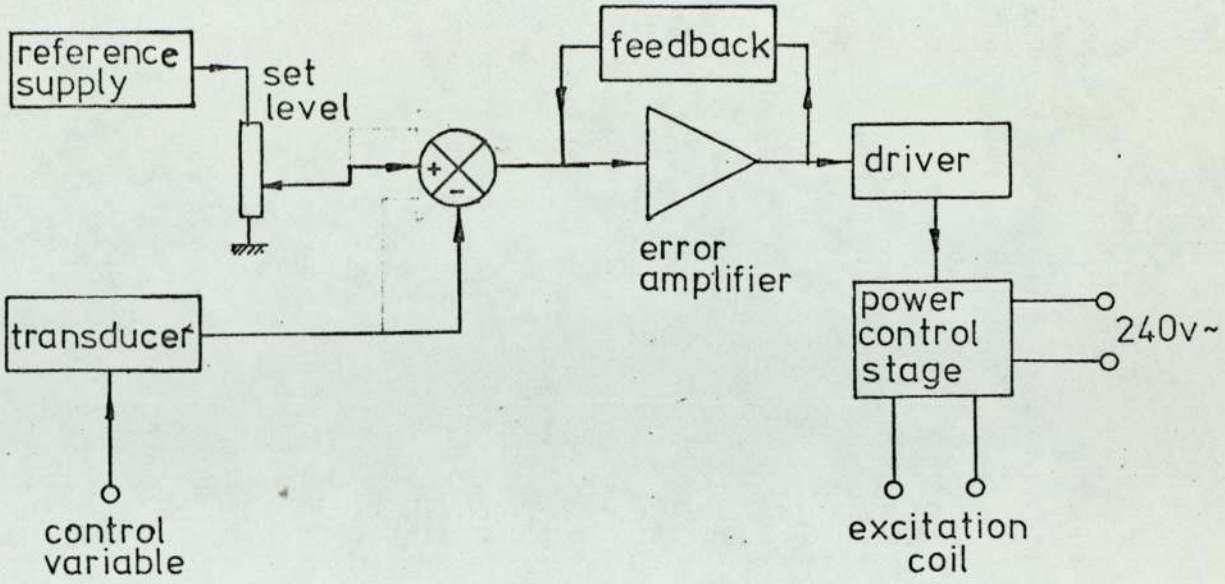

Fig. 4.4 Simple Analogue Controller

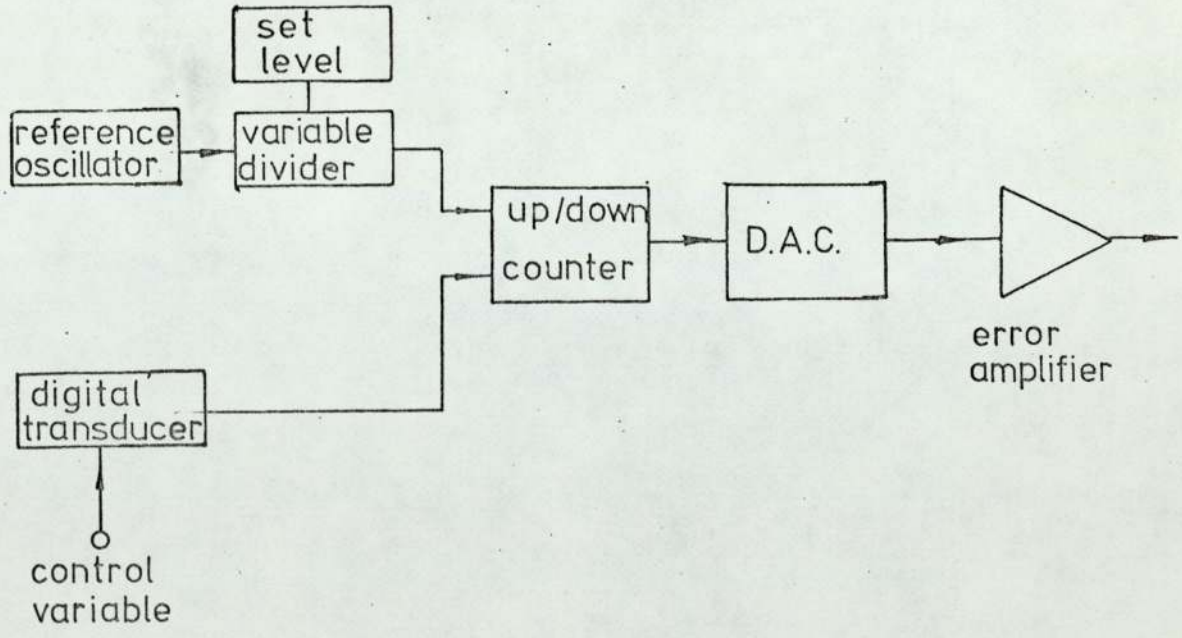

Fig. 4.5 Simple Digital Error Signal Processor.

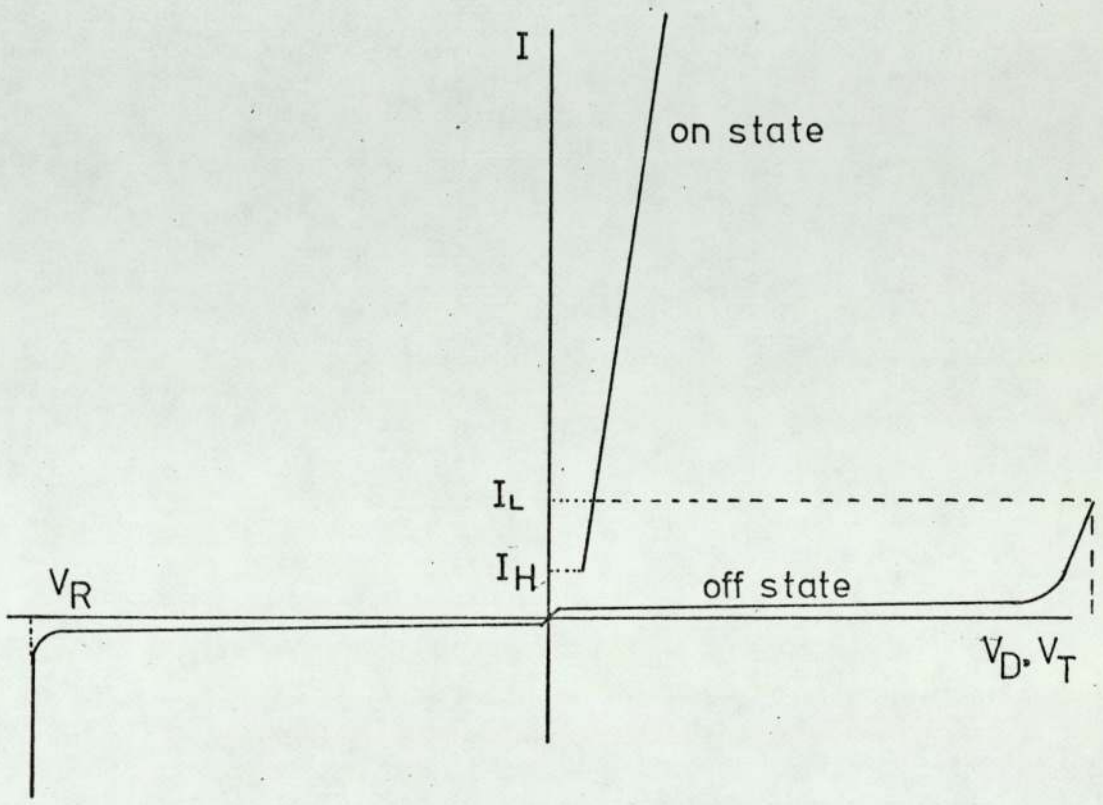

Fig. 4.6 Thyristor Operating Characteristics.

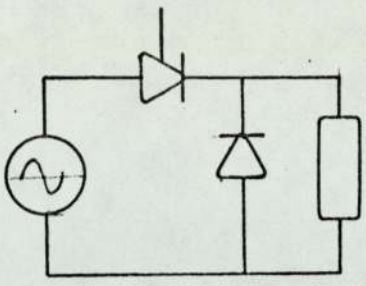

a.

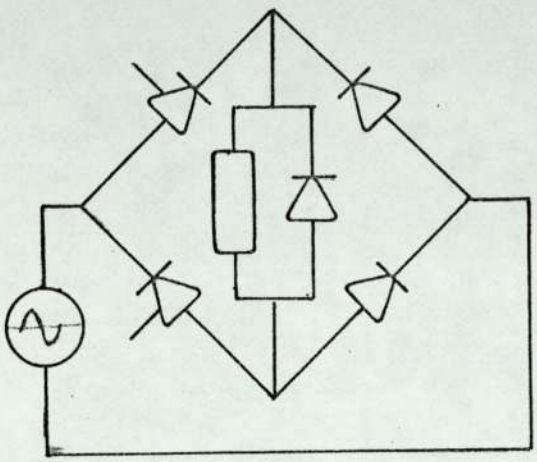

b.

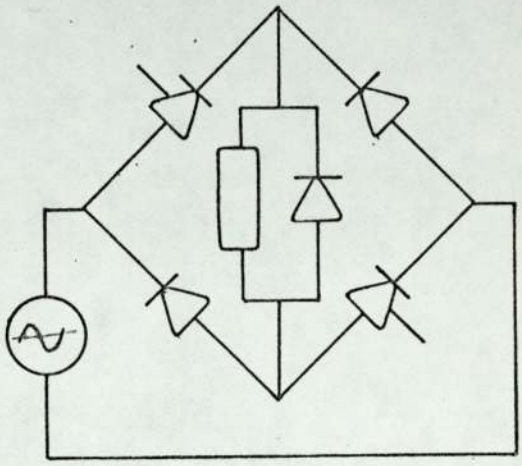

c.

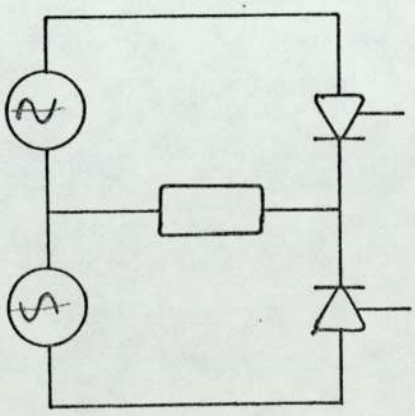

d.

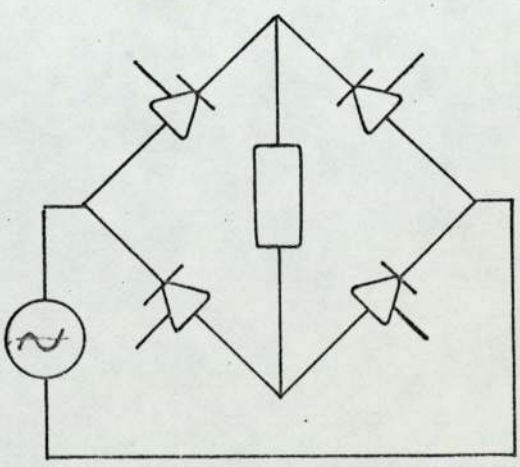

e.

Fig. 4.7 Controlled Rectifier Configurations.